ÇUKUROVA UNIVERSITY

INSTITUTE OF NATURAL AND APPLIED SCIENCES

MSc THESIS

Helin BOZKURT

OPTIMAL DESIGN OF A HYBRID PV-BATTERY SYSTEM FOR ON-GRID APPLICATIONS

DEPARTMENT OF ELECTRICAL AND ELECTRONICS ENGINEERING

ADANA, 2022

ÇUKUROVA UNIVERSITY
INSTITUTE OF NATURAL AND APPLIED SCIENCES

OPTIMAL DESIGN OF A HYBRID PV-BATTERY SYSTEM FOR ON-GRID APPLICATIONS

Helin BOZKURT

MSc THESIS

DEPARTMENT OF ELECTRICAL AND ELECTRONICS ENGINEERING

We certify that the thesis titled above was reviewed and approved for the award of degree of the Master of Science by the board of jury on 04/10/2022.

…….....	……..	……..……..
Prof. Dr. Ahmet TEKE	Assoc. Prof. Sami ARICA	Asst. Prof. Dr. Oğuzhan TİMUR
SUPERVISOR	MEMBER	MEMBER

…….....	…….
Asst. Prof. Dr. Özgür ÇELİK	Asst. Prof. Dr. Kasım ZOR
CO-SUPERVISOR	MEMBER

This MSc Thesis is written at the Department of Institute of Natural and Applied Sciences of Çukurova University.
Registration Number:

Prof. Dr. Sadık DİNÇER
Director
Institute of Natural and Applied Sciences

ABSTRACT

MSc THESIS

OPTIMAL DESIGN OF A HYBRID PV-BATTERY SYSTEM FOR ON-GRID APPLICATIONS

Helin BOZKURT

ÇUKUROVA UNIVERSITY
INSTITUTE OF NATURAL AND APPLIED SCIENCES
DEPARTMENT OF ELECTRICAL AND ELECTRONICS DEPARTMENT

Supervisor : Prof. Dr. Ahmet TEKE
Co-Supervisor : Asst. Prof. Dr. Özgür ÇELİK
Year: 2022, Pages: 183
Jury : Prof. Dr. Ahmet TEKE
: Assoc. Prof. Sami ARICA
: Asst. Prof. Dr. Oğuzhan TİMUR
: Asst. Prof. Dr. Kasım ZOR
: Asst. Prof. Dr. Özgür ÇELİK

Photovoltaic (PV) systems with integrated battery energy storage systems (BESs) play a crucial role in promoting energy efficiency, sustainability, and the use of renewable energy sources. The main aim of this study is to develop an artificial neural network (ANN) based maximum power point tracking (MPPT) method that eliminates the drawbacks of conventional perturb & observe (P&O) and incremental conductance (INC) MPPT methods. Moreover, an optimal operation of the grid-connected hybrid PV-BES system is presented by considering the real atmospheric data taken from the Turkish State Meteorological Service. MATLAB/Simulink is used to design and test the constructed 12 kW PV system with 10 kWh capacity BES. In this study, a scenario is created for all operating modes of the hybrid system. The solar irradiation curve of a-determined day is created from the real meteorological data of Tarsus/Mersin. In addition, simulation results for constant irradiation values as 1000 W/m^2 and for 500 W/m^2 at 25°C are analyzed separately. It is observed from the simulation results that the presented ANN-based MPPT method gives better total harmonic distortion (THD) results than conventional MPPT methods for variable atmospheric conditions and all operating modes of the system. Especially at low irradiance values, the ANN-based MPPT illustrate better performance values for parameters such as efficiency, THD, and tracking capability.

Keywords: Battery Energy Storage System (BESs), Total Harmonic Distortion (THD), ANN-Based MPPT, Grid Connected Hybrid Systems.

ÖZ

YÜKSEK LİSANS TEZİ

ŞEBEKE BAĞLANTILI HİBRİT FV-BATARYA SİSTEMİNİN OPTİMAL TASARIMI

Helin BOZKURT

ÇUKUROVA ÜNİVERSİTESİ
FEN BİLİMLERİ ENSTİTÜSÜ
ELEKTRİK ELEKTRONİK MÜHENDİSLİĞİ BÖLÜMÜ

Danışman : Prof. Dr. Ahmet TEKE
2. Danışman : Dr. Öğr. Üyesi Özgür ÇELİK
Yıl: 2022, Sayfa: 183
Jüri : Prof. Dr. Ahmet TEKE
: Doç. Dr. Sami ARICA
: Dr. Öğr. Üyesi Oğuzhan TİMUR
: Dr. Öğr. Üyesi Kasım ZOR
: Dr. Öğr. Üyesi Özgür ÇELİK

Entegre pil enerji depolama sistemlerine sahip fotovoltaik (FV) sistemler, enerji verimliliğini, sürdürülebilirliği ve yenilenebilir enerji kaynaklarının kullanımında çok önemli bir rol oynamaktadır. Bu çalışmanın amacı, şebeke bağlantılı hibrit sistemin optimal tasarımını sağlayarak, en yaygın kullanılan geleneksel yöntemler olan Değiştir & Gözlemle ve Artan İletkenlik maksimum güç noktası takibi (MGNT) yöntemlerinden daha iyi sonuçlar veren yapay sinir ağları (YSA) tabanlı bir MGNT yöntemi geliştirmektir. MATLAB/Simulink 10 kWh kapasiteli akü depolama sistemi ile 12 kW FV sisteminden oluşan hibrit sistemi tasarlamak ve test etmek için kullanılır. Bu çalışmada hibrit sistemin tüm çalışma modları için bir senaryo oluşturulmuştur. Tarsus/Mersin'in gerçek meteorolojik verilerinden oluşan bir günün güneş ışınım eğrisi oluşturulmuş ve sistem bu ışınım eğrisi ile simüle edilerek, MGNT yöntemleri karşılaştırılmıştır. Ayrıca 25°C'de 1000 W/m^2 ve 500 W/m^2 için simülasyon sonuçları ayrı ayrı analiz edilmiş ve karşılaştırılmıştır. Sunulan YSA tabanlı MGNT yönteminin, değişken atmosfer koşulları ve sistemin tüm çalışma modları için diğer yöntemlere göre daha iyi toplam harmonik bozulma (THD) sonuçları simülasyon sonuçlarından gözlemlenmiştir. Özellikle düşük ışınım değerlerinde geleneksel MGNT yöntemleri daha yüksek THD değerlerine sahipken, önerilen YSA tabanlı MGNT yöntemi ile bu durum önlenmiş ve düşük ışınıma sahip hava koşulları için daha verimli bir sistem elde edilmiştir.

Anahtar Kelimeler: Batarya Enerji Depolama Sistemi, Toplam Harmonik Bozulma, YSA Tabanlı MGNT, Şebekeye Bağlı Hibrit Enerji Sistemleri.

EXTENDED SUMMARY

The interest in renewable energy sources has increased due to the continuous grow in energy need, environmental friendliness, and inexhaustibility. The demand for power storage systems has risen to obtain more efficiency from renewable energy sources and to ensure uninterrupted energy flow. In this study, the optimal design of a hybrid system consisting of PV and BES is carried out. The Hybrid System is designed and tested in MATLAB/Simulink. This design consists of 4 stages. These are *(i)*; production of maximum power from the PV system, *(ii)* battery design, *(iii)* design of current controlled DC-AC inverter, and *(iv)* determination of the scenario that operates the whole system.

In order to obtain maximum power from the PV system, MPPT controlled DC-DC interleaved converter is designed. The DC-DC interleaved boost converter is used for the connection of PV and inverter, thus dividing the current into two branches and reducing transmission losses. The traditional P&O and INC methods are compared with the proposed ANN-based MPPT method. The installed power of the PV system is selected as 12.48 kW. Considering the variable weather conditions and shading effect, the PV system is designed as two separate arrays.

The capacity of BES system is determined as 10 kWh. A bidirectional buck-boost converter is designed so that the BES system can transmit power in two directions over DC-link. When the battery is charged, the converter works in buck mode, the battery is fed via DC-link, this is achieved by controlling the battery current and voltage. In case the battery is discharged, the converter works in boost mode and power is transferred to the DC-link, in this case, battery current and DC-link voltage control is provided. The maximum and minimum values of the state of charge (SOC) are 90% and 50% respectively.

A current-controlled DC-AC inverter is designed to transfer the produced power from PV to grid and the stored power from battery to grid. Active and reactive

power control is provided in the system, but only active power support mode is used. LCL filter is designed in order to eliminate the harmonics generated by the inverter.

A working scenario has been designed in order to use the generated power more efficiently and to ensure that the power flows to the grid or the battery can be realized at the right time intervals. The study consists of three ANN-based forecasting models; long short-term memory (LSTM), recurrent neural network (RNN), feedforward backpropagation neural network (FFBPNN) that estimates the daily total solar irradiation by using real meteorological data of Tarsus/Mersin in order to run the scenario depending on the weather conditions. The accuracy of this estimation is evaluated by normalized mean absolute error (NMAE), weighted mean absolute error (WMAE), normalized root mean squared error (NRMSE) and mean absolute percentage error (MAPE) which are more suitable and frequently used to evaluate meteorological forecasts. The FFBPNN model gives the best results among the other methods with 3.64% for NMAE, 5.40% for WMAE, 6.70% for NRMSE and 7.46% for MAPE. An energy management scheme is created based on the estimated total daily solar irradiation. As a result of the irradiation forecast for the next day, the SOC of the battery can be decided by considering the cloudy and sunny weather conditions.

In the operating scenario of the system, the aim is to ensure the most efficient use of the generated and stored power. Therefore, when the battery PV power generation is sufficient, the battery is charged until the SOC reaches 90%. While the battery is being charged, the power generated from the PV system is transferred to both the battery and the grid. In cases where PV power generation cannot meet the energy needs, that is, if PV cannot produce power, the battery will discharge until its SOC is 50%. In this case, the energy stored in the battery is transferred to the grid. Thus, energy continuity is ensured by using the stored power produced from PV during the daytime, for night hours when the PV system cannot benefit. The system is simulated and tested in MATLAB/Simulink and the results are taken for 1000 W/m^2, 500 W/m^2 and an irradiation curve of Tarsus/Mersin created by the real data

obtained from meteorology. The system's charge mode, discharge mode and PV-to grid mode are simulated separately for these irradiation values and the results are compared. Higher THD values are especially encountered at low irradiance values for the system operated with traditional MPPT methods. On the other hand, it is seen that the system operated with the proposed ANN-based MPPT method has lower THD values even at low irradiance values for all operating modes. In addition, the oscillations and tracking capability of the proposed MPPT are far superior when the traditional MPPT methods are considered. As a result, when the battery, inverter output, DC-link voltage and THD graphs given for all operating modes are examined, it is seen that a more stable and lower THD system is designed with the ANN-based MPPT method developed in this study.

GENİŞLETİLMİŞ ÖZET

Enerji ihtiyacının sürekli artması, çevre dostu ve tükenmez olması nedeniyle yenilenebilir enerji kaynaklarına olan ilgiyi artmıştır. Yenilenebilir enerji kaynaklarından daha fazla verim elde etmek ve kesintisiz enerji akışını sağlamak için güç depolama sistemlerine olan talep de artmıştır. Bu çalışmada, FV ve batarya depolama sisteminden oluşan hibrit bir sistemin optimal tasarımı gerçekleştirilmiştir. FV ve batarya enerji depolama sisteminden oluşan hibrit sistem MATLAB/Simulink 'te tasarlanmış ve test edilmiştir. Sistem tasarımı 4 aşamadan oluşmaktadır. Bunlar; FV sistemden maksimum güç üretimi, batarya tasarımı, akım kontrollü DC-AC evirici tasarımı ve tüm sistemi çalıştıracak senaryonun belirlenmesidir.

FV sistemden maksimum güç elde etmek için MGNT kontrolörleri tarafından kontrol edilen DC-DC serpiştirmeli dönüştürücü tasarımı yapılmıştır. DC-DC serpiştirmeli dönüştürücü sayesinde FV sistemi ile DC bağlantı noktası arasındaki bağlantı gerçekleştirilir ve akım iki kola bölünerek iletim kayıpları azaltılır. Geleneksel yöntemlerden P&O ve INC yöntemleri, önerilen YSA tabanlı yöntemle karşılaştırılır. FV sistemin kurulu gücü 12.48 kW olarak belirlenmiş ve değişken hava koşulları ve gölgeleme etkisi göz önünde bulundurularak PV sistemi iki ayrı dizi olarak tasarlanmıştır.

Batarya depolama sisteminin kapasitesi 10 kWh olarak belirlenmiştir. Batarya sisteminin DC bağlantı noktası üzerinden gücün iki yönde iletebilmesi için çift yönlü bir alçaltıcı-yükseltici dönüştürücü tasarlanmıştır. Batarya şarj edildiğinde dönüştürücü alçaltıcı modunda çalışır, batarya DC bağlantı noktası üzerinden beslenir, bu batarya akımı ve voltajı kontrol edilerek gerçekleştirilir. Bataryanın boşalması durumunda dönüştürücü yükseltici modunda çalışır ve DC bağlantı noktasına güç aktarılır, bu durum batarya akımı ve DC bağlantı noktasının gerilim kontrolü sağlanarak gerçekleştirilir. Batarya şarj yüzdesinin maksimum ve minimum değerleri sırasıyla %90, ve %50'dir.

Akım kontrollü bir DC-AC evirici, FV sistem tarafından üretilen gücün şebekeye aktarılması ve bataryada depolanan gücün şebekeye aktarılması için tasarlanmıştır. Sistemde aktif ve reaktif güç kontrolü sağlanır ancak sadece aktif güç destek modu kullanılmıştır. LCL filtre sistemdeki bozulmaları ortadan kaldırmak ve sistemde oluşan harmoniklerin azaltılması için tasarlanmıştır.

FV sistem tarafından üretilen gücün verimli kullanılması ve sistemler arasında doğru zamanda güç akışının sağlanması için bir çalışma senaryosu tasarlanmıştır. Bu çalışmada, senaryonun daha anlamlı hale gelebilmesi ve batarya çalışma şeklinin hava koşullarına göre belirlenebilmesi amacıyla Tarsus/Mersin'in gerçek meteorolojik verileri kullanılarak günlük toplam güneş ışınımını tahmin eden yapay sinir ağı tabanlı metotlarından olan uzun kısa süreli bellek, tekrarlayan sinir ağı ve ileri geri yayılım tahmin modelleri oluşturulmuştur. Bu modellerin tahmin doğruluğu, NMAE, WMAE ve NRMSE gibi sık kullanılan performans endeksleriyle değerlendirilmiştir. En iyi tahmin sonucu ileri geri yayılım modelinden NMAE için %3,64, WMAE için %5,40, NRMSE için %6,70 ve MAPE için %7,46 olarak elde edilmiştir. Ertesi gün için tahmin edilen toplam günlük güneş ışınımına dayalı olarak bir enerji yönetim şeması oluşturulmuştur. Bu sayede, bir sonraki gün için yapılan tahmin sonucunda, bulutlu ve güneşli hava koşulları göz önünde bulundurularak bataryanın doluluk oranı yüzdesine karar verilebilir. Bu çalışmada verilen senaryo güneşli hava koşulları için verilmiştir. Bu senaryoda, yüksek güneş ışınımının olduğu saat dilimlerinde bataryanın doluluk yüzdesi %90'ın altındaysa, batarya %90'a kadar şarj edilir. Güneş ışınımının elektrik üretimi için yetersiz olduğu saat dilimlerinde ise FV sistemi elektrik üretimini durdurur. Bu durumda bataryanın doluluk yüzdesi %50'den fazla ise batarya doluluk yüzdesi %50 olana kadar bataryadan şebekeye güç aktarılır. Böylece gündüz FV sistemden üretilen ve bataryada depolanan güç, FV sisteminden yararlanılamayan gece saatlerinde kullanılarak enerji sürekliliği sağlanır. Sonuç olarak, sistem 1000 W/m^2, 500 W/m^2 ve Tarsus/Mersin'e ait gerçek bir günün ışınlama eğrisi için test edilir. Sistemin şarj modu, deşarj modu ve FV' den şebekeye modu bu ışınlama değerleri için ayrı ayrı

incelenerek sonuçlar alınır ve karşılaştırılır. Geleneksel MGNT yöntemleri ile çalıştırılan sistemde, özellikle düşük ışınım değerlerinde daha yüksek THD değerleri ile karşılaşılmaktadır. Önerilen YSA tabanlı MGNT yöntemi ile çalıştırılan sistemin tüm çalışma modlarında daha düşük ayar süresine sahip olduğu ve düşük ışıma değerlerinde bile düşük THD değerlerinde çalıştığı görülmektedir. Sonuç olarak tüm çalışma modları için verilen batarya, evirici akım gerilim çıkışı, DC-bağlantı noktası gerilimi ve THD grafikleri incelendiğinde, bu çalışmada geliştirilen YSA tabanlı MGNT yöntemi ile daha kararlı ve düşük THD sistemi tasarlandığı görülmektedir.

ACKNOWLEDGMENTS

First and most importantly, I would like to express my deepest thankfulness to my supervisors Prof. Dr. Ahmet TEKE, co-supervisor Asst. Prof. Dr. Özgür ÇELİK for their specialty, assistance, complete support, and patience throughout this thesis. Their scientific approach has enabled me to successfully conclude this study. Also, I would like to thank my colleague Res. Asst. Ramazan MACİT for his friendship and supports. Finally, I would like to express my thanks to Assoc. Prof. Sami ARICA, Asst. Prof. Dr. Oğuzhan TİMUR, and Asst. Prof. Dr. Kasım ZOR, who participated in my thesis jury for their contribution to eliminate the deficiencies in my thesis.

CONTENTS **PAGE**

LIST OF TABLES

LIST OF FIGURES

LIST OF SYMBOLS AND ABREVIATIONS

ACO : Ant Colony Optimization
ANN : Artificial Neural Network
BESS : Battery Energy Storage System
CS : Cuckoo Search
CSI : Current Source Inverter
D : Duty Cycle
D_{buck} : Duty cycle of buck converter
D_{boost} : Duty cycle of boost converter
FFBPNN : Feed Forward Back Propagation Neural Network
F_{grid} : Grid frequency
F_s : Switching frequency
GMPP : Global Maximum Power Point
GWO : Grey Wolf Optimization
INC : Incremental Conductance
I_{out} : Output current
I_{bat} : Battery current
L_{crit} : Critical value of inductance
MAPE : Mean Absolute Percentage Error
MPP : Maximum Power Point
MPPT : Maximum Power Point Tracking
MSE : Mean Squared Error
NRMSE : Normalized Root Mean Squared Error
NMAE : Normalized Mean Absolute Error
OCV : Open Circuit Voltage
P&O : Perturb and Observe
PI : Proportional -Integral
PV : Photovoltaic

PLL : Phase Locked Loop

P_{pv} : PV Power

PSO : Particle Swarm Optimization

RES : Renewable Energy Sources

R_i : Input side impedance

R_L : Load impedance

R_{MPP} : Optimum impedance

SCC : Short Circuit Current

SSE : Steady State Error

STC : Standard Test Conditions

SOC : State of Charge

TETC : Turkish Electricity Transmission Corporation

THD : Total Harmonic Distortion

V_{bat} : Battery voltage

Vdc : DC-link Voltage

V_H : Voltage of high side

V_{in} : Input side voltage

V_L : Voltage of low side

VSI : Voltage Source Inverter

V_{out} : Output voltage

WMAE : Weighted Mean Absolute Error

1. INTRODUCTION

1.1. Statement of Problem and Research Motivation

Nowadays, the interest in renewable energy sources (RESs) has gradually increased due to the depletion of traditional energy sources, their harm to the environment and the inability to meet sufficient energy demand. RESs are inexhaustible and clean energy sources that comes from nature such as geothermal, biomass, sun, wind, hydropower and tidal. The solar power is one of the most effective sources among the other RESs for several reasons such as being sustainability, economical, pollution free and easy to install (Chauhan and Singh, 2021).

Photovoltaics (PVs) convert sunlight into electrical energy by using the photoelectric effect. The sun's radiation is directly converted into usable electricity by PV systems that are made of photovoltaic modules, which are semiconductor devices. PV power depends highly on solar irradiation and temperature (Iqbal, 2017). In consequence, maximum power extraction from the PV system plays a crucial role in increasing the efficiency of the solar power generation for all weather conditions. Therefore, an appropriate MPPT technique to track the MPP is of high need (Bollipo et al., 2021).

The Figure 1.1. shows the current versus voltage (I-V) and power versus voltage (P-V) characteristics for constant temperature variable irradiation values, the I-V and P-V characteristics for constant irradiation variable temperature values for a PV cell.

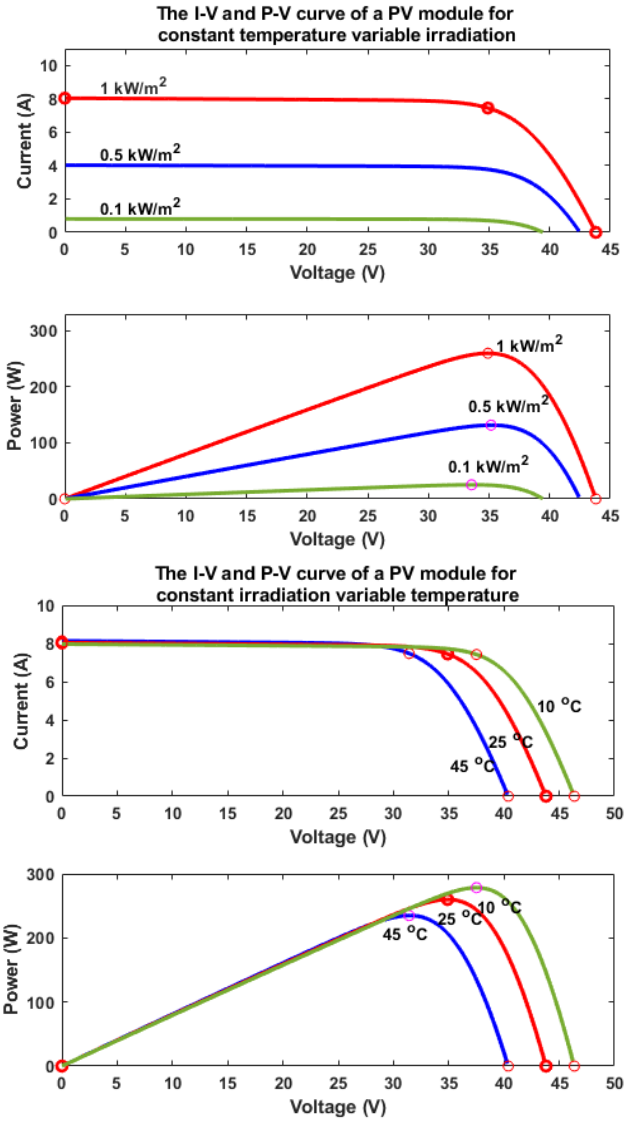

Figure 1.1. I-V and P-V characteristics of a PV module at specified temperature-variable radiation values & specified radiation-variable temperature values

Since the power generation of the PV panel is directly dependent on the weather conditions, the behavior of the generated PV power is discontinuous. Therefore, it is not always possible for the PV array to meet the load demand alone

at every time (Narayanan et al., 2020). This causes power mismatch and imbalance in the system. In order to minimize these problems occurring in the system and to increase the efficient use of the energy produced BESs is used with PV system. BESs has some benefits over traditional energy sources, which include fast and steady response, adaptability, controllability, environmental friendliness, and geographical independence, and are considered as a potential solution to the global warming problem (Hannan et al., 2021). The main components of the renewable energy and battery energy storage system (RE-BESs) include the energy supply, energy storage, grid integration, load control and energy management (Liu et al., 2020).

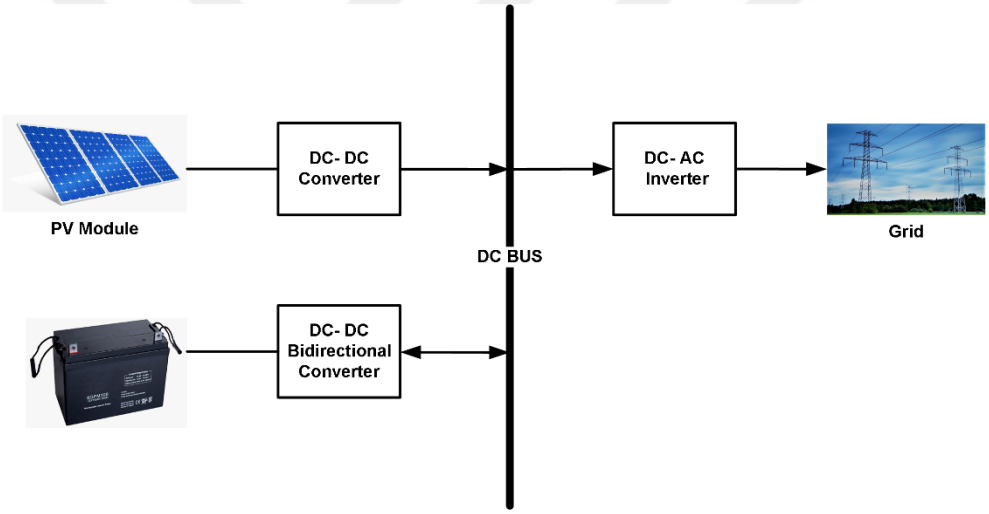

Figure 1.2. A block diagram of a hybrid PV-BES grid connected system

The basic structure of a grid connected PV-BES system is shown in Figure 1.2. The system consists of a DC-DC converter that controlled by a MPPT algorithm to obtain the maximum power from PV arrays. The BESs is connected DC-link with a bidirectional DC-DC converter that is controlled with a battery controller algorithm to set the dc voltage, battery voltage, battery current and state of charge (SOC) at desired values while the system is charging and discharging. In addition, DC-AC inverter that is controlled with current controller is used for grid integration.

1.2. Objective and Outline of the thesis

The main objective of these thesis is modelling and simulating a grid tied PV-BES system with an optimal energy management algorithm and proposed ANN-based MPPT algorithm by use of MATLAB/Simulink. The model consists of interleaved DC-DC boost converter, ANN-based MPPT controller, DC-DC bidirectional buck-boost converter, proportional-integral (PI) controller for charging discharging processes, three phase current controlled DC-AC inverter, and LCL filter. In addition, traditional MPPT methods, that are mostly used, are modeled, and simulated to demonstrate the superiority of the proposed method. In this study, it is aimed to manage the produced energy better, mitigate harmonics, not to decrease the efficiency obtained from the system, stabilize the system earlier in sudden changing temperature and radiation values compared to conventional MPPT methods.

After an introductory section in which the problem statement, research motivation and contribution of the study are introduced, the structure of this thesis is as follows:

In Chapter 2, the current state of the world and Turkey in terms of renewable energy is summarized, the system overview is presented and the extensive literature review of the converters' topologies, controllers' algorithms, energy storage and energy management strategies are presented in detail.

In Chapter 3, the power circuit parameters of grid-tied hybrid system model components are designed in MATLAB/Simulink program for simulation cases. The proposed system and the working principle of whole system are detailed with the energy management scheme.

In Chapter 4, different case results are given for both conventional MPPT methods and proposed MPPT method. The results are given as graphically.

In Chapter 5, the conclusions of the study are explained and the future work topics on optimal energy management and BESs are explained.

1.3. Contributions of Thesis

The important contributions of this thesis can be summarized as follows:

- This study emphasizes the importance of uninterrupted, continuous, and efficient use of energy, and focuses on the use of grid tied PV-BES systems at low power to spread the usage of renewable energy sources at every power level.
- Recent studies on the design of grid-connected PV-BES systems are reviewed and a summary of the current literature on the main topics of this thesis is made.
- The results of MPPT methods for variable weather conditions are clearly given and compared.
- Mitigation of harmonics in grid tied PV-BES system is carried out as follows for different operating cases with proposed ANN-based MPPT method.
  - ✓ PV to grid and battery for 1000 W/m^2 at charging mode THD% < 1.5%
  - ✓ PV to grid mode for 1000 W/m^2 THD% < 1%
  - ✓ Battery to grid mode at discharging mode THD% < 3%
  - ✓ PV to grid and battery for 500 W/m^2 at charging mode THD% < 3%
  - ✓ PV to grid mode for 500 W/m^2 THD% < 2%
- Energy management is required for more efficient use of solar energy. It also helps increase battery life by adjusting the lower and upper limits of SOC. In order to make the working scenario applied to the system more meaningful, this study is supported by the total daily solar irradiation estimation performed with the real meteorological data of Tarsus / Mersin with LSTM, RNN, and FFBPNN models. In this way, we can make our energy plan by estimating the energy to be produced from our PV plant.

- In order for the power estimation to be more rational and understandable, irradiation estimation result is evaluated with performance metrics such as NRMSE, NMAE, WMAE and MAPE.
- An operation scenario is created for sunny weather conditions and the irradiation curve of a day is created from the real meteorological data of Tarsus/Mersin and it is observed how the system works with created scenario. Thus, it is seen that this study, which is carried out in the simulation environment, also works at low THD for suddenly changing weather conditions and settles more quickly that the conventional MPPT methods.

2. LITERATURE REVIEW

2.1. Renewable Energy

Today, the ever-increasing need for energy plays a crucial and fundamental role in determining the economic and political levels of countries. Energy dependence is the most important factor in specifying the level of development of a country in all aspects of life. The total energy consumption of world between 1965 and 2021 is shown in the Figure 2.1.

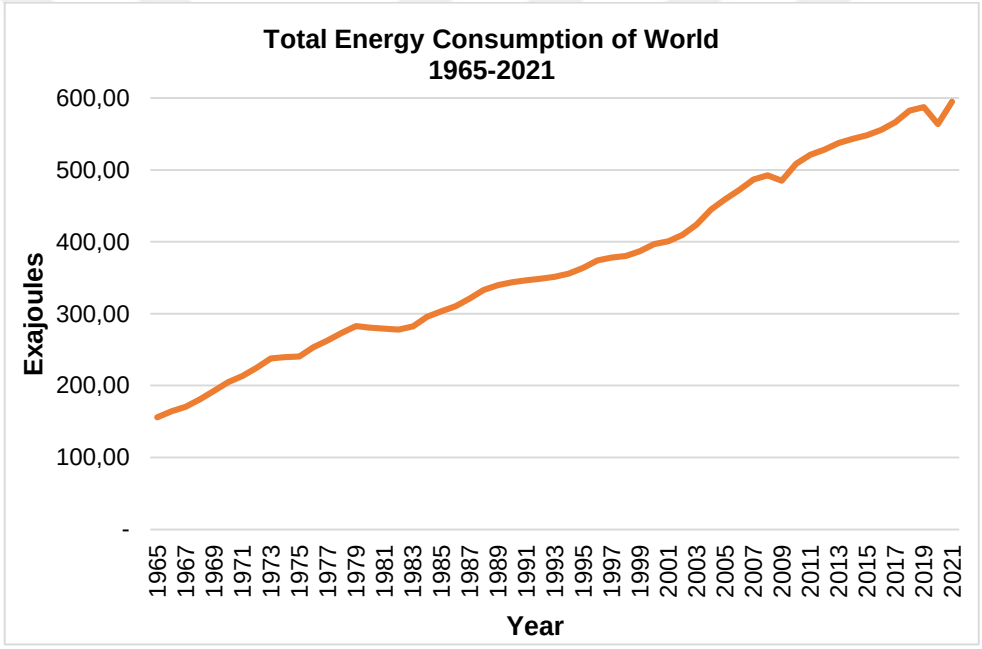

Figure 2.1. The total energy consumption of world

Energy is obtained from renewable and non-renewable energy sources. Conventional energy sources, also called non-renewable and exhaustible, are carbon-based. While producing energy from these sources, carbon-based gases are released into the environment, and these gases cause the world to warm up and cause permanent climate change. Renewable energy attracts worldwide attention due to

environmental concerns. New policies require grid operators to supply a certain percentage of their load from RES or face high penalties (Mohandes et al., 2021). Since it is inexhaustible and reduce the carbon footprint, greenhouse gases around the world, it become the focal point of developed and developing countries. Considering all these situations, various international environmental agreements such as 'Paris Agreements' have been signed, aiming for all living creatures in the world to live in a cleaner, healthier, more permanent world, and in line with these agreements, it is aimed to provide the produced energy mostly from renewable energy sources. The total energy consumption of the world in 2020 and 2021 by fuels is presented in Figure 2.2. As can be seen from the graph, a significant portion of the consumed energy is obtained from renewable energy.

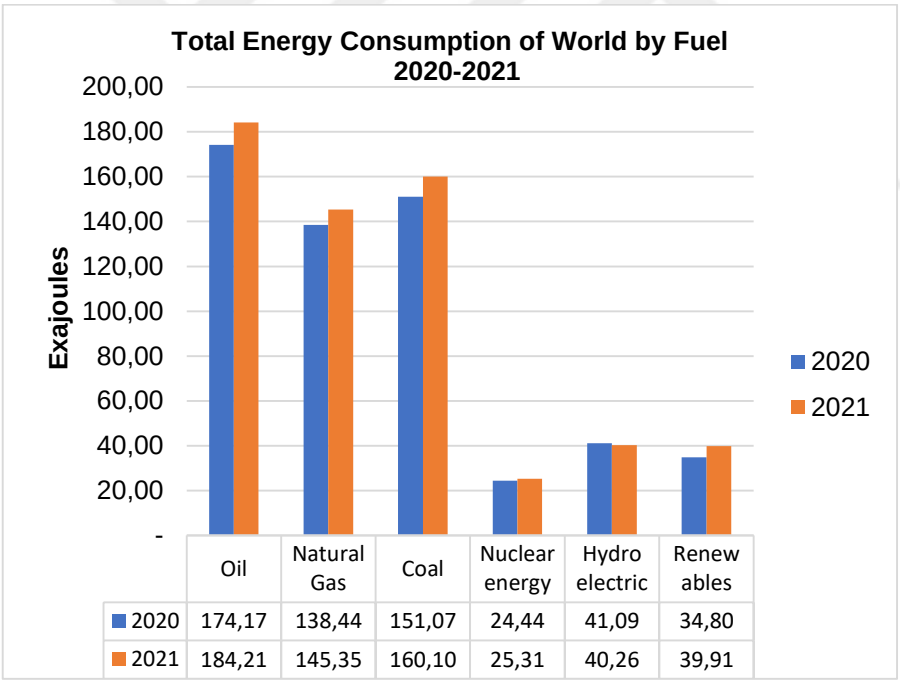

	Oil	Natural Gas	Coal	Nuclear energy	Hydro electric	Renewables
2020	174,17	138,44	151,07	24,44	41,09	34,80
2021	184,21	145,35	160,10	25,31	40,26	39,91

Figure 2.2. Total energy consumption of the world by fuel 2020-2021

As the need for energy increases, the need for electricity also increases. Growth of population, increase in production, settled life, hospitals, basic life needs

are the main reasons for the rise of electricity productions. The total Electricity generation of world between 1985 and 2021 is shown in Figure 2.3 and in Figure 2.4 the total electricity generation of world by fuel for 2020-2021 years is presented.

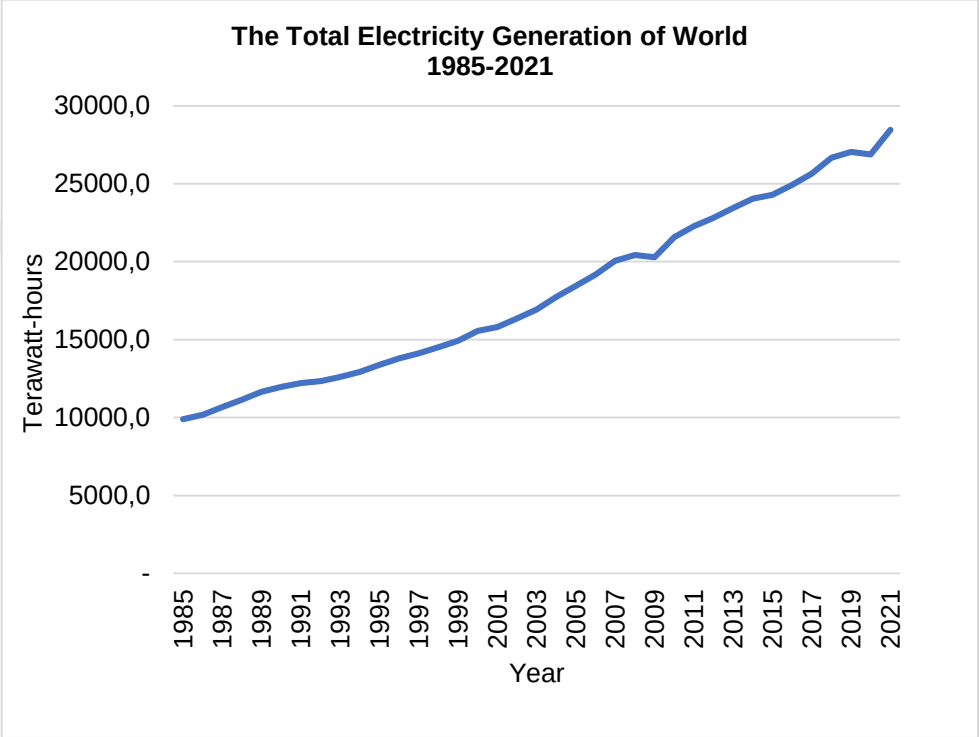

Figure 2.3. The total electricity generation of world 1985-2021

As seen in Figure 2.4, 11% of the total electricity produced in the world in 2020 was provided by renewable energy. In 2022, this rate increased to 12.84%. The undeniable contribution of renewable energy to energy and the environment has brought all types of renewable energy into focus. One of them is undoubtedly solar energy. The use of photovoltaic electricity is constantly increasing around the world since there is no fuel problem, ease of use, no mechanical wear, modularity, commissioning in a very short time, working smoothly for many years and being a clean energy source. According to the 2021 world energy report published by BP-

Statistics, while the total installed PV power in the world was 710281MW in 2020, this is increased by 19% in 2021 and reached 843086 MW.

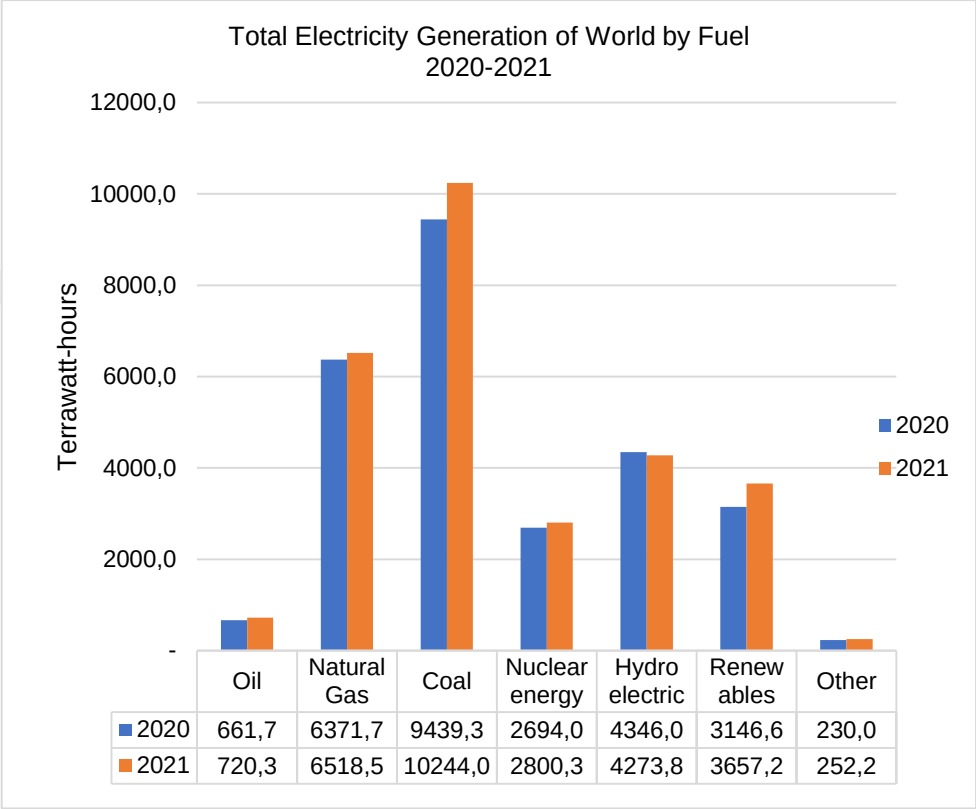

	Oil	Natural Gas	Coal	Nuclear energy	Hydro electric	Renew ables	Other
2020	661,7	6371,7	9439,3	2694,0	4346,0	3146,6	230,0
2021	720,3	6518,5	10244,0	2800,3	4273,8	3657,2	252,2

Figure 2.4. Total electricity generation of world by fuel 2020-2021

In parallel with the world, energy consumption in Turkey also increases over the years. According to the latest energy reports of announced by Turkish Electricity Transmission Corporation (TETC), Turkey's installed capacity is shown in Figure 2.5 between 1980 and 2020 with 5 years intervals. Although the statistical data for 2021 has not been published yet, it is mentioned that in 2021, 31.4% of our electricity production come from coal, 32.7% from natural gas, 16.8% from hydraulic energy, 9.4% from wind, 4% from solar, 3.2% from 2% was obtained from geothermal

energy and 2.4% from other sources. Furthermore, the installed capacity of Turkey is announced as 101,518.3 MW in the June 2022 report by TETC.

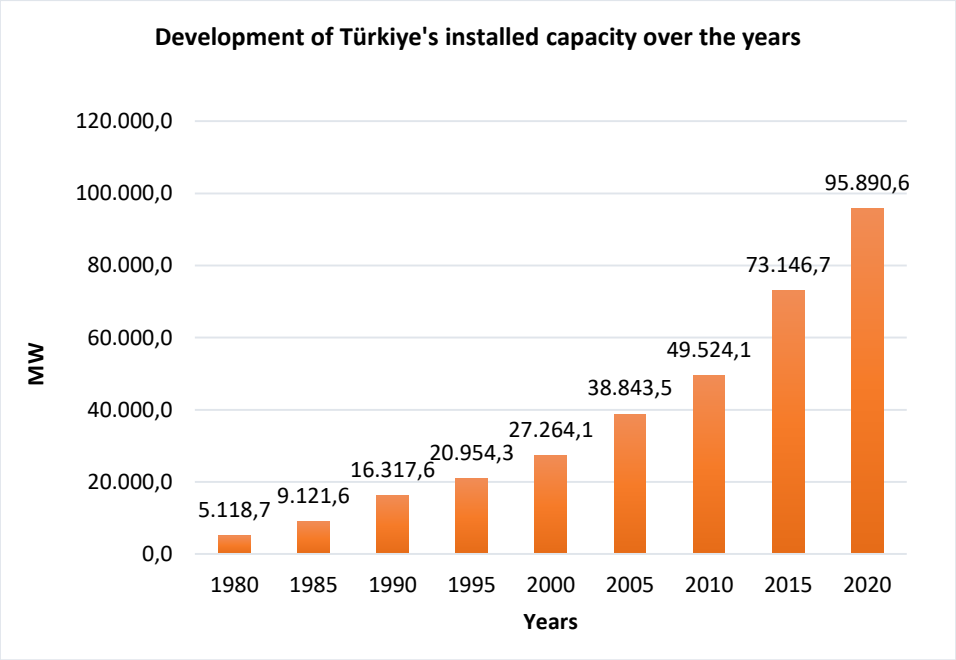

Figure 2.5. Development of Turkey's installed power over the years

The main reasons that lead all countries of the world to seek new energy sources, such as the ever-increasing need for energy, depleting energy resources, and foreign dependency in energy, have led Turkey to make incentives and investments in RESs. Figure 2.6 shows the graph of Turkey Installed Power Development by Primary Energy Sources (2010-2021). As can be seen from the Figure 2.6, solar energy meets a significant part of our energy needs.

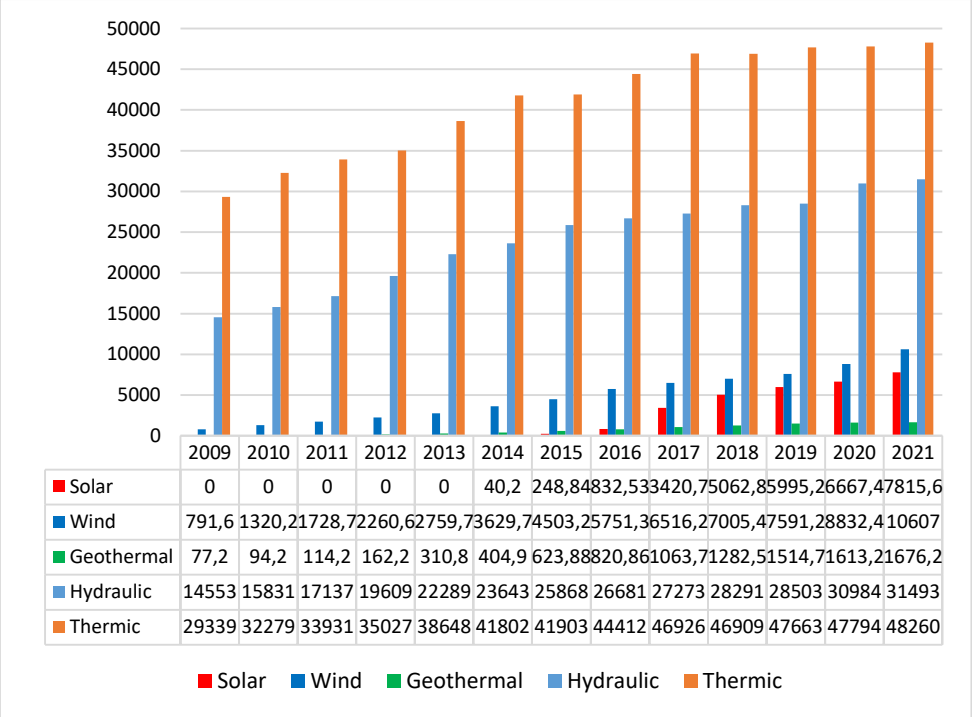

	2009	2010	2011	2012	2013	2014	2015	2016	2017	2018	2019	2020	2021
Solar	0	0	0	0	0	40,2	248,84	832,53	3420,75	5062,85	5995,26	6667,47	7815,6
Wind	791,6	1320,2	1728,72	2260,62	2759,73	3629,74	4503,25	5751,36	6516,27	7005,47	7591,28	8832,4	10607
Geothermal	77,2	94,2	114,2	162,2	310,8	404,9	623,88	820,86	1063,71	1282,51	1514,71	1613,21	1676,2
Hydraulic	14553	15831	17137	19609	22289	23643	25868	26681	27273	28291	28503	30984	31493
Thermic	29339	32279	33931	35027	38648	41802	41903	44412	46926	46909	47663	47794	48260

Figure 2.6. Turkey's installed power development by primary energy sources 2010-2021

In the June 2022 installed power report that is published by TETC, it was stated that renewable energy has reached 54,871.5 MW and renewable energy power plants constituted 54.05% of the total installed power and the installed power of solar power plants increased to 8479.1 MW.

2.2. System Overview and Grid Connection Standards

In this part of study, there is literature review of the main topologies and control algorithms that make up the grid-connected PV-BES hybrid system seen in Figure 2.7.

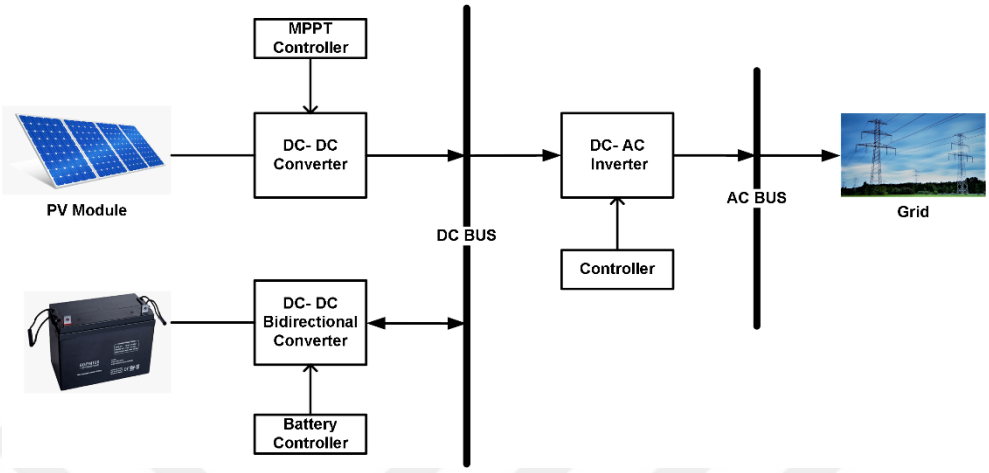

Figure 2.7. The overview of proposed system

The DC-DC interleaved boost converter is designed for boosting the output voltage of PV array. MPPT is used for extracting the maximum power from PV arrays. Among the MPPT methods, P&O, INC methods which are commonly used also called traditional methods, and proposed ANN-based MPPT method are used. Battery PI controller is designed for defining the reference signals for DC-DC bidirectional buck-boost converter based on the operating scenario of the system. Thus, our DC-DC bidirectional converter can buck DC-link voltage for charging process or boost the battery voltage for discharging process for specified values. So, the DC-link voltage is constantly controlled. The power controller-controlled DC-AC inverter which integrates the system into the grid is designed. Synchronization with the grid is a very important problem, so before networking the PV system, it is necessary to evaluate how the network is affected. PV systems that will be integrated into the grid must be designed to provide the necessary rules and standards for essential integration. With the use of these standards, the technical conditions that must be complied with in the electricity transfer system of the countries are provided. These rules vary from country to country. There are also well-known international standards, such as Institute of Electrical and Electronics Engineers (IEEE) and International Electro technical Commission (IEC).

In Turkey these regulations are demonstrated in ELECTRICITY MARKET GRID REGULATION (EMGR) with the latest version that is published in Official Gazette of the Republic of Turkey no 29013 on 28/5/2014 (EPDK, 2014).

- Frequency: The rated frequency of the system is controlled by TETC. It is determined in the operating range of 47.5-51.5 Hz and around 50 Hertz (Hz). When the operating frequency drops below 47.5 Hz or rises above 51.5 Hz, the system must be disconnected from the mains.

2.3. DC–DC Switch Mode Converter

2.3.1. Topologies

The DC-DC converters are divided into two main groups as isolated and non-isolated converters. In non-isolated topologies, power is transferred without magnetic isolation, they have a simpler structure. Although they cannot take advantage of some of the important advantages of galvanic isolation, they are not affected by the disadvantages either. It is suitable for use in applications where size and weight are important. (Gorji et al., 2019). The classification of the non-isolated DC-DC converters are shown in Figure 2.8.

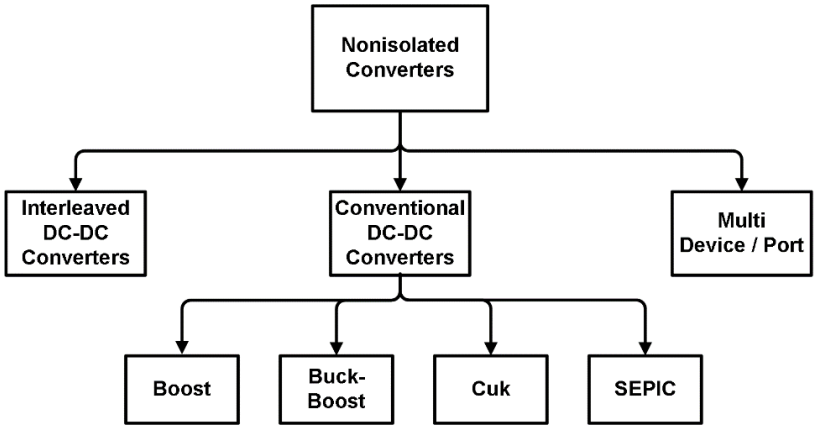

Figure 2.8. Non-isolated DC-DC converters

Insulation implies the existence of an electrical barrier between the inputs and outputs of the converter. A high frequency transformer can act as this barrier. The main advantage of this barrier is its use for high voltage applications. In addition, these isolated transducers can be configured as positive or negative (Kummara et al., 2020). Isolated Converters are shown in Figure 2.9.

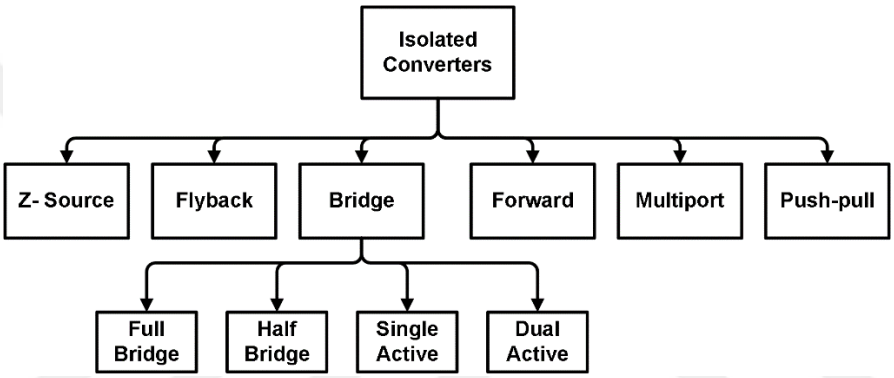

Figure 2.9. Isolated DC-DC converters

In the literature there are various studies on DC-DC Converter topologies. In (Amir et al., 2019) , comparative analysis of isolated and non-isolated DC-DC converters, focusing on transformer-less topology for high voltage gain in photovoltaic systems is studied under different situations such as ideal and non-ideal conditions. In (G and Singh, 2017), it has been shown that the choice of converter has an effect on the performance of the PV system, and a comprehensive literature review for non-isolated topologies for the selection is given. In (Mumtaz et al., 2021) non-isolated DC-DC converters are analyzed based on different controlling algorithms for renewable energy systems. In (Sivakumar et al., 2016) , a comparative performance analysis of non-isolated converters such as buck-boost, cuk, sepic, luo, and state space modelling of these converters are figured out.

2.3.1.1. Buck Converter

Buck converter which is also called step down converter is used for obtaining a lower voltage level at the output than the voltage level at the input. The circuit topology is given in the Figure 2.10. This topology can be used to connect high module voltages to low load or battery voltages (Taghvaee et al., 2013).

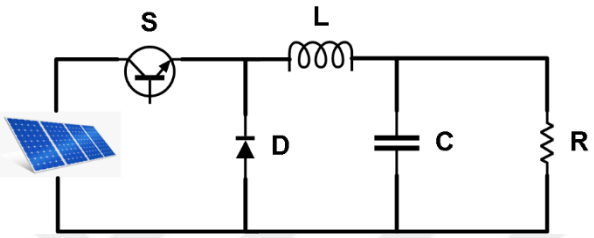

Figure 2.10. Buck converter topology

Buck converter operates when the load impedance (R_L) bigger than the optimum impedance (R_{MPP}). In the operating mode intervals, it changes the duty cycle (D) to obtain maximum power. At the maximum power point R_{MPP} equal to input side impedance (R_i). The duty cycles determine the on and off state of the IGBT for the relationship between the input and output voltages. When the switch is ON state, the diode is reverse biased and the inductor current rises its maximum value and stores the energy, in the OFF state of switch the inductor transfers its energy to the capacitor and load. The average of the output voltage is zero.

$$(V_{out} - V_{in}) * t_{on} - V_{out} * t_{off} = 0 \tag{2.1}$$

$$\frac{V_{out}}{Vin} = \frac{t_{on}}{(t_{on} + t_{off})} = D \tag{2.2}$$

2.3.1.2. Boost Converter

Boost converter is one of the widely used DC-DC converter types for increasing the output voltage level. It is also called as step-up converter. The boost

converter topology is shown in Figure 2.11. Boost converter is a basic DC-DC voltage booster circuit with a variety of features that make it suitable for various applications in products ranging from low-power portable devices to high-power stationary applications (Forouzesh et al., 2017).

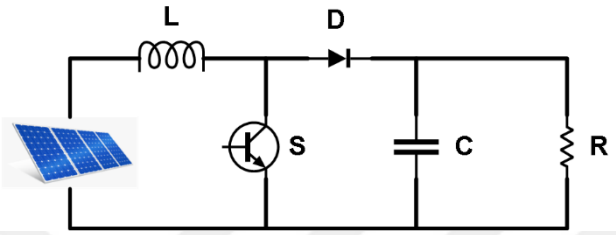

Figure 2.11. Boost converter topology

Boost converter operates while the R_L is smaller than the R_{MPP}. At the maximum power point R_i is equal to R_{MPP}. Duty cycle determines the operation states of IGBT. At the ON state of switch inductor stores energy, the inductor current rises to its maximum value, the diode is in OFF position. At the OFF state of switch the inductor current decreases its minimum value because of releasing its energy to load and capacitor, the diode is in ON position and the output voltage occurs. The average of the output voltage is zero.

$$(\Delta iL)open + (\Delta \dot{I}L)closed = 0 \tag{2.3}$$

$$V_i * (D + 1 - D) - V_o * (1 - D) = 0 \tag{2.4}$$

$$V_o = \frac{V_i}{1 - D} \tag{2.5}$$

2.3.1.3. Bidirectional Buck-Boost Converter

Bidirectional DC-DC converters are used to transfer power in both directions between two dc sources (Iqbal, 2017). The basic bidirectional converter is presented based on the original buck and boost converter (Gorji et al., 2019). The basic topology is shown in Figure 2.12.

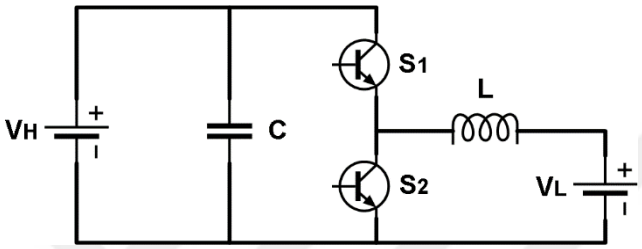

Figure 2.12. Bidirectional buck-boost converter topology

A bidirectional buck-boost DC-DC converter has two dc voltages levels: high and low. It consists of two switches, one inductor and one capacitor. While the circuit is in buck mode in the operation of S_1, the boost mode is applied in the operation of S_2. In this way, since it is a bidirectional circuit topology, it is widely used in various applications consisting of 2 separate voltage levels. The duty cycles of the switches determine the operating modes of S_1 and S_2. The duty cycles for buck and boost operating modes are expressed as follows.

$$Dbuck = \frac{VL}{VH} \tag{2.6}$$

$$Dboost = 1 - \frac{VL}{VH} \tag{2.7}$$

2.3.1.4. Interleaved Boost Converter

DC-DC converters are typically employed as power electronics interfaces in the photovoltaic generators and other renewable energy sources (Abdelkhalek et al., 2020). Although the use of boost converter is very common, it has many

disadvantages such as input current and output voltage fluctuations. These disadvantages are eliminated by using an interleaved boost converter by sharing the current among the elements (Mohammed and Devaraj, 2015a).

Interleaved boost converters consist of two or more boost converters in parallel combination. The interleaved boost converter topology is shown in as displayed Figure 2.13 with two switches (MOSFETs) and two inductors connected in parallel to split the input current among the inductors that improves the reliability and efficiency with smaller size of filter component and less ripple voltage and current over conventional boost converter (Nahar and Bashir Uddin, 2019; Alharbi et al., 2020).

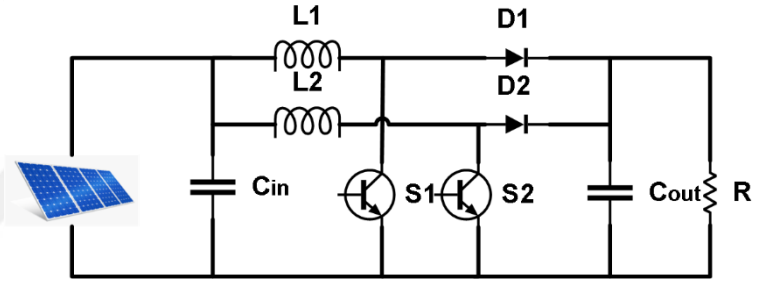

Figure 2.13. Interleaved Boost Converter Topology

The interleaved boost converter design equations are as follows.

$$D_{max} = \frac{V_{out} + V_d - V_{inmin}}{V_{out} + V_d - V_{on}} \tag{2.8}$$

$$D_{min} = \frac{V_{out} + V_d - V_{inmax}}{V_{out} + V_d - V_{on}} \tag{2.9}$$

$$L_{crit} = \frac{(V_{inmin} - V_{on})D_{max}(1 - D_{max})}{f_s I_{out}} \tag{2.10}$$

The interleaved boost converter topology is widely used in PV applications because of low current ripples while comparing with the conventional boost converters. The interleaved converters have the wider continuous current mode, the reduced output voltage ripple, the low switching losses and the high efficiency (Sefa and Özdemir, 2009) by reducing the conduction losses (I^2R) with sharing the current in two paths (Abdelkhalek et al., 2020).

2.3.2. MPPT Control Techniques

Dynamic performance of MPPT algorithms is important to ensure high-power output under practical operating conditions (Li et al., 2021). MPPT techniques are classified as; conventional, intelligent, optimization and hybrid tracking methods as seen in Figure 2.14 (Bollipo et al., 2021).

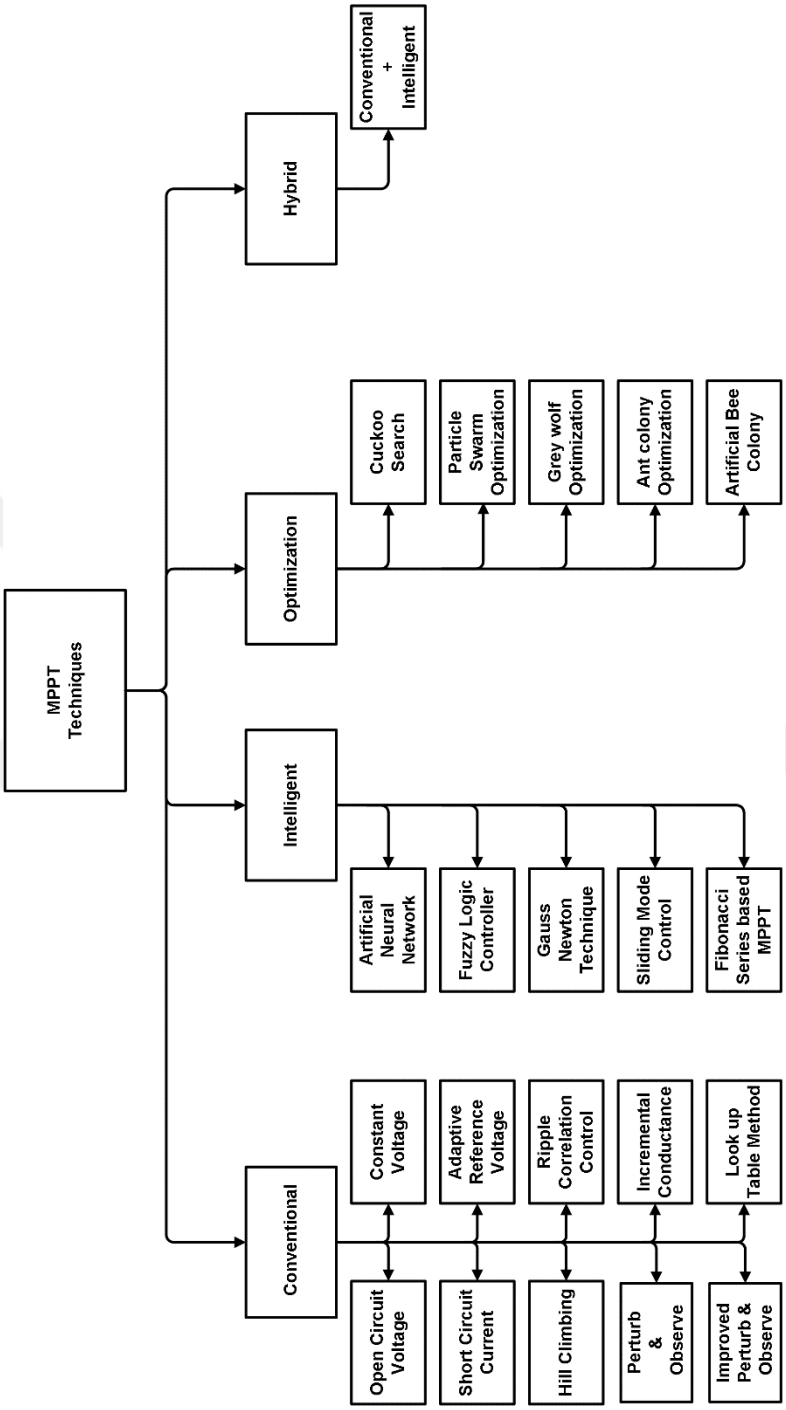

Figure 2.14. MPPT techniques

Conventional MPPT methods contain short circuit current (SCC), open circuit voltage (OCV), ripple correlation control, constant voltage, hill climbing, P&O, INC, and adaptive reference voltages methods. these methods are mostly used for uniform weather conditions as the PV generates only one global maximum power point (GMPP). conventional MPPT methods are implemented easily but have oscillations around MPP that cause the system to lose power.

Intelligent MPPT methods contain ANN, fuzzy logic controller, gauss newton technique, sliding mode control and Fibonacci series based MPPT methods. These techniques have faster response to track MPP. ANN technique responds more quickly to changing weather conditions, but big data processing is needed to perform the training task. Fuzzy logic controller can solve the limitations of traditional MPPT techniques, which include high settling time and steady state error (SSE), but it has difficulties in creating fuzzy rules. The gauss-newton method is the fastest one among the mathematical computational MPPT techniques. It is mainly used to solve nonlinear problems associated with the least squares approximation (Bollipo et al., 2020). Tracking of MPP causes increased computation time and big data storage problem, this problem is solved by Fibonacci-based tracking algorithm by limiting the search and moving to look the range for optimal operating point (Bollipo et al., 2021). The artificial intelligence based MPPT algorithms are reviewed by (Yap et al., 2020) and merits and demerits of all ANN methods are shown in tables and recent studies are also shown. A comparative performance analysis of ANN-based MPPT methods with different training algorithms for PV systems is performed by (Roy and Amin, 2021).

Optimization MPPT methods contain particle swarm optimization (PSO), artificial bee colony, cuckoo search (CS), grey wolf optimization (GWO) and ant colony optimization (ACO). Particle swarm optimization is a stochastic optimal algorithm inspired by the living mechanisms and social behavior of flocks of birds and fish for finding food and traveling together (S. U. Khan et al., 2015). The PSO has some advantages such as robustness, flexibility, and rapidity, during the tracking

process, but it is easy for the MPP to fall into the local optimum that resulting in inability to reach the global peak (Ibrahim et al., 2020). Cuckoo search (CS) is a meta-heuristic optimization algorithm stimulated from observing the life style of Cuckoo birds in their survival strategy along with the behavior of Lévy flight (Alrashidi et al., 2019). Grey wolf optimization imitates the hunting mechanism of gray wolves. In descending order of leadership, gray wolves are called alpha, beta, delta, and omega. Hunting consists of mathematically applied prey search, siege and attack operations to perform optimization (Behera et al., 2019). Ant colony optimization (ACO) is another swarm optimization technique based on the phenomenon of ants searching for the shortest path to their colony (Besheer and Adly, 2012). Nowadays, ACO is often applied in conjunction with different MPPT techniques to determine GMPP in often varying weather conditions, with only a pair of voltage and current sensors capable of continuously monitoring the changes in real time (A. Ali et al., 2020). Artificial bee colonies (ABC) emerge from the foraging process of honeybees. Honeybees living in colonies search for food by dividing into groups. Honey bees are generally divided into three types; worker, lookout and scout (Gonzalez-Castano et al., 2021) likewise, the best MPP is sought by assigning an individual tracking procedure.

Hybrid MPPT methods are created by mixing two different tracking methods to increase the system efficiency. In the literature there are various combination of MPPT techniques. Some of the hybrid studies in the literature are as follows: An experimental estimation of hybrid ANFIS-PSO-based MPPT for PV grid integration under fluctuating sun irradiance is performed by (Priyadarshi et al., 2020). In (Figueiredo and Aquino, 2021) hybrid MPPT technique PSO-P&O is applied to photovoltaic systems under uniform and partial shading conditions. An efficient fuzzy-logic based variable-step INC MPPT method for grid-connected PV systems is performed by (M. N. Ali et al., 2021). A hybrid MPPT method based on iterative learning control and P&O method is performed by (Zhang et al., 2021) to eliminate

the steady-state oscillations, and errors, when the operation point is close to the MPP or a small irradiance variation occurs.

2.3.2.1. Incremental Conductance

INC MPPT algorithm is one of the most used algorithms due to its ease of implementation. The INC is tried to track the MPP by considering the P-V characteristic of the PV module. The Inc. strategy depends on the way that the derivative of the output power P with respect to the panel voltage V is equivalent to zero at the MPP (Bollipo et al., 2021). The change in voltage, current and power determines the perturbation direction as in the tracking principle in Figure 2.15.

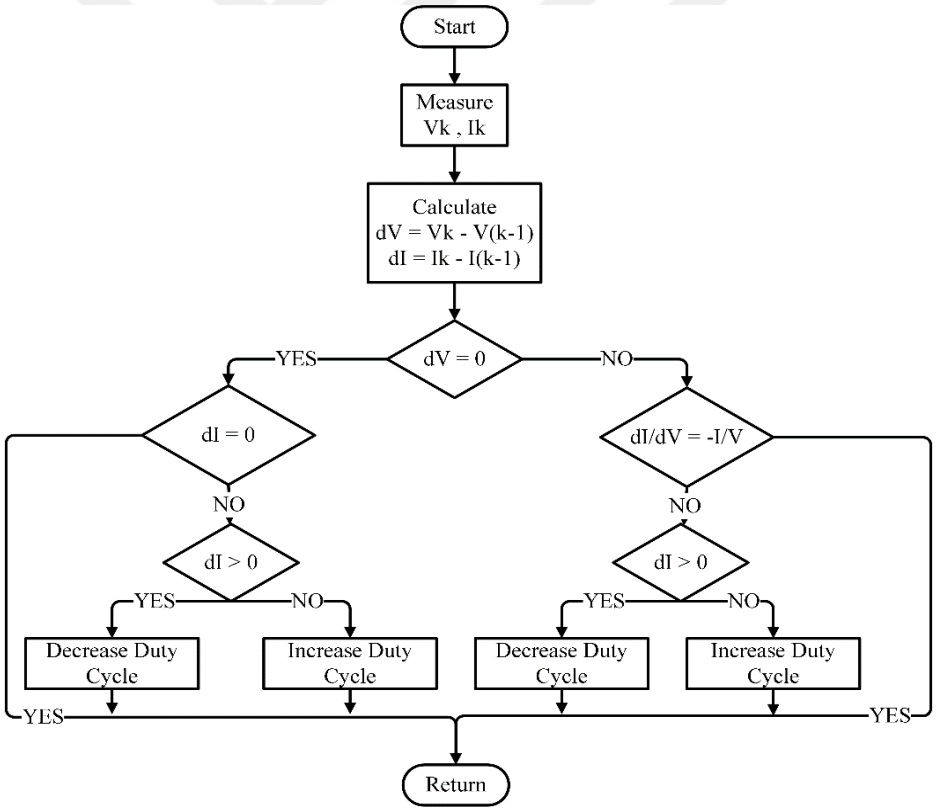

Figure 2.15. The flowchart of INC method

This technique is fundamentally based on the fact that the derivative of the PV panel output with its voltage as given in equations below (Safari and Mekhilef, 2011).

$$\frac{dP}{dV} = 0 \tag{2.11}$$

$$\frac{d(IV)}{dV} = I + V\frac{dI}{dV} \cong I + V\frac{\Delta I}{\Delta V} \tag{2.12}$$

The equation can be described as follows.

$$\frac{\Delta I}{\Delta V} = -\frac{I}{V} \text{ at MPP} \tag{2.13}$$

$$\frac{\Delta I}{\Delta V} > -\frac{I}{V} \text{ , left of MPP} \tag{2.14}$$

$$\frac{\Delta I}{\Delta V} < -\frac{I}{V} \text{ , right of MPP} \tag{2.15}$$

The algorithm continuously tracks the PV output and adjust the duty cycle of the converter by increasing and decreasing the perturbation based on equations adjusts the duty cycle (D) of the converter to achieve MPP (Mohammed and Devaraj, 2015b). The INC method has many advantages such as tracking speed, tracking accuracy and efficiency. Despite these advantages, INC algorithm has two major disadvantages; the continuous oscillations even after reaching the steady state, and the incapability to effectively track sudden changes in operating conditions (Bhattacharyya et al., 2021).

2.3.2.2. Perturb & Observe

P&O method is one of the simplest and commonly used online MPPT technique. Fundamentally, this strategy checks for the change in PV cell power (dP),

then checks for the sign of PV cell voltage (dV). The flow chart of the conventional P&O approach is presented in Figure 2.16. In the process, the reference voltage is perturbed, and the system response is observed. This determines the direction of the next perturbation (Zongo, 2021).

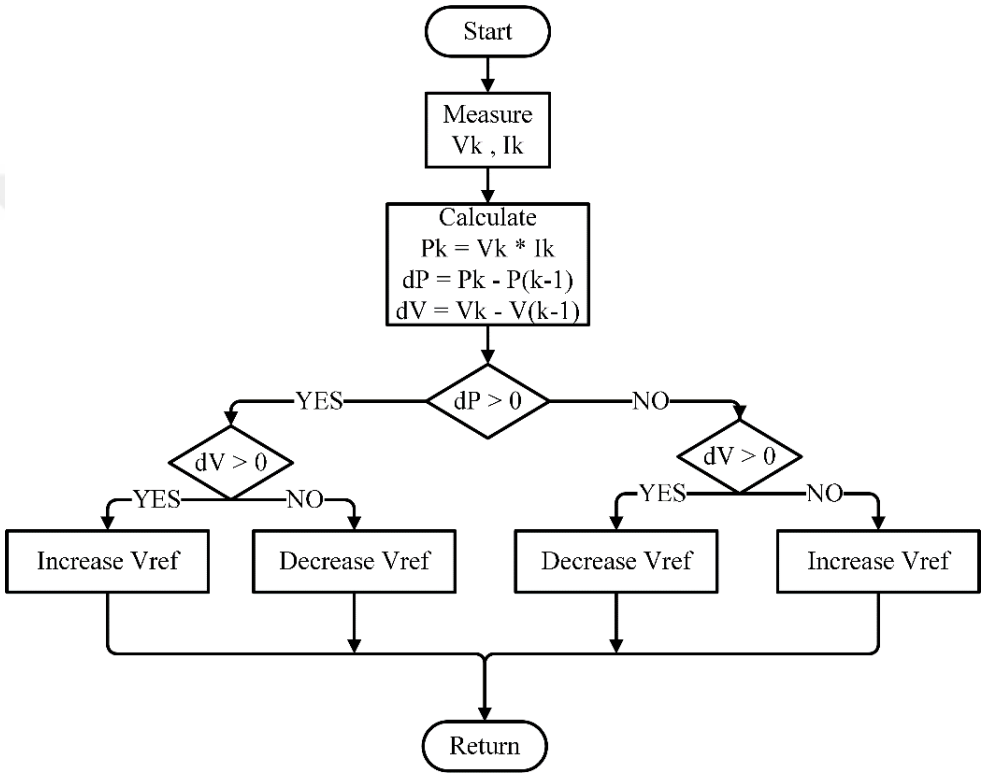

Figure 2.16. The flowchart of P&O method

The position of MPP of P&O method determine the position of the operation point relative to the MPP based on the non-linear characteristics of the solar array, moving it back and forth to achieve the MPP by injecting a perturbation in the PV voltage/current/duty ratio (Sher et al., 2015). The position of MPP is defined by use of below equations.

$$\frac{dP}{dV} = 0 \quad \text{at MPP} \tag{2.16}$$

$$\frac{dP}{dV} > 0 \quad \text{, left of MPP} \tag{2.17}$$

$$\frac{dP}{dV} < 0 \quad \text{, right of MPP} \tag{2.18}$$

The P&O MPPT technique has some disadvantages that significantly affect the output power of the PV system. One of them is the perturbation size, which limits the rate of convergence and determines the amplitude of oscillations around V_{mpp}. The other drawback is that this method causes power loss at the time of a perturbation and it fails to track the MPP at diverse irradiation and temperature conditions (Basha and Rani, 2020).

2.3.2.3. ANN-Based MPPT Methods

ANNs are computational models inspired by the human brain (Guerra et al., 2021). It is generally used for complex and nonlinear problems by regulating weights and biases (Ibnelouad et al., 2021). ANN can be defined as a parallel distributed information processing structure consisting of inputs and at least one hidden layer and one output layer. These layers have processing elements called interconnected neurons (Talbi et al., 2021).

LSTM networks are a type of iterative neural network that can handle difficult nonlinear approximation tasks of time series (Alnejaili et al., 2021). The LSTM network structure consists of forget gate, input gate, and output gate as shown in Figure 2.17. These gates can be opened or closed to add results to the calculation of the current layer, depending on whether the output in that layer reaches the threshold. In LSTM, inputs can learn mapping for temporal dependency relation (Sun et al., 2018a).

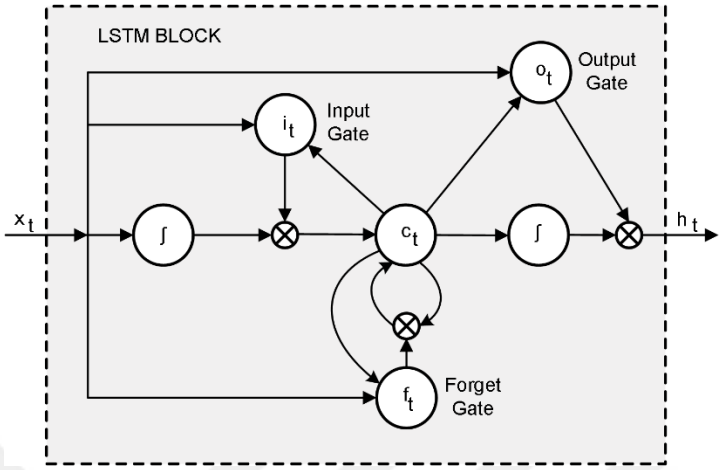

Figure 2.17 The basic LSTM structure (Sun et al., 2018b)

The RNN is one time-series model that is similar to FFBPNN except that there is feedback from each hidden layer's neurons to input layer (Shafique and Tjernberg, 2021). Unlike traditional neural networks, in RNN, inputs are dependent on each other (Garud et al., 2021). The learning mechanism used to calculate new states recursively by applying activation functions over the inputs and previous states of the network is called RNNs (Teke, 2022). The structure of RNN is shown in Figure 2.18.

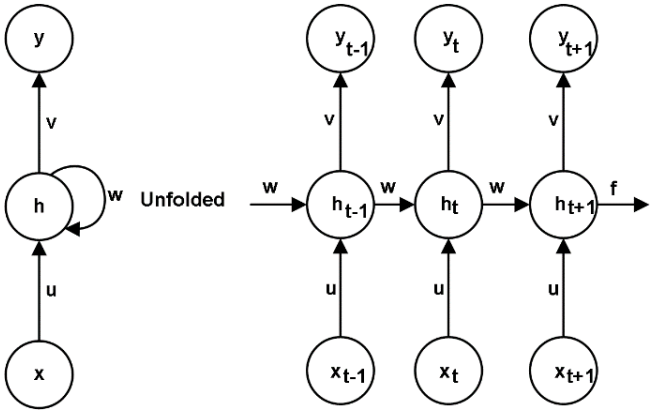

Figure 2.18. The basic RNN structure

The FFBPNN is a supervised learning method that used to obtain the relationship between input and output variables by adjusting the weights and biases for minimizing the error value. The basic structure of FFBPNN model is illustrated in Figure 2.19. The FFBPNN consists of an input layer, an output layer and at least one hidden layer.

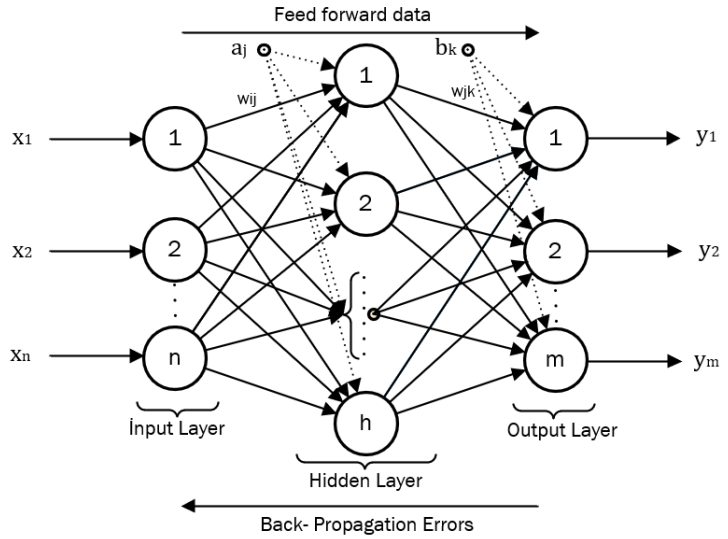

Figure 2.19. The FFBPNN structure (Teke, 2022)

For PV applications, FFBPNN is used to train and test the nonlinear relationship between I-V and P-V. From input current, input voltage, irradiance, temperature to metrological data, ANN takes these inputs and constantly learns to match the behavior of the solar system for maximum power (Basha and Rani, 2020). The output of the model can be reference voltage or duty cycle for PWM which smoothens the switching operation of IGBT (Roy and Amin, 2021). The accuracy of the created model depends on many features such as the learning algorithm used, the number of layers, the size of the data, the activation function used, the ratio between training data and testing data etc.

The ANN method reduces the steady-state oscillations at the MPP during dynamic irradiation conditions (Basha and Rani, 2020). ANN-based MPPT is proven to exhibit the capability of tracking MPP with the minimum transient time and low ripple under the real operation climatic condition. However, an accurate, standardized and appropriate training dataset is the main limitation for optimal performance of ANN without high training error (Yap et al., 2020).

2.4. DC–AC Switch Mode Inverter

The DC-AC inverters are known as power electronic converters that enable the transfer of DC power to AC power. They are classified as current source inverters (CSIs) that control AC output in current waveform and voltage source inverters (VSIs) that control AC output in voltage form. In (Zeb et al., 2018), dissimilarity between VSI and CSI are given as a table. VSIs are favorable for PV applications due to cost, efficiency, and size over CSIs (M. N. H. Khan et al., 2020). The main purpose of these topologies is to design a three-phase voltage source that controls the amplitude, phase, and frequency of the voltages. In (Tahir et al., 2018) , a comprehensive review for VSIs topologies and their controlling techniques are given.

Single-phase VSI with half-bridge and full-bridge topologies are used for the low power range. Three-phase VSIs are used in medium to high power applications. The full bridge VSI topology is shown in Figure 2.20.

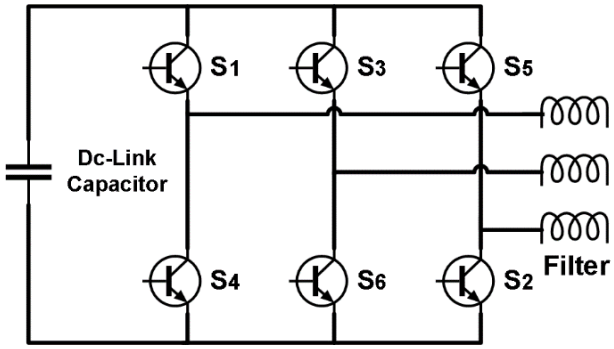

Figure 2.20. Three phases full bridge VSI

To obtain the three-phase AC current in three phases VSI, six gating signals need to be sent to the switches of the inverter. S1, S3, S5 are 3 phase symmetrical switching functions with phase shift 120° (Permatasari, 2015). Both switches in the same leg cannot be turned ON at the same time, as it would short the input voltage violating the Kirchhoff's Voltage Law. The switching states of the three-phase inverter is shown in Table 2.1.

Table 2.1. The switching states of three phase full bridge VSI

State	S1	S2	S3	S4	S5	S6	Vab	Vbc	Vca
1	on	on	off	off	off	on	Vdc	0	Vdc
2	on	on	on	off	off	off	0	Vdc	Vdc
3	off	on	on	on	off	off	Vdc	Vdc	0
4	off	off	on	on	on	off	Vdc	0	Vdc
5	off	off	off	on	on	on	0	Vdc	Vdc
6	on	off	off	off	on	on	Vdc	Vdc	0
7	on	off	on	offf	on	off	0	0	0
8	off	on	off	on	off	on	0	0	0

In this thesis, a full-bridge two-level VSI is designed, which is suitable for the system power rating range. It is aimed to obtain pure sinusoidal current, low harmonic distortion and unity power factor by applying it with an efficient controller.

2.4.1. Synchronous Reference Frame – Phase Locked Loop

The DC-AC controllers regulate the required gate signals for three phase inverters to work. The structure and control system of the inverter should take advantage of capabilities such as harmonic detection, power control and power factor correction. Also, the grid voltage phase is added to the control system implemented by the phase locked loop. As a result, the PLL is used to synchronize the base reference current and the grid (Athari et al., 2017).

The active and reactive power control (PQ) is applied in PLL based on the d-q reference frame. The primary purpose of using PQ control is to maintain constant active power and reactive power at source terminals when the frequency and terminal voltage fluctuates within the recommended limits (Ansari et al., 2021). The power control of inverter is achieved by implementing the power controller, voltage controller and current controller, respectively. The scheme of these processes is given in Figure 2.21 (Pogaku et al., 2007).

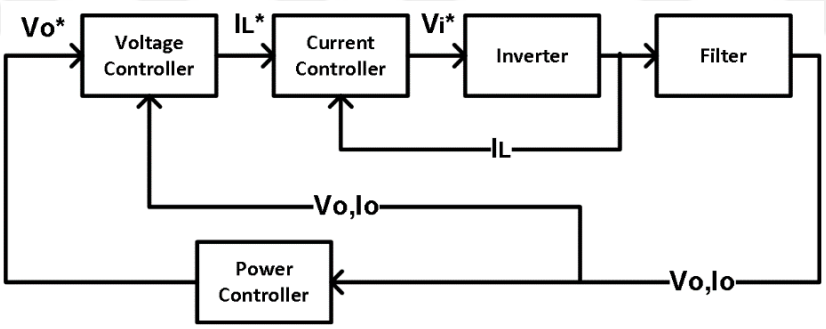

Figure 2.21. The scheme of inverter controller

The Figure 2.22 shows the block diagram of the voltage controller. The reference voltage for voltage controller is obtained from the output of the power controller as seen in Figure 2.21. The obtained reference voltage is controlled by implementing the PI controller after the necessary feedforward and feedback processes as seen in Figure 2.22, and the reference of the current controller is seen at the output.

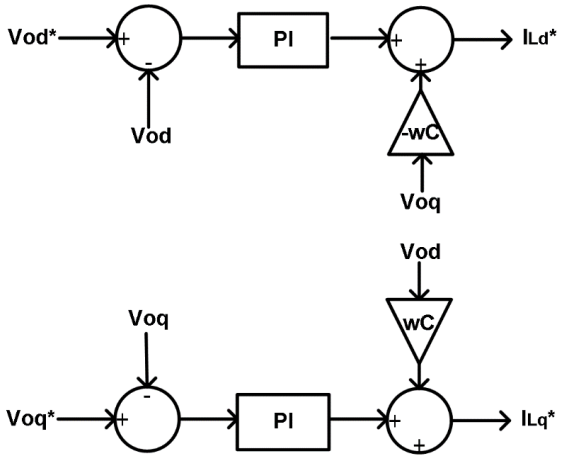

Figure 2.22. The voltage controller

The same process is achieved for current controller as shown in The Figure 2.23. The reference voltage for current controller is obtained from the output of the voltage controller as seen in Figure 2.22. The obtained reference current is controlled by implementing the PI controller after the necessary feedforward and feedback processes as seen in Figure 2.23, and the voltage reference for d-q components of - are obtained at the output.

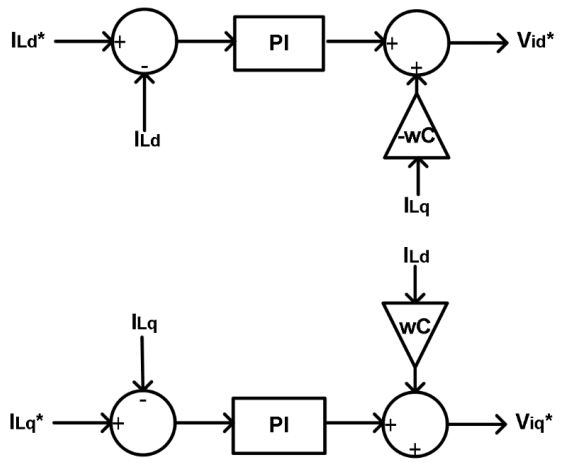

Figure 2.23. The current controller

2.5. LCL Filter

The use of power converters is crucial in maximizing the power transfer from renewable energy sources such as wind, solar, or even a hydrogen-based fuel cell to the utility grid (Reznik et al., 2014). Switching frequency harmonics by inverters leads to a new dimension of research problems and solutions. A suitable filter is required to connect inverters to grid (Poongothai and Vasudevan, 2019). The generation of harmonics around the switching frequency can be filtered out by the large inductance connected to the output of the converter. However, large inductance reduces the dynamics of the system and the operating range of the converter. The inverter can be equipped with an LCL filter instead of inductance (Bauer, 2010). The LCL filter model is shown in Figure 2.24. The following equations are used to obtain the correct LCL filter parameters (ÇELİK, 2019).

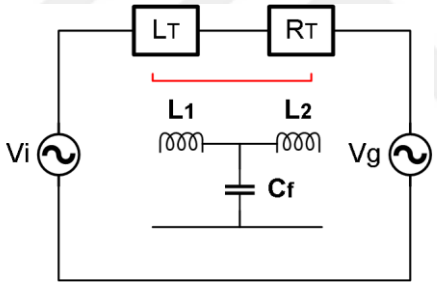

Figure 2.24. The LCL filter

To extracting the transfer function, the current flowing through the filter is given as in equation.

$$i_{Li} - i_c - i_{Lg} = 0 \tag{2.19}$$

The voltages in ‘s’ domain are given as

$$V_i = i_{Li} L_i s + V_c \tag{2.20}$$

$$V_g = -i_{Lg} L_g s + V_c \tag{2.21}$$

$$V_c = i_c \left(\frac{1}{C_f s} + R_d \right) \tag{2.22}$$

$$i_{Li} = \frac{1}{L_i s}(V_i - V_c), i_{Lg} = \frac{1}{L_g s}(V_c - V_g) \tag{2.23}$$

$$V_i = \left(L_i s + \frac{1}{C_f s} + R_d \right) i_{Li} - (\frac{1}{C_f s} + R_d) i_{Lg} \tag{2.24}$$

$$V_g = \left(\frac{1}{C_f s} + R_d \right) i_{Li} - (L_g s + \frac{1}{C_f s} + R_d) i_{Lg} \tag{2.25}$$

2.6. Harmonic Mitigation

With the increasing number of renewable distributed generation (DG) units connected to utility power grids, the deterioration of power quality at the PCC point is becoming a major concern (Liang and Andalib-Bin-karim, 2017). In power quality, harmonics are an important concern in all the utility sectors (Alexander, 2016). As one of the clean energy sources, PV can provide abundant and free energy from the sun, its use has increased in recent years. However, compared to other renewable technologies, the PV system still has disadvantages such as high cost and low efficiency. In addition, fluctuating energy from the sun creates harmonics in the generated power that can lead to undesirable system performance. THD is the ratio of the distorted power to the main power of the signal and is most commonly used to indicate the amount of signal degradation (Alhafadhi and Teh, 2020). Also it is the measure that quantifies “how close the waveform is to pure sine” for both current and voltage (Alexander, 2016). In other words, THD value is essential for system continuity and efficiency. The formulas given in equations in (2.26) and (2.27) are used to calculate voltage and current THD’s.

$$V_{THD\_F} = \frac{100 * \sqrt{\sum_{h=2}^{N} V_{h,rms}^2}}{V_{1,rms}} \tag{2.26}$$

$$I_{THD\_F} = \frac{100 * \sqrt{\sum_{h=2}^{N} I_{h,rms}^2}}{I_{1,rms}} \tag{2.27}$$

Various studies have been conducted in the literature showing the harmonic mitigation in PV systems. In (Alexander and Manigandan, 2014), the intelligent techniques such as Genetic Algorithm, ANN and particle swarm optimization methods are used for PWM generation of fifteen level multilevel inverter in solar system to reduce the harmonics. In (Reveles-Miranda et al., 2020), a passivity-based control scheme is conducted to control a grid-connected PV inverter under the presence of nonlinear loads and reactive power with continuous operation for THD mitigation and power factor correction. In (Gowtham et al., 2022), various MPPT controlling methods such as P&O, optimized P&O, gravitational search algorithm are used to generate inter harmonic emissions for improving source voltage and current. The output power is also improved by reducing the THD value with optimized P&O MPPT controlling method. In (Sorte et al., 2021), the comparison between PSO and current reference control based MPPT are examined with an adaptive power management algorithm for a grid connected PV-Battery system according to MPP tracking efficiency, dc voltage settling time and THD. In (Tofigh et al., 2021), harmonic reduction for a grid tied PV system is conducted based on fast Fourier Transform. In (Liang and Andalib-Bin-karim, 2017), diverse controlling methods such as current control method, voltage control method, hybrid control method, active filtering methods are reviewed to reduce harmonics in grid connected renewable energy sources.

2.7. Energy Storage and Energy Management System Control Strategies for On Grid Applications

As the need for energy increases day by day, it has become an inevitable end that renewable energy sources will be used in all areas of life, such as homes, workplaces, factories, schools. In this way, hybrid energy systems have been included in our lives in order to use the obtained energies more efficiently and to compensate for the fluctuating and unpredictable features of PV power generation (Liu et al., 2019). The most common of these are PV included battery systems. Each hybrid systems are created differs in energy management; this mostly depends on the operating purpose of the system. The purpose of the hybrid system can be to feed a critical load, to support the grid mode, or just to meet its own energy at any time of the day or etc. That is, the working scenario of each system is created to be different and unique. But they all have some striking common points; to obtain maximum power with MPPT, to ensure that the DC-link voltage is stable, to create the necessary conditions for the grid integration and to ensure that the produced and stored energy is used in the most efficient way.

In the literature there are diverse studies on energy management of PV battery hybrid systems. In (Khezri et al., 2022), the optimal planning PV and battery hybrid system for on grid residential sector is reviewed with the care of technical data, energy management, electricity pricing, design parameters based on rooftop availability, country policies, import/export power, power balance features of the system. In (Qays et al., 2020) an intelligent controlling method based on SOC estimation with use of back propagation neural network algorithm is developed for battery management system to control charging, discharging and islanding processes to increase battery lifetime. In (Hong et al., 2019), energy management is conducted with an integrated three-port power converter that shares the power switches both for DC-DC full bridge converter and bidirectional converter to balance the power switches for MPPT and charging/discharging processes. In (Malar et al., 2020), a power management algorithm based on the PSO-firefly algorithm tuned PI is

proposed to enhance DC-link voltage and dynamic, steady-state responses of hybrid system that consists of wind turbine, PV cell, BES and load. In (Wu et al., 2015), a demand side management is conducted with the care of battery size, PV power output and minimizing the electricity cost based on a developed open loop optimal controlling method for 24h and a closed loop model predictive control for uncertain disturbances. In (Di Piazza et al., 2019), the hybrid PV-BES integration to grid is enhanced by reducing the peak-to-mean ratio with an energy management algorithm. In (Rates, 2021), new practical rule-based energy management for an Australian house with PV-BES grid integrated system is examined based on 4 different options for a sunny week in summer and a cloudy week in winter by use of real data. In (Yonis Buswig et al., 2020), a battery management system is designed based on SOC estimation for controlling a PV-BES system and the real data used for SOC estimation by use of BPNN algorithm with an 0.082% error rate. In (Khezri et al., 2022), a comprehensive review on designing, energy controlling, pricing programs and the-state-of-the-art methods for a grid connected PV-BES system is conducted.

2.8. The Performance Evaluation Metrics

Performance evaluation metrics are used to calculate the accuracy of unobservable results by performing a statistical accuracy assessment. The G_t is the actual daily total solar irradiation value while the G'_t is the predicted daily total solar irradiation value. The equations of the performance metrics are as follow. (Nespoli et al., 2019)

$$NRMSE\ (\%) = \frac{\sqrt{\frac{\sum_{t=1}^{N} |G_t - G'_t|}{N}}}{\frac{1}{N}\sum_{t=1}^{N} G_t} . 100 \tag{2.28}$$

$$WMAE\ (\%) = \frac{\frac{1}{N}\sum_{t=1}^{N}|G_t - G'_t|}{\sum_{t=1}^{N} G_t}\ .100 \tag{2.29}$$

$$NMAE\ (\%)\ = \frac{1}{NC}\sum_{t=1}^{N}|G_t - G'_t|.100 \tag{2.30}$$

$$MAPE\ (\%) = \frac{1}{N}\sum_{t=1}^{N}\left|\frac{G_t - G'_t}{G_t}\right|.100 \tag{2.31}$$

2.9. Summary

In this section the literature review of the main topics of thesis are given with an extended literature review. Previous studies on the MPPT techniques, the converter topologies, the BESs, energy management methods, harmonic reduction are mentioned.

3. DESIGN AND OPERATION OF PROPOSED SYSTEM

In this study, it is aimed to reduce the current harmonic by developing a FFBPNN-based MPPT method compared to the traditional-based MPPT methods P&O and INC, by targeting the optimal design for the grid-connected PV-BES system. The proposed system outline diagram is shown in the Figure 3.1. The system is simulated by use of MATLAB/Simulink.

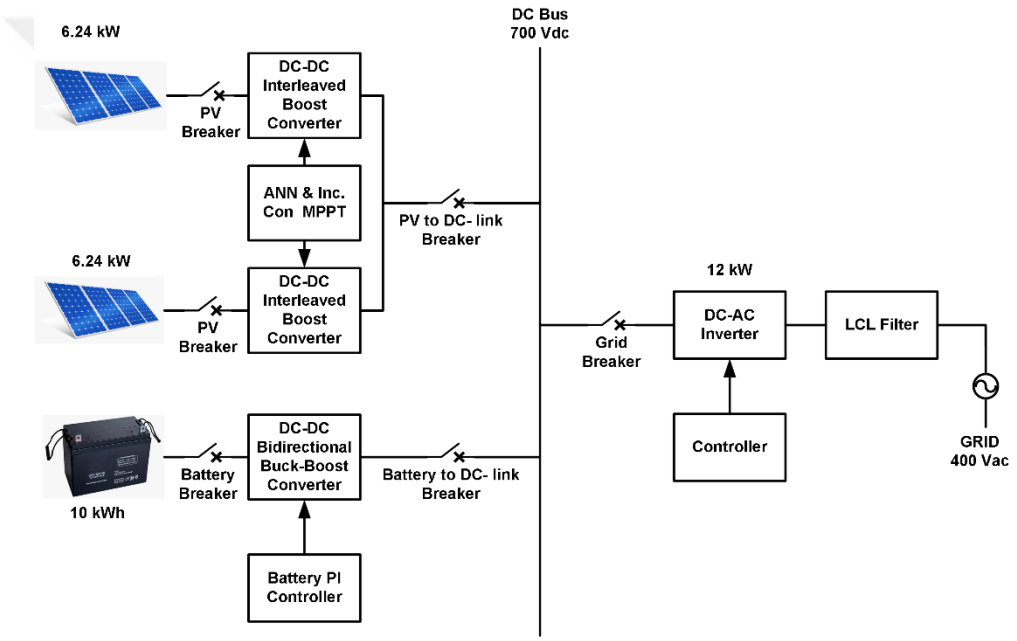

Figure 3.1. The proposed PV-BES on grid system

In this section, the design of the whole system is explained in 4 sections. Solar power design with DC-DC interleaved boost converter design, BES system design with DC-DC bidirectional buck-boost converter design, DC-AC inverter design controlled by PLL controller and finally the scenario that ensures that efficient and continuous operation of the whole system is designed.

3.1. Solar Power

In this section, the design of solar power, that forms our PV-BES grid-connected system, starting from temperature and radiation to the integrated part of power generation into the DC-link, is explained. PV array design, DC-DC interleaved boost converter design, conventional and proposed ANN-based MPPT design are explained, respectively, under the sub-titles that make up this section.

3.1.1. PV Array

The solar power in the system is positioned by dividing into two parts, assuming shading situations, in this way it is aimed to make the power produced more realistic considering the variable weather condition. The PV module specifications that make up the solar power system are mentioned in Table 3.1.

Table 3.1. The PV module specifications

Technical Properties of Utilized Solar Power System	
Solar power total capacity	12.48 kW
PV Array-1	6.24 kW
PV Array-2	6.24 kW
Technical Properties of Utilized Photovoltaic Module	
Nominal max. power (P_{max})	260 W
Opt. operating voltage (V_{mp})	30.7 V
Open circuit voltage (V_{oc})	37.8 V
Short circuit current (I_{sc})	8.99 A
Module efficiency	16.16%
Max. system voltage	1000 V (IEC) or 600 V (UL)
Application classification	Class A
Power tolerance	0 ~ + 5 W

The PV module I-V and P-V characteristics are shown as graphs in Figure 3.2 for 1000 W/m^2, 500 W/m^2 and 100 W/m^2 irradiances at 25 ˚C.

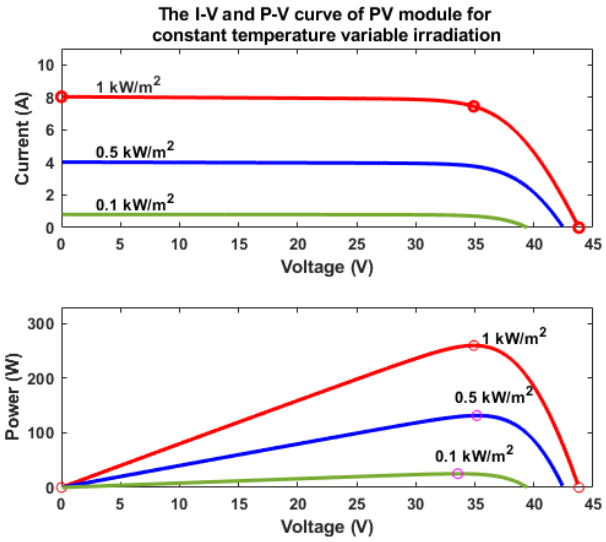

Figure 3.2. PV module I-V and P-V characteristic

Solar power system with a total power of 12.48 kW is considered at 2 separate points and the power is divided into two. Thus, by creating 2 separate arrays specified in Table 3.1, the power of each array is determined as 6.24 kW. These PV arrays are obtained by connecting 2 strings in parallel, consisting of 12 serial connected modules per string of the PV module whose specifications are given in Table 3.1. The PV arrays I-V and P-V characteristic graphs are shown in Figure 3.3 for 1000 W/m^2, 500 W/m^2 and 100 W/m^2 irradiances at 25 ˚C.

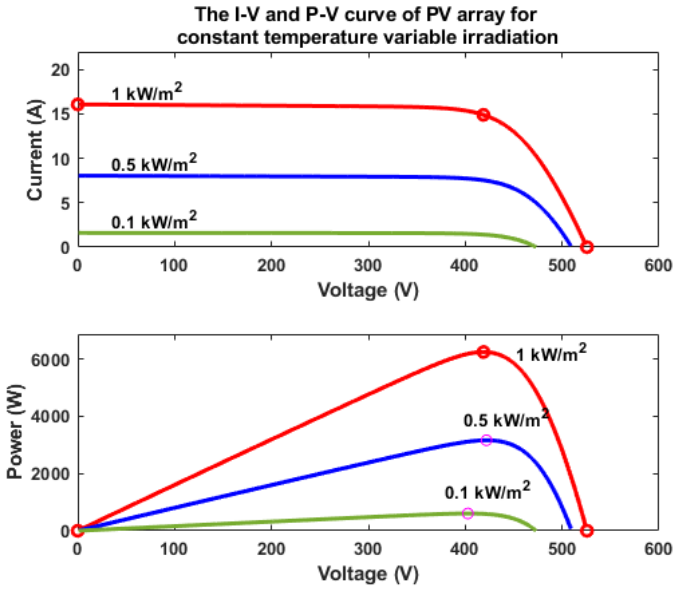

Figure 3.3. PV array I-V and P-V characteristic graphs

The PV arrays output voltage, current and power are shown in Table 3.2 for standard test conditions (STC) for 1000 W/m^2 at 25 ˚C.

Table 3.2. The specifications of PV arrays

Technical Properties of Utilized PV Arrays	
Number of series connected modules per strings	12
Number of parallel connected strings	2
Voltage at MPP under STC	418.8 V
Current at MPP under STC	14.9 A
Maximum output power under STC	6.24 kW

3.1.2. DC-DC Interleaved Boost Converter Design

A two-layer DC-DC interleaved boost converter is designed to operate the PV system at MPP. The interleaved boost converter is described in our previous sections 2.3.1. Two separate switches work with 180˚ phase shift with the control of MPPT controller and act as 2 separate boost converters. By dividing the current into

2 branches, the transmission losses (I^2R) are reduced, thus a more efficient operating system is obtained. The converter also reduces the ripples for voltage and current at the output. The interleaved boost converter consists of input and output capacitors, power switches and the inductors. Choosing the appropriate inductor and capacitor is quite important. This is because fluctuations in the input and output waveform affect the controller performance and thus the overall efficiency of the system. The limit values of fluctuations in input current and output voltage are defined as 10% and 1%, respectively. For the design, the equations in the interleaved boost converter section are used and the parameters in the Table 3.3 are obtained. The Figure 3.4 shows the simulink model of the interleaved boost converter.

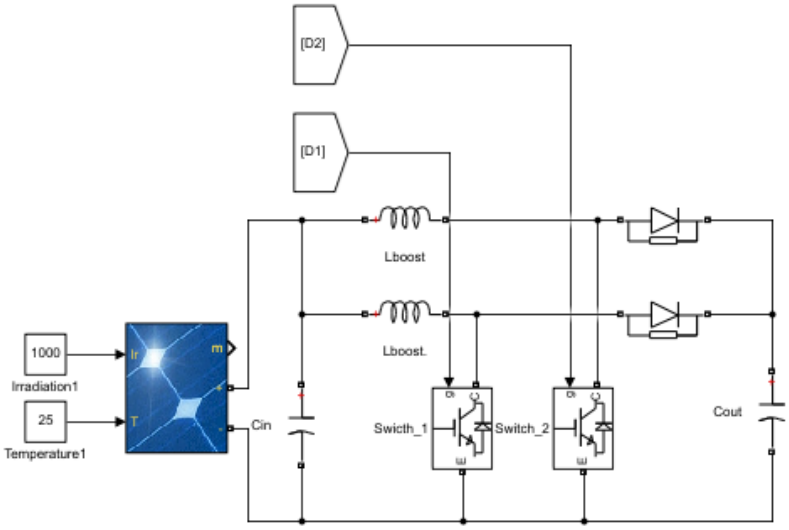

Figure 3.4. The DC-DC interleaved boost converter MATLAB/Simulink

Table 3.3. The DC-DC interleaved boost converter design parameters

Parameters of Interleaved Boost Converter for Each PV Array	
Rated Power	6.24 kW
Vin-min	250 V
Vin-max	418.8 V
Vout	700 V
$I_{in\text{-}max}$	12.48 A
$\Delta I_{in\text{-}max}$	1.24 A
Switching Frequency	20 kHz
Input Current Ripple	%10
Output Voltage Ripple	%1
L_{boost}	6.8 mH
C_{in}	0.1 mF
Duty Cycle (D)	0.41

The duty cycle is defined for power switches of interleaved boost converter by subtracting the output voltage of the MPPT controller from the panel output voltage and feeding this difference with the PI (Proportional-Integral) parameters. This signal is then compared with a reference signal in the range (0-1) and the power switches in the converter are fed by these signals for operating as shown in Figure 3.5.

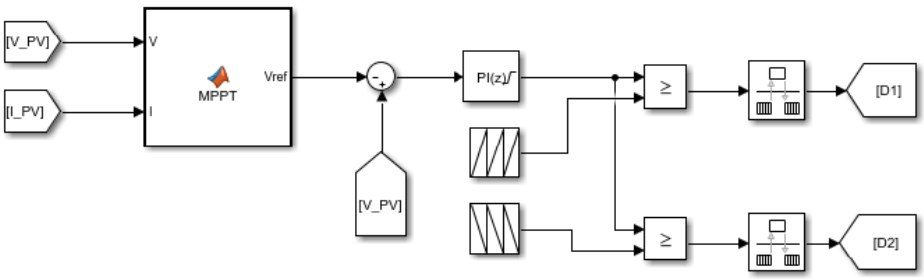

Figure 3.5. The duty signals of switches

3.1.3. ANN-Based MPPT Controller Design

The proposed MPPT controller is designed based on ANN. The purpose of designing an artificial intelligence-based controller is to provide an earlier response to variable weather conditions and to ensure continuous operation of the system and to eliminate the drawbacks of conventional MPPT techniques in terms tracking speed, tracking accuracy, oscillations, and overall system efficiency. However, this method is more complex, and its accuracy highly relies on PV panel characteristics. The power obtained from the PV modules is directly affected by the variable weather conditions and this negatively affects the operation of the whole system, the more we purify the system from fluctuations, the more stable the system becomes. The MATLAB neural network training tool is used for network creation.

Data collection is the first and most important step in creating an ANN-based forecast. For this reason, firstly, a voltage variation table is created at the output against the temperature and radiation changes determined as input for the PV module. The obtained data is divided into 80% training data and 20% testing data. Different combinations of the single hidden layer between the input and output layers have been tried more than a hundred times. The network was created as in Figure 3.6.

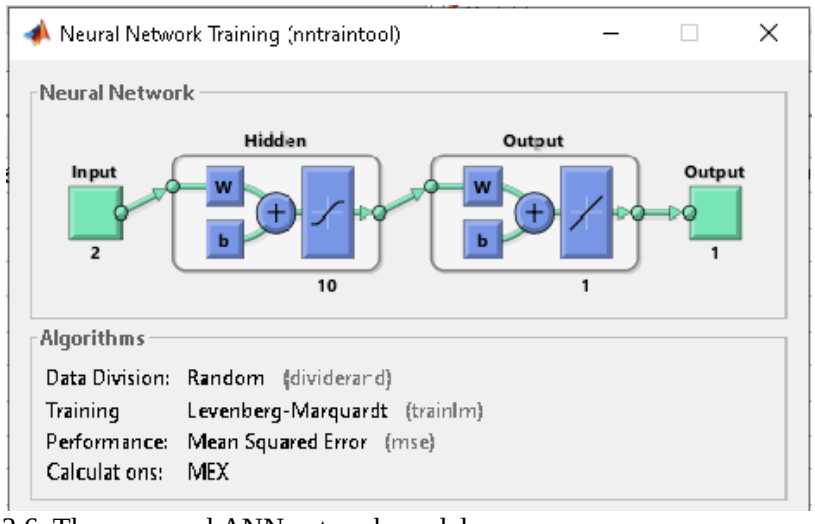

Figure 3.6. The proposed ANN network model

As the PV voltage is a nonlinear output of temperature and irradiation the FFBPNN type and Levenberg-Marquart training function is used to solve non-linear least squares problems based on nonlinear activation function tangent sigmoid transfer function. The regression graphic of the trained proposed network is shown in Figure 3.7.

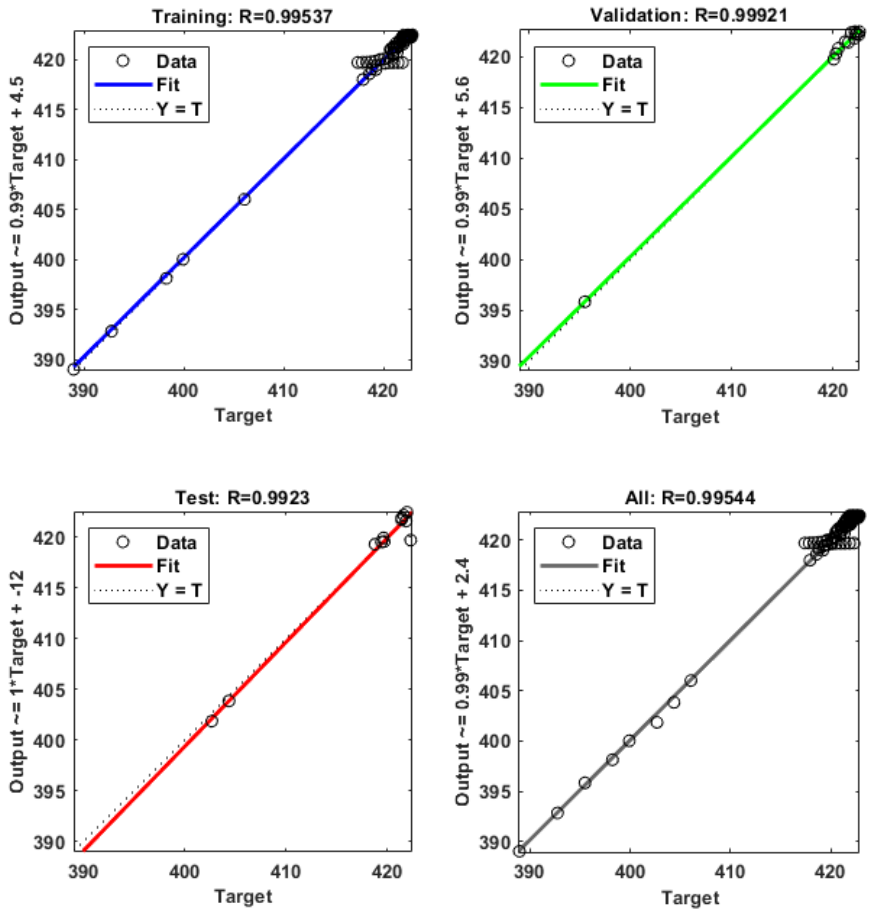

Figure 3.7. The regression graph of ANN-based network

The performance of proposed network is evaluated based on mean squared error (MSE) as in the Figure 3.8.

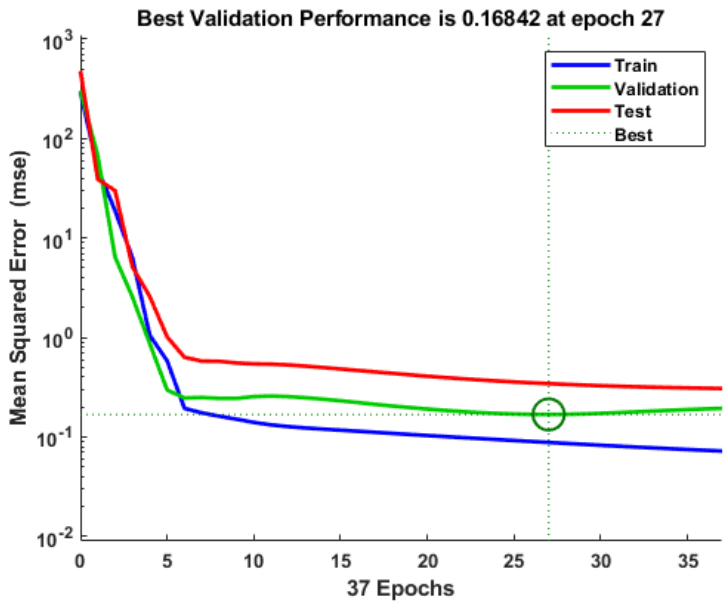

Figure 3.8. Performance of ANN-based network

3.2. Battery Energy Storage System

The BES system has started to be used in many areas together with solar energy. While this provides a more ecological energy cycle for the environment, it also provides a technological solution for rural areas. Although the first thing that comes to mind is to use this hybrid system in rural areas, today this system is used in homes, schools, factories etc.

In the BES system, respectively; the design of the battery, the design of the DC-DC bidirectional buck-boost converter, the design of the PI controller for the charge and discharge processes of the battery are very essential for the creation of the system.

For the battery design the lithium-ion battery is chosen in battery block of MATLAB/Simulink with 420 nominal voltage and 24 Ah (ampere-hour) rated

capacity. The battery power capacity is specified as 10 kW. The lower and upper limits of SOC are determined as 50% and 90%, respectively. That is, a battery that discharge up to 50% and charge up to 90% has been designed. The battery block parameters configuration in Simulink is shown in Figure 3.9.

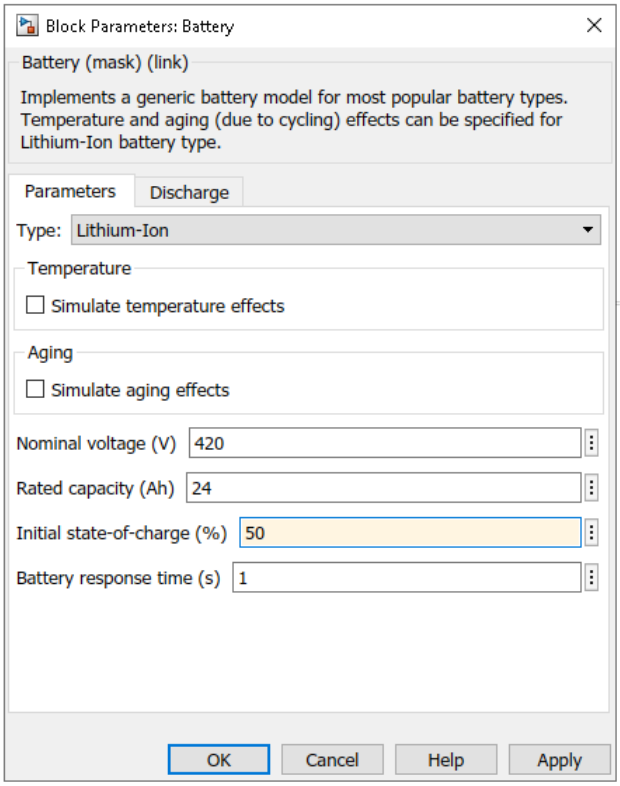

Figure 3.9. Battery block parameters

The battery is connected to DC-link with a bidirectional buck-boost converter to decrease and increase voltage levels as specified during the charging and discharging processes. The Simulink model of DC-DC bidirectional buck-boost converter is conducted as shown in the Figure 3.10. The DC-link voltage is specified with 700 V as the high voltage side of the bidirectional buck-boost converter. The battery voltage is specified with 455 V as the low voltage side of the converter.

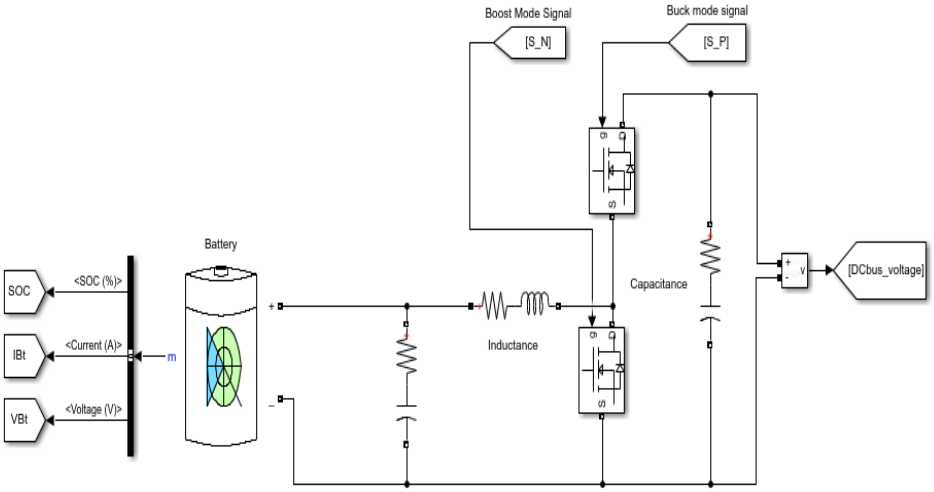

Figure 3.10. The DC-DC bidirectional buck-boost converter model in MATLAB/Simulink

The design features of the circuit elements used in the bidirectional buck-boost converter are also given in the Table 3.4.

Table 3.4. DC-DC bidirectional buck-boost converter parameters

Parameters of DC-DC Bidirectional Buck-Boost Converter	
Rated Power Capacity	10 kW
V_L - Battery voltage	455 V
V_H – DC-link voltage	700 V
Switching Frequency	20 kHz
Input Current Ripple	%10
Output Voltage Ripple	%1
$L_{crit\text{-}buck}$	3.62 mH
$L_{crit\text{-}boost}$	3.61 mH
$C_{crit\text{-}buck}$	3 µF
$C_{crit\text{-}boost}$	36 µF
L_{chosen}	3.7 mH
C_{chosen}	40 µF
D_{buck}	0.64
D_{boost}	0.36

The most important point after the circuit design is the correct feeding of the operating signals of the switches. The charging and discharging states of the battery are studied separately.

In the charging state, the difference between the voltage of the battery and the reference voltage is taken and this difference is controlled by the PI parameters and multiplied by (-1) to obtain the reference charging current (IB_ref) for battery at the output. Thus, both the battery voltage is controlled, and the reference charging current is determined depending on the battery voltage. This process for charging is shown in Figure 3.11. The reference voltage is specified as 455 V that is the voltage of the battery at 90% SOC and the maximum charging current is determined as 10.43 A with reference to the nominal discharge current of the battery in the battery block. After the reference charging current for the battery is determined, the difference between this value and the measured current of the battery is controlled by the PI

parameters. The PI output is then compared with a reference signal in the (0, 1) range to generate gate signals for charging processes. The charging process is end up when the SOC of the battery reaches 90%.

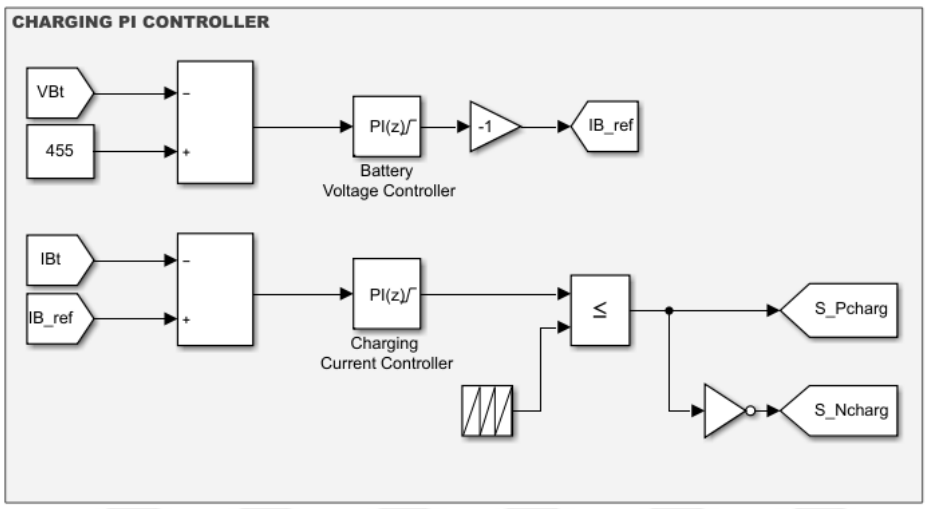

Figure 3.11. The charging process control of the battery

In the discharging process the difference between DC-link voltage and the reference voltage is feed by PI parameters to obtain the reference discharging current for the battery. In this way, both the DC-link voltage is controlled and the maximum discharging current (IB_ref) of the battery is determined as 10.43 A. This processes for discharging are shown in Figure 3.12. After the reference discharging current for the battery is determined, the difference between this value and the measured current of the battery is controlled by the PI parameters. The PI output is then compared with a reference signal in the (0, 1) range to generate gate signals for discharging processes. The discharging process is end up when the SOC of the battery reaches 50%.

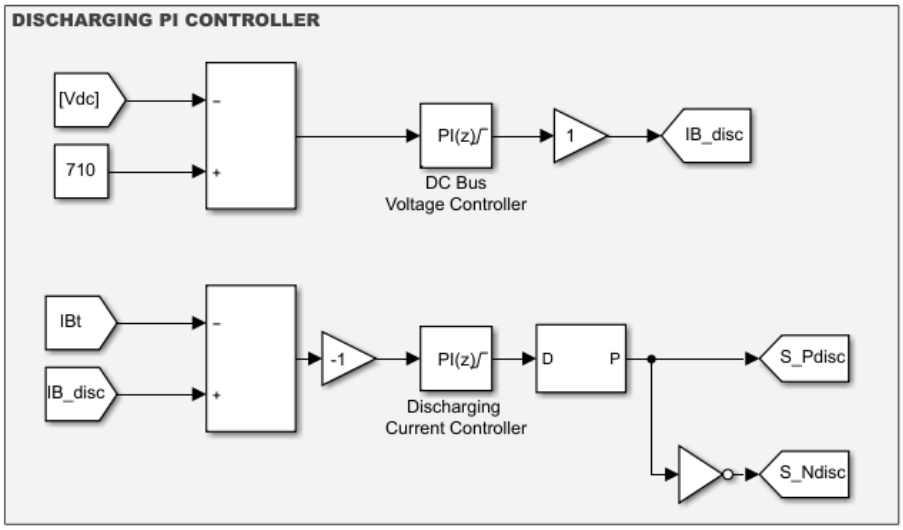

Figure 3.12. The discharging process control of the battery

3.3. Current Controller for DC-AC Inverter

The output current control of the power converter as magnitude and phase angle provides control of active and reactive power in the system. In this thesis the balance between active and reactive power is provided with PLL controller. The PLL block of MATLAB is used to transfer the output phase to ground voltage V_{abc} to phase angle (Ph) as seen in Figure 3.13.

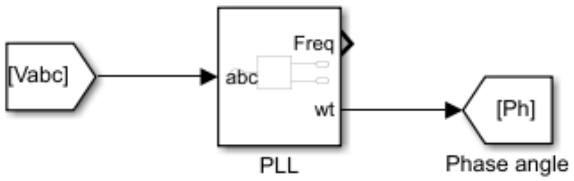

Figure 3.13. The PLL block

This obtained phase angle is used in the direct-quadrature-zero (d-q-0) transformation of V_{abc} that is the measured phase to ground voltage after the LCL

filter and I_{abc} that is the measured phase to ground current of the inverter before LCL filter as seen in Figure 3.14.

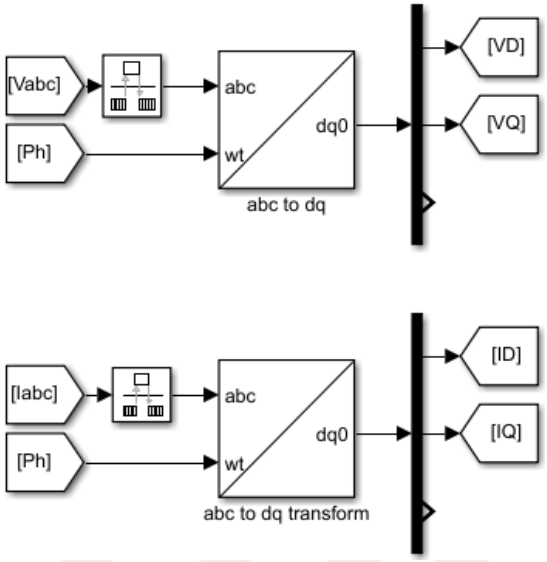

Figure 3.14. The d-q-0 transformation of the voltage and current

The ID, IQ, and VD, VQ components extracted from I_{abc} and V_{abc}, respectively, are used in a closed loop designed for active and reactive power control. For active power control, the voltage controller and the current controller are respectively involved in this loop. Voltage control is provided by subtracting the VD value from the determined reference voltage and passing the obtained value through the PI controller. The reference voltage is specified as 330 V. Voltage PI controller output is the default reference current value of 18 A. The value obtained by subtracting the ID value from the reference current is passed through the PI controller to provide current control. In this way, the ED component is obtained as a result of these processes shown in Figure 3.15.

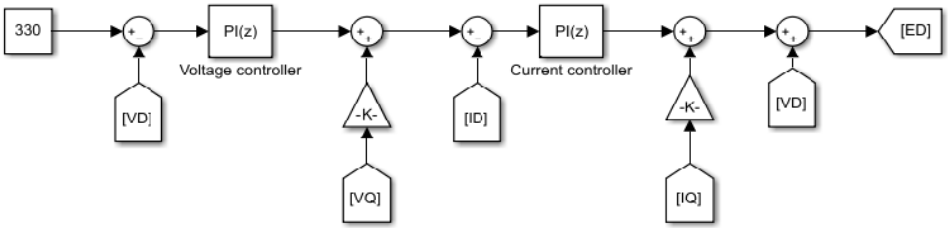

Figure 3.15. The active power controls

For reactive power control, the voltage controller and current controller are respectively involved in. Voltage control is achieved by subtracting the VQ value from the determined reference voltage and passing the obtained value through the PI controller. The reference voltage for reactive power control is assumed to be zero. Current control is provided by passing the value obtained by subtracting the IQ value from the result obtained after the voltage control is passed through the PI controller. EQ component is obtained as a result of these processes that shown in Figure 3.16.

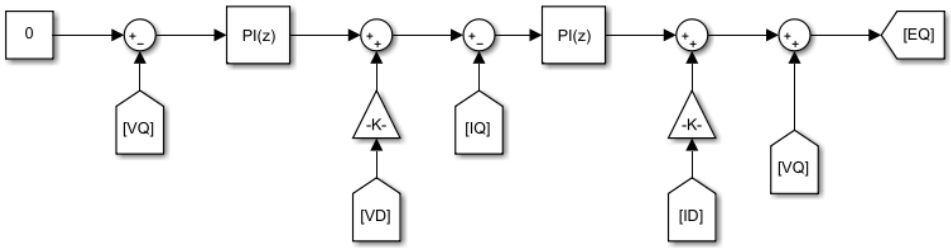

Figure 3.16. The reactive power controls

By obtaining the ED and EQ values suitable for the system, the conversion from d-q-0 to abc is re-established. By using the reference voltages obtained after the abc conversion, pulse signals that determine the operation of the IGBTs forming the DC-AC inverter are obtained as shown in Figure 3.17.

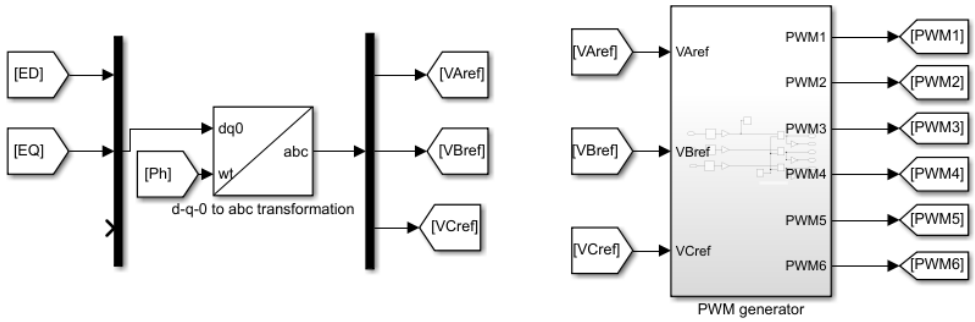

Figure 3.17. PWM generation

3.4. LCL Filter Design

A high-order LCL filter is used to smooth out the output current of the voltage source inverter. This improves the transient behavior by reducing the harmonics and improves the operating range of the inverter. The design parameters of the inverter are calculated by the equations in section 2.5 and listed in Table 3.5.

Table 3.5. The design parameters of LCL filter

Design Parameters of LCL Filter	
L_1	2.5 mH
L_2	2.5 mH
C_f	30μF
$R_{damping}$	2 Ω

3.5. System Operating Scenario

The operating scenario of the system is designed to support the most effective consumption of the generated power. The consumption rates of electrical energy vary throughout the day. Different tariffs are applied for different time zones depending on low and high consumption. There are 3 different tariff zones in Turkey; it is the daytime period between the hours 06.00-17.00, the peak period between the 17.00-22.00 and the night period between 22.00-06.00. Between these periods, the highest energy consumption occurs between 17.00 and 22.00 that is the peak period.

The energy consumption tariffs applied vary for these three periods. The tariff applied during the night period is cheaper than the day period, while the highest tariff is applied during the peak period. For this reason, it is very important to use the energy produced correctly, that is, to manage it correctly. The daily total solar irradiation estimation is performed by use of the real meteorological data of Tarsus obtained from the Turkish Meteorological Service to support this study in terms of energy management. The estimation is performed with LSTM, RNN and FFBPNN methods. The accuracy of these estimations is evaluated with performance metrics such as NRMSE, NMAE, MAPE and WMAE. The estimated daily total solar irradiation value gives us information about the weather conditions of the next day and the amount of power to be produced from the PV panel used. In this way, considering whether the next day will be sunny or cloudy, it is decided whether the power in the battery is not consumed, consumed, or consumed up to a limited SOC value. As a result, the irradiation estimation indirectly allows us to estimate the power that will be produced from the PV system, which gives the opportunity to decide how the system will work according to the weather conditions. The flow diagram describing this energy management is given in Figure 3.18.

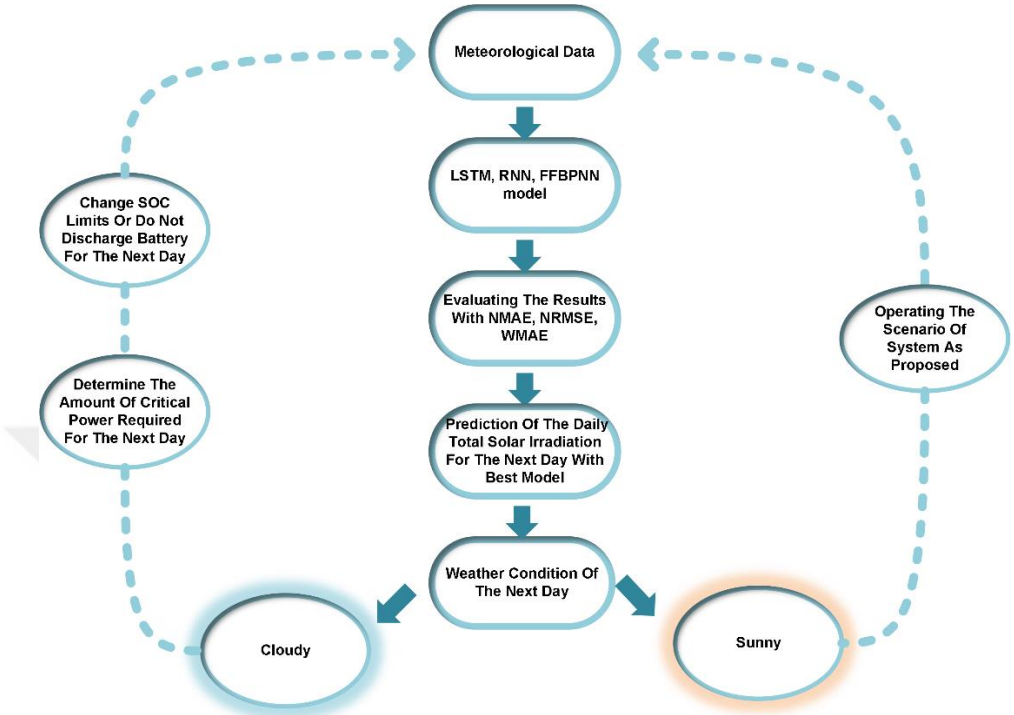

Figure 3.18. The energy management of the system

Meteorological data consists of daily average temperature, daily average wind speed, daily average humidity, daily total sunshine duration and daily total solar irradiation for ten years from 2010 to 2020. While examining meteorological data, deficiencies in the data and data beyond the theoretical limits are observed. To fit the data into ANN models, the data should be fully organized before ANN models are created. The deficiencies and anomalies found in the data are corrected. In this dataset, linear interpolation method is used to process abnormal data, followed by data filtering and data splitting. 3622 days are used for training process and 183 days for testing purpose.

Literature studies and the MATLAB help tool is reviewed to decide how to choose the training option for LSTM from stochastic gradient descent with momentum (SGDM), root mean square spread (RMSProp), and adaptive moment estimation (ADAM). The ADAM optimizer uses similar update parameters as

RMSProp with an additional momentum term and drift correction. ADAM is also used for less feature data and generally achieves a faster-than-normal convergence rate. It is known as one of the best optimizers. Different combinations of model parameters are tried and the parameters that give the best results of the model created with LSTM for daily total irradiation estimation are as in the Table 3.6.

Table 3.6. The LSTM model parameters

The LSTM Model Parameters	
NumHiddenUnits	200
TrainingOptions	Adam
MaxEpoch	350
MiniBatchsSize	16
GradientThreshold	1
InitialLearnRate	0.005
LearnRateSchedule	Piecewise
LearnRateDropPeriod	250
LearnRateDropFactor	0.2
Verbose	1

The RNN model is created in MATLAB. Various combination of training functions with different number of hidden neurons are tried. The best result for RNN model is obtained with 10 hidden neurons. The network of RNN model is shown in Figure 3.19. The Levenberg-Marquardt training function is used with tangent sigmoid transfer function to predict nonlinear output waveform of daily total solar irradiation.

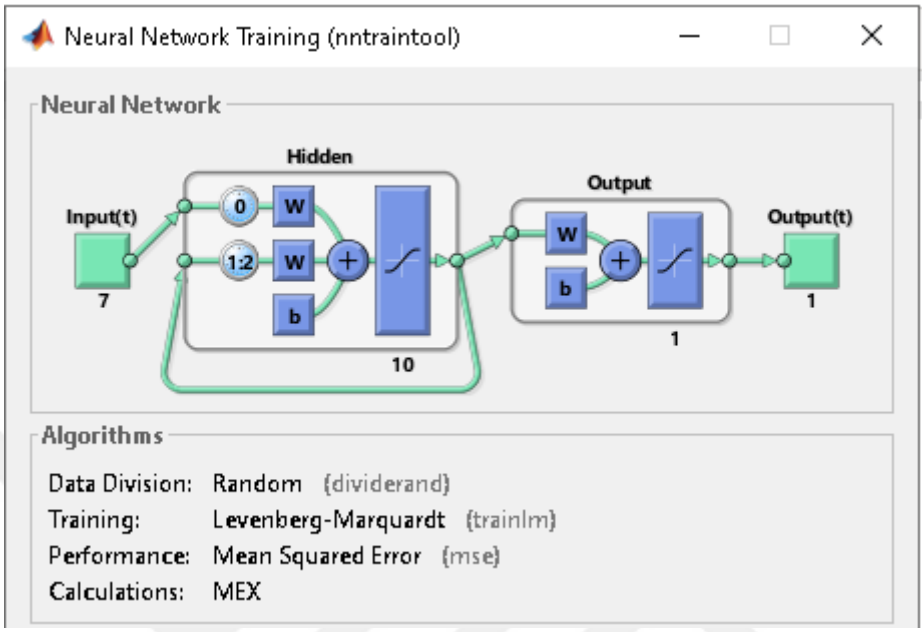

Figure 3.19. The network of RNN model

The daily total solar irradiation estimation is performed by creating FFBPNN-based model in MATLAB. The network model of FFBPNN model is shown in Figure 3.20. Various training functions with different transfer functions and hidden layer numbers are tried, and the best result is performed with the Levenberg-Marquardt training function with tangent sigmoid transfer function to predict nonlinear output waveform of daily total solar irradiation.

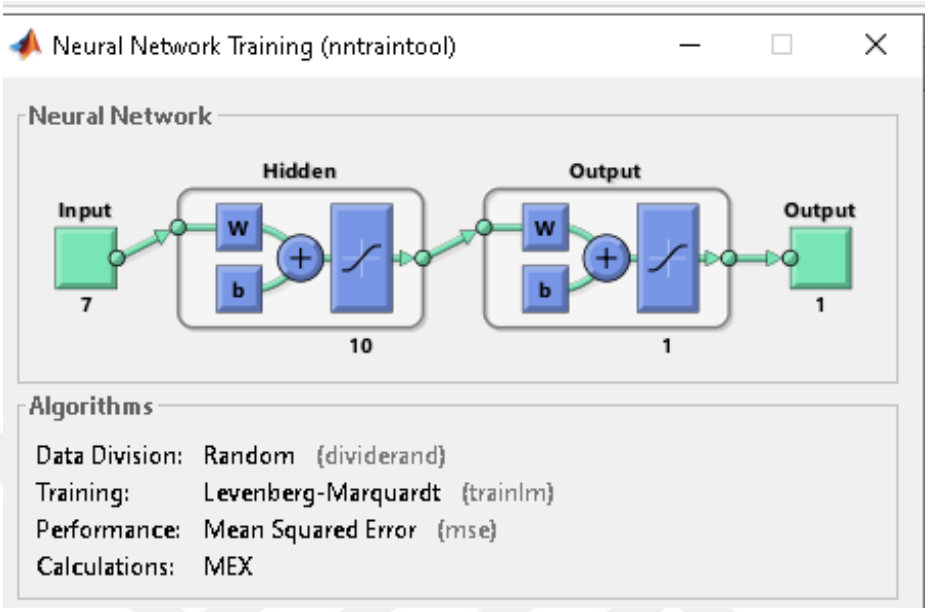

Figure 3.20 .The network of FFBPNN model

The regression graphs of these three ANN-based models created in MATLAB are given in the Figure 3.21. As can be seen from the graphs, the FFBPNN model give the best results.

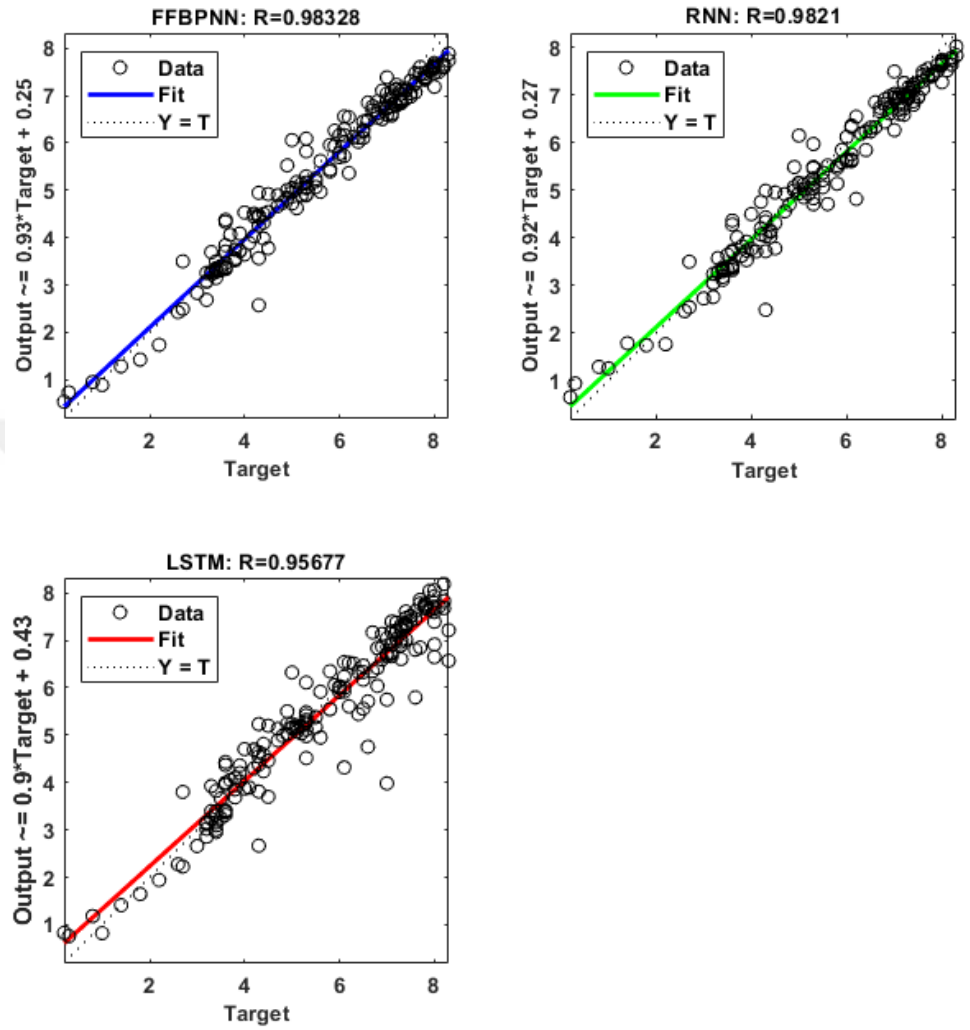

Figure 3.21. The regression graphs of ANN models

The actual total daily solar irradiation vs ANN models' predictions and error magnitudes are shown in Figure 3.22.

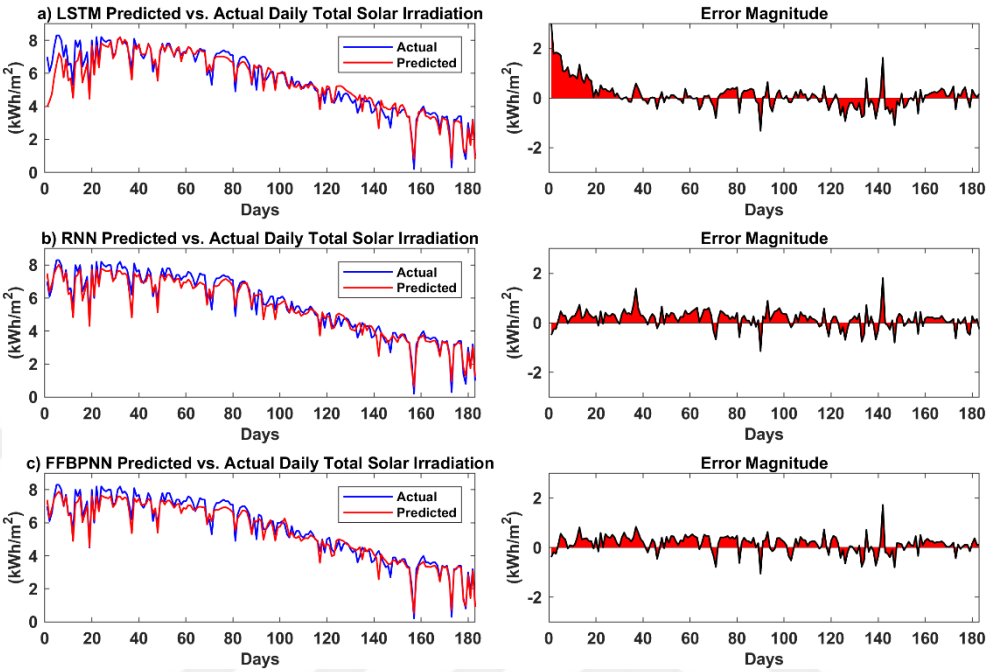

Figure 3.22. The actual total daily total solar irradiation vs ANN models' predictions and error magnitudes

The accuracy assessment of the models' predictions is evaluated with performance metrics and given in the Table 3.7. The best results for LSTM model are taken with the parameters in Table 3.6. Both RNN and FFBPNN models consist of 10 hidden layers. In order to obtain the best results, the created ANN models run with different training functions in different combinations.

Table 3.7. The evaluation of ANN-based model on the performance indices

Model	NMAE%	WMAE%	NRMSE%	MAPE%
LSTM	4.39	6.55	9.99	11.89
RNN	3.65	5.42	6.93	8.47
FFBPNN	3.61	5.36	6.70	7.46

In the creation of the scenario for the system, the limit values shown in the Figure 3.21 are considered. MATLAB function block is used for the algorithm. Firstly, the total produced PV power $P_{PV,}$ the grid frequency F_{grid}, the irradiation and the SOC of the battery are measured as function inputs. The function outputs are defined as grid breaker, PV to DC-link breaker, and battery to DC-link breaker. The specified limit values for the inputs determines whether the breakers are on and off. The lowest and highest values for the grid frequency are specified as 47.5 Hz and 51.5 Hz respectively according to grid connection standards. The lower value of P_{PV} is determined as 620 W for continuous and stable solar power.

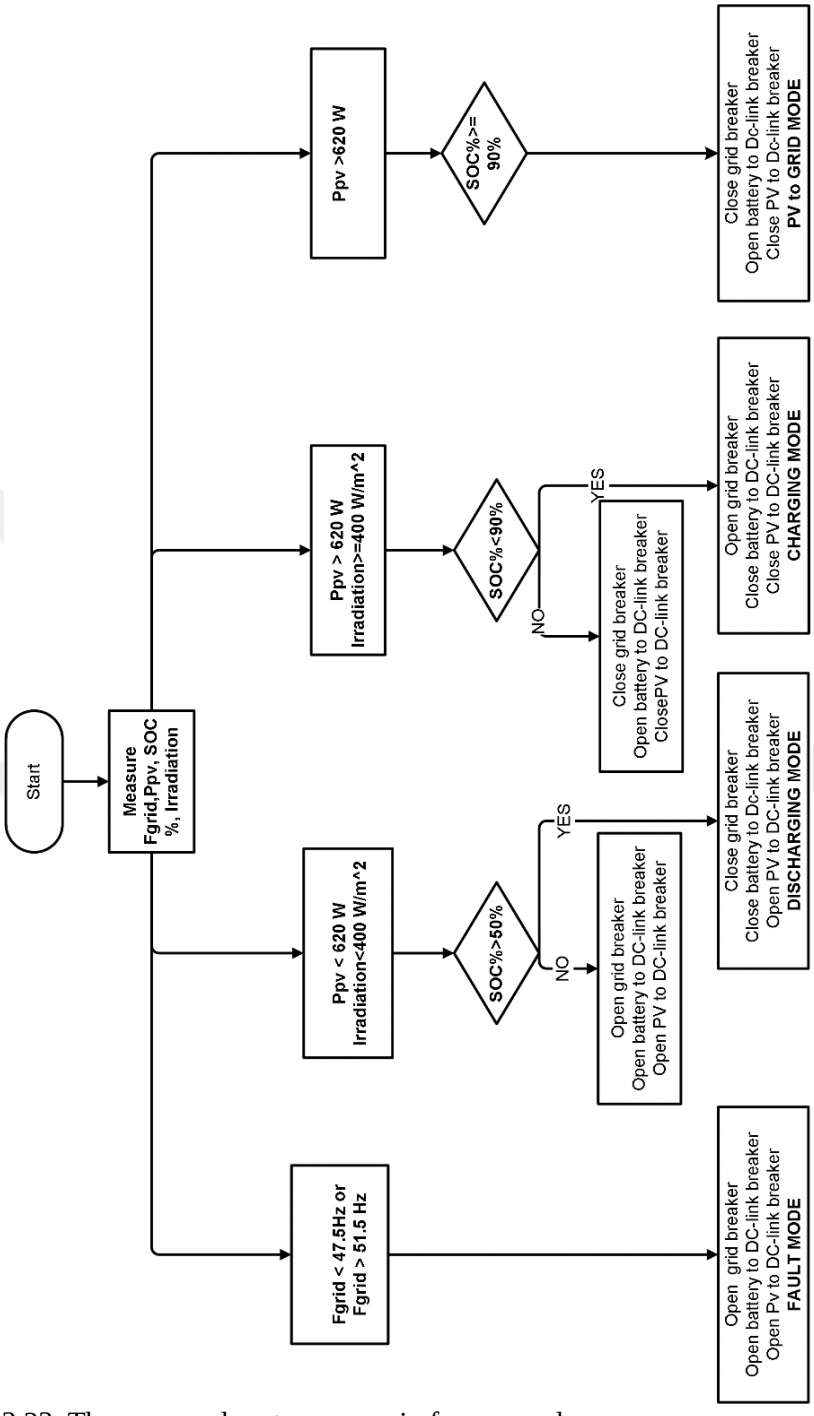

Figure 3.23. The proposed system scenario for sunny days

3.5.1. Charging Mode (PV to Battery)

The mode of charging the battery in the system occurs when the P_{PV} > 620 W, the irradiation > 400 W/m^2 and the SOC < 90%. In other words, if the PV produces power during the daytime and is stable, if the power is produced at a level that can charge the P_{PV} battery, and if the battery's SOC < 90%, the battery is charged until it reaches 90% SOC. In this way, the battery is ready for the peak time interval to support the grid. The irradiation must not be less than 400 irradiances for charging the battery. This is because the battery is at 50% SOC before it starts charging. In other words, since there is 5 kW of power in the battery, we must have P_{PV} more than 5 kW to be able to press current to the battery. When the function inputs meet these conditions, the function outputs allow the battery to be charged by opening the grid breaker and closing the battery breaker and DC-link breaker. In this way, the energy flow is only ensured between the PV system and the battery until it reaches 90% SOC.

3.5.2. Discharging Mode (Battery to Grid)

The mode of discharging the battery in the system occurs when the P_{PV} < 620 W and the SOC > 50%. In other words, when the power generation of the PV system stops and the battery's SOC > 50%, the battery is discharged until it reaches 50% SOC. In this way, the battery is ready for the peak time interval to support the grid. When the function inputs meet these conditions, the function outputs close the grid breaker, the battery breaker and open the DC-link breaker, allowing the battery to discharge. In this way, the energy flow is only provided between the battery and the grid until the battery reaches 50% SOC.

3.5.3. PV to Grid Mode

It is the time when all the power produced by the PV is transmitted to the grid. For the system to work in this mode; P_{PV} > 620 W and SOC should be at least 90%. When the inputs meet these conditions, the battery breaker determined as the

output will be in the open position, the grid breaker and the DC-link breaker will be in the closed position.

3.5.4. Fault Mode

This mode occurs when the network frequency value is outside the determined values and the transmission of the generated power to the grid is stopped.

3.6. Summary

In this section, the details of the system designed in MATLAB/Simulink are given. PV system, DC-DC interleaved boost converter, DC-DC bidirectional converter, LCL filter, current-controlled DC-AC inverter, battery parameters, energy management scheme, the daily total solar irradiation estimation from meteorological data, proposed ANN-based MPPT method and scenario created for sunny days are given in detail.

4. TEST RESULTS AND DISCUSSIONS

The test results of the proposed system and its comparison with other MPPT methods are examined in this section. MATLAB/Simulink is used for hybrid system design. The operation of the system is investigated depending on different weather conditions. This study is examined at 25 °C, 1000 W/m^2 and 25 °C, and 500 W/m^2 and 25 °C with the irradiation of a day created from real meteorological data of Tarsus/Mersin. Charging mode, discharging mode, PV to grid mode is given separately for each weather conditions. System THD, inverter current-voltage, battery SOC, battery current-voltage, DC-link voltage and power efficiency results are obtained for each mode separately for all weather conditions.

4.1. Perturb & Observe

4.1.1. Charging Mode

4.1.1.1. 1000 W/m^2 at 25 ˚C

The charging mode of the battery is simulated for 1000 W/m^2 irradiation at 25 ˚C temperature for the P&O method, and graphic results are given in this section. For this situation to occur, the SOC of the battery must be below 90%. The maximum and minimum charging current is determined as 10. 43 A, 8.5 A respectively, for this situation. Figure 4.1 shows the SOC, current and voltage graphs when the battery is charging at 1000 W/m^2 from PV system. The initial SOC value of the battery is given as 50% and it is observed on the graph that SOC increases. The battery is charged with a voltage value varying between 454 V and 456 V. The current value is between the maximum and minimum current values.

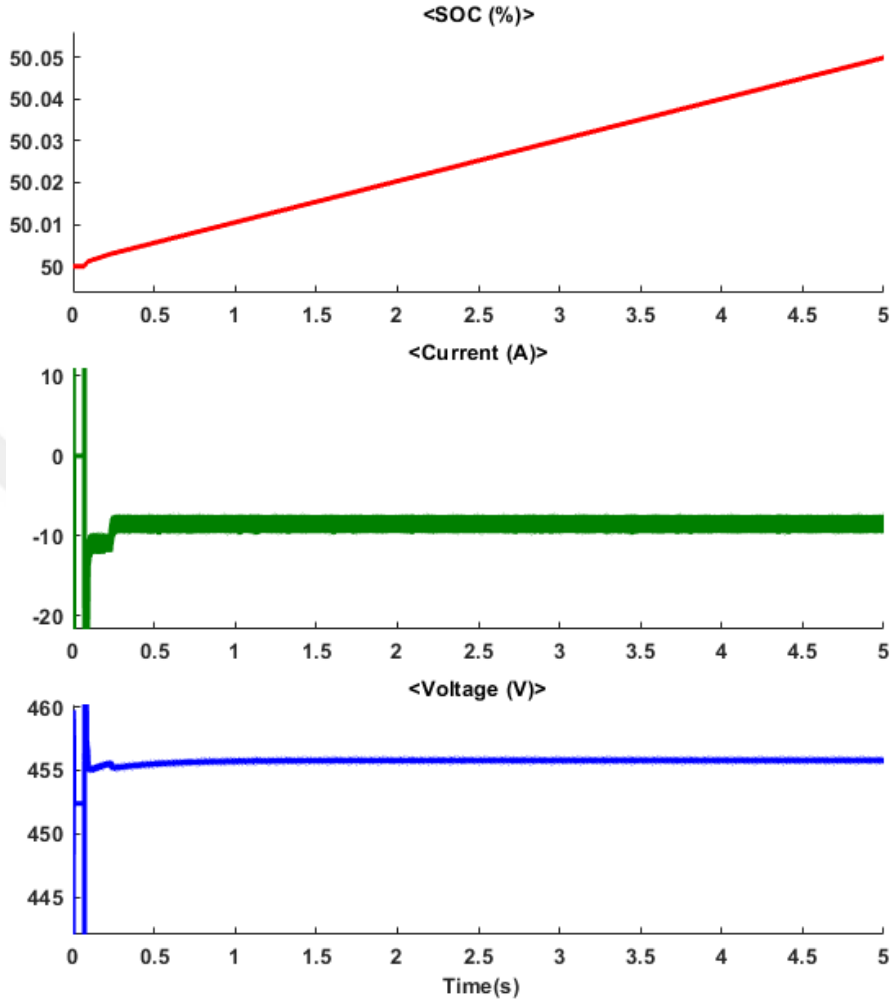

Figure 4.1. The SOC, voltage and current of the battery at charging mode with P&O at 1000 W/m^2

The produced PV power is shown in Figure 4.2. With the P&O method, it is seen that the power produced by the PV is at the level of 12.46 kW.

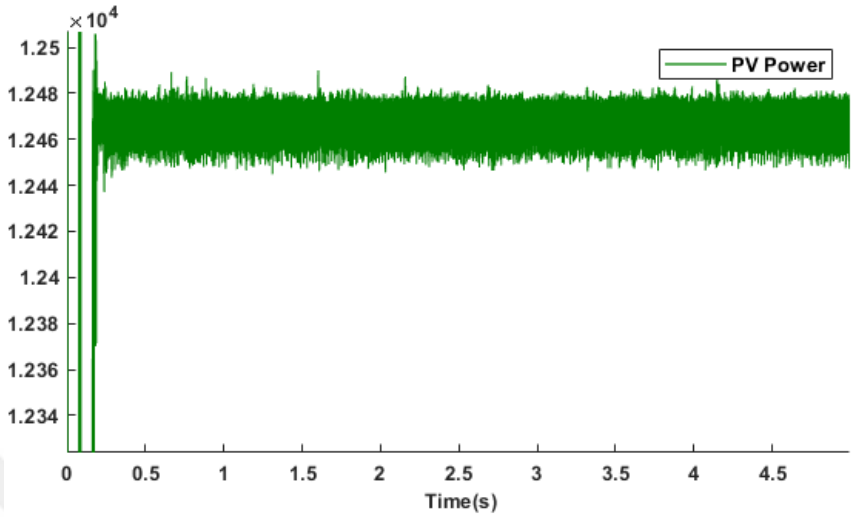

Figure 4.2. The produced PV power with P&O for charging mode at 1000 W/m^2

The power transferred to the battery from this generated power is shown in the Figure 4.3.

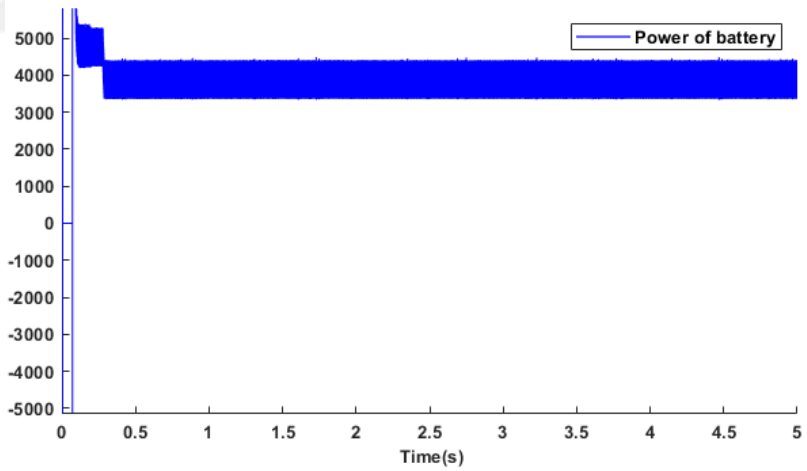

Figure 4.3. The power transferred to battery at charging mode with P&O at 1000 W/m^2

The power transferred to the grid from this generated power is shown in the Figure 4.4.

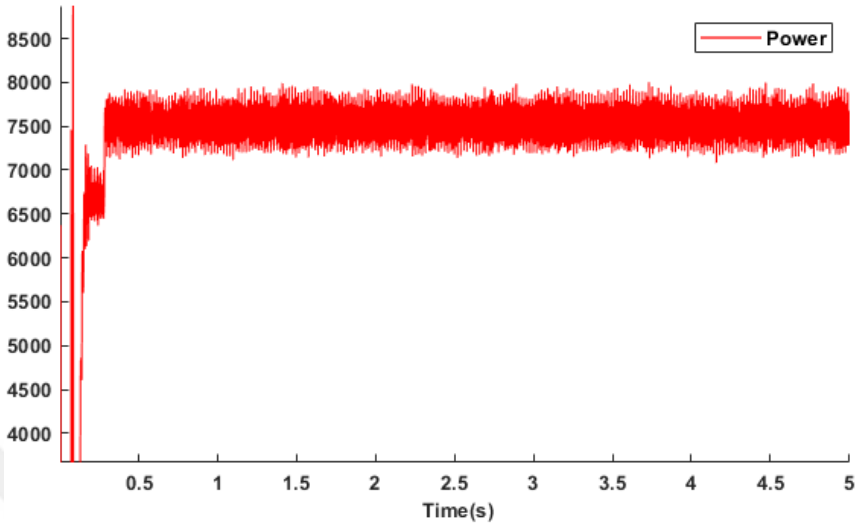

Figure 4.4. The power transferred to the grid at charging mode with P&O at 1000 W/m^2

In the charging state of the battery the inverter voltage and current graphs are shown in Figure 4.5. As can be seen from the graphs, the pf value is zero, the current and voltage graphs have the same phase angle.

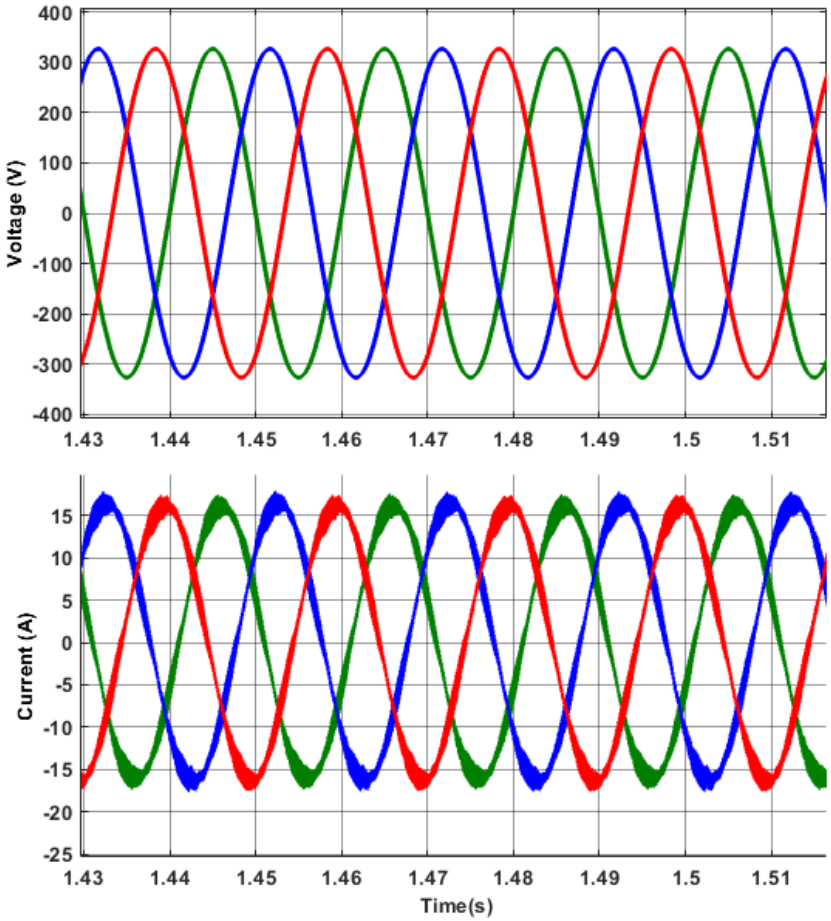

Figure 4.5. The voltage and current of inverter output at charging mode with P&O at 1000 W/m^2

While power transfer is provided from the PV system to both the battery and the grid, the DC-link voltage must also be at the specified level for stability. Figure 4.6 and 4.7 shows that this voltage oscillates around 710 V.

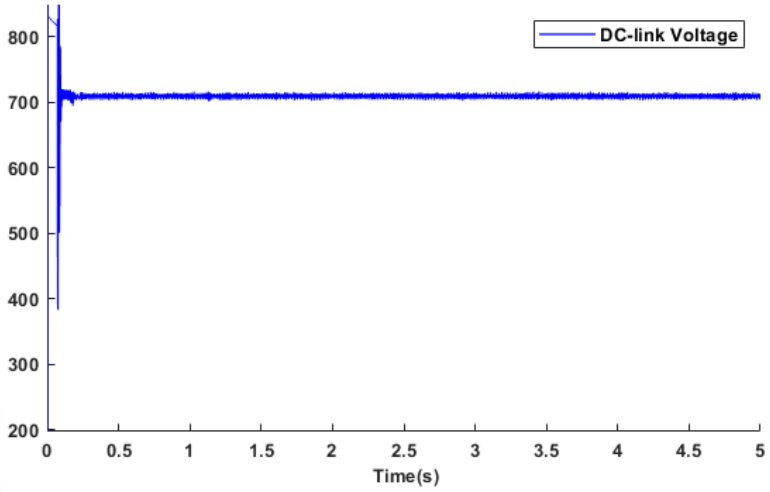

Figure 4.6. The DC-link voltage at charging mode with P&O at 1000 W/m^2

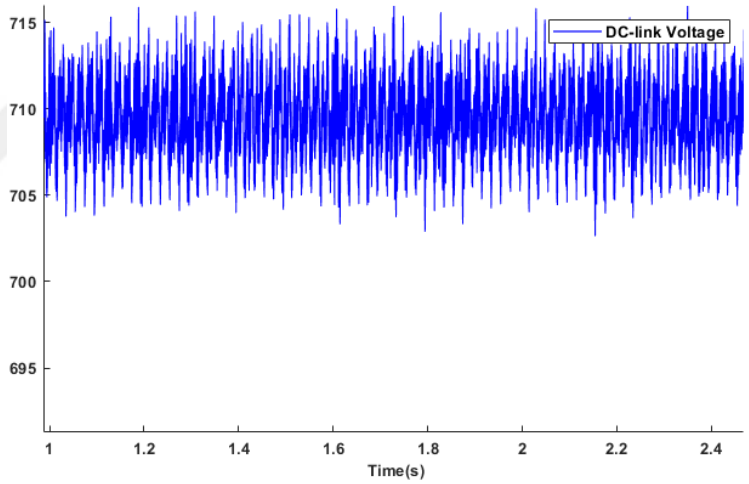

Figure 4.7. The DC-link voltage at charging mode with P&O at 1000 W/m^2

The measurement of power efficiency in simulation studies is constantly changing due to small step size values, so efficiency is measured by use of the 'mean' block, which is averaged power efficiency over the simulation period. The power efficiency graph is seen in Figure 4.8. It is just below 92%.

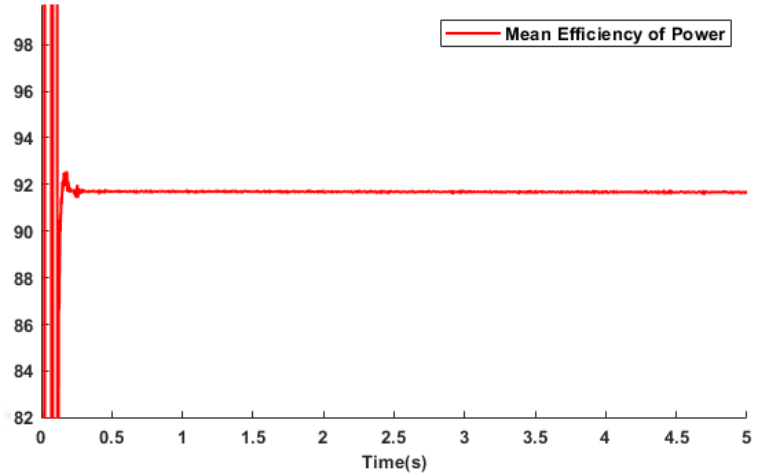

Figure 4.8. The efficiency of produced power at charging mode with P&O at 1000 W/m^2

The THD for charging state is shown in Figure 4.9. Although it is seen that THD falls below 1.5%, it is also seen that there are times when it is above 2%.

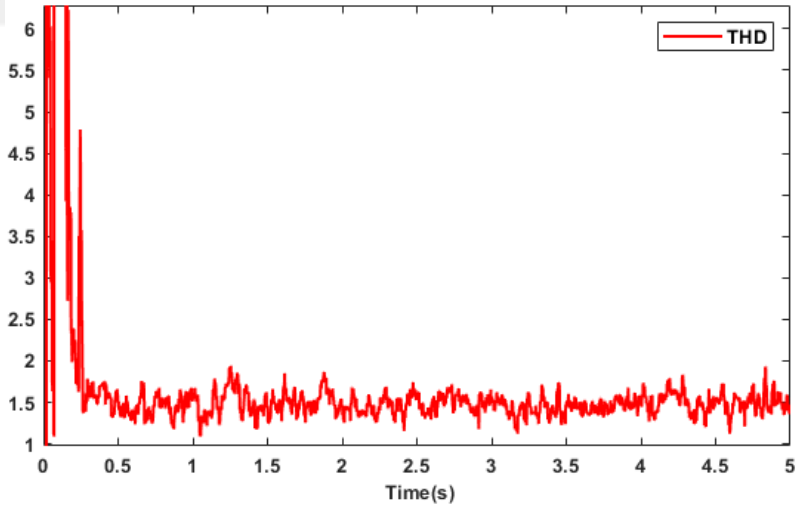

Figure 4.9. The THD of system at charging mode with P&O at 1000 W/m^2

4.1.1.2. 500 W/m^2 at 25 ˚C

The charging mode for P&O method is analyzed for 500 W/m^2 irradiance at 25 ˚C temperature. The power generated from the PV system is transferred to both the battery and the grid. While examining this situation, the charging current of the battery is re-evaluated by calculating the power that the irradiation value can produce. While this transfer takes place, the generated power is distributed to the grid and the battery in a balanced way. If the battery is storing power with maximum current, large filters are needed for the power transferred to the grid. To avoid this situation, the charging current for 500 W/m^2 irradiation is determined as 5 A, as shown in Figure 4.10.

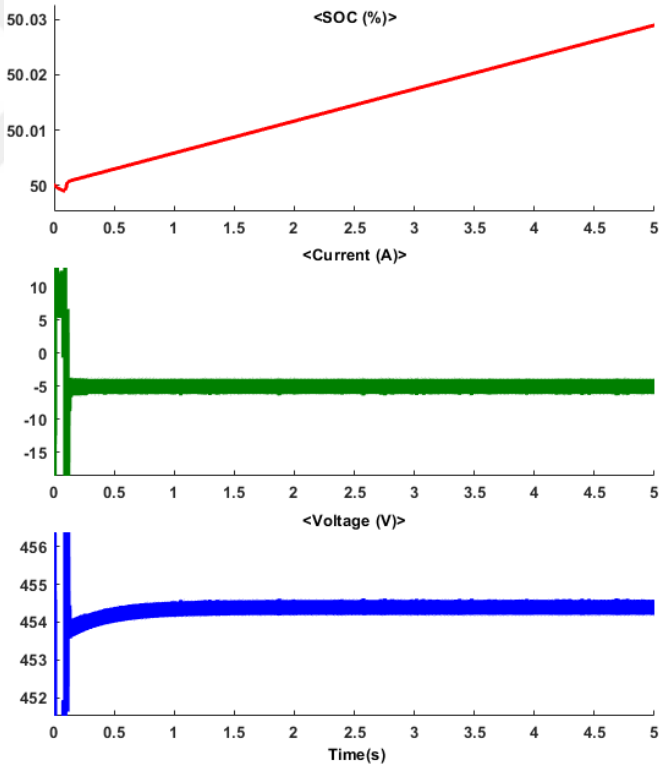

Figure 4.10. The SOC, voltage and current of the battery at charging mode with P&O at 500 W/m^2

The produced PV power is shown in Figure 4.11. With the P&O method, it is seen that the power produced by the PV is at the level of 6.3 kW.

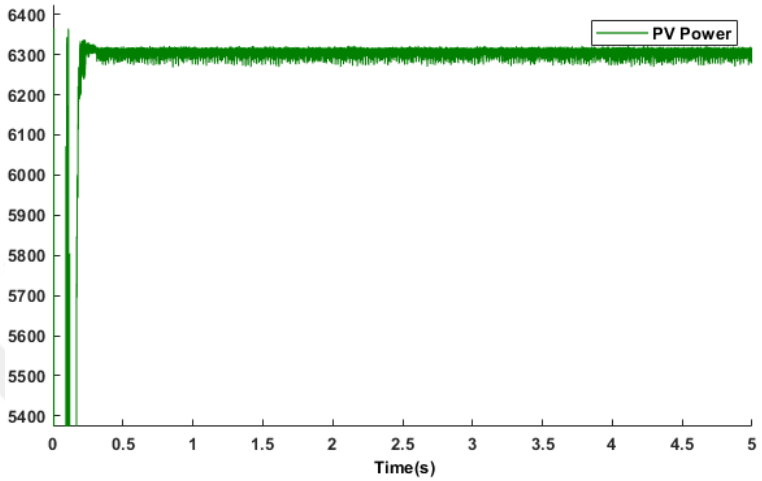

Figure 4.11. The produced PV power with P&O for charging mode at 500 W/m^2

The power transferred to the battery from this generated power is shown in the Figure 4.12.

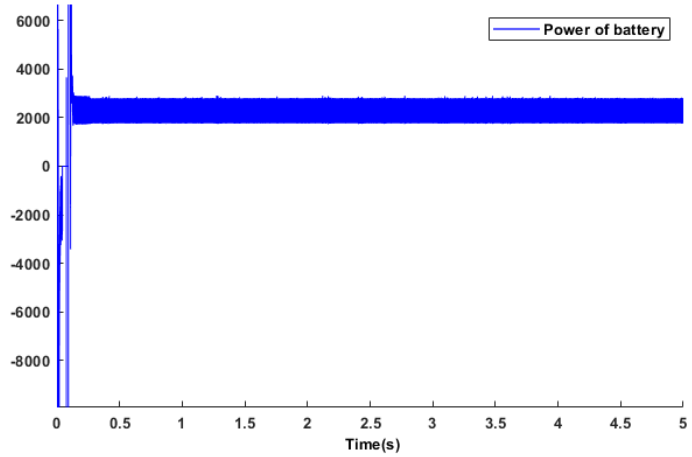

Figure 4.12. The power transferred to battery at charging mode with P&O at 500 W/m^2

The power transferred to the grid from this generated power is shown in the Figure 4.13.

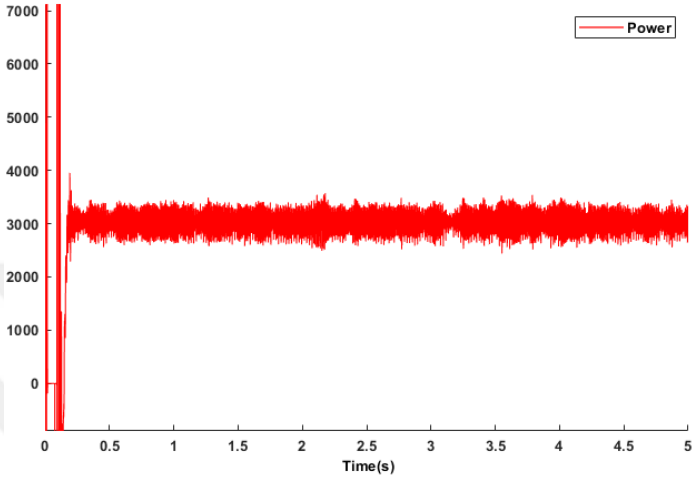

Figure 4.13. The power transferred to grid at charging mode with P&O at 500 W/m^2

Inverter output voltage and current graphs are shown in Figure 4.14. The sum of the currents of the PV and the battery shows that the system is at 500 W/m^2. It is seen that there is no phase difference between current and voltage and pf is zero.

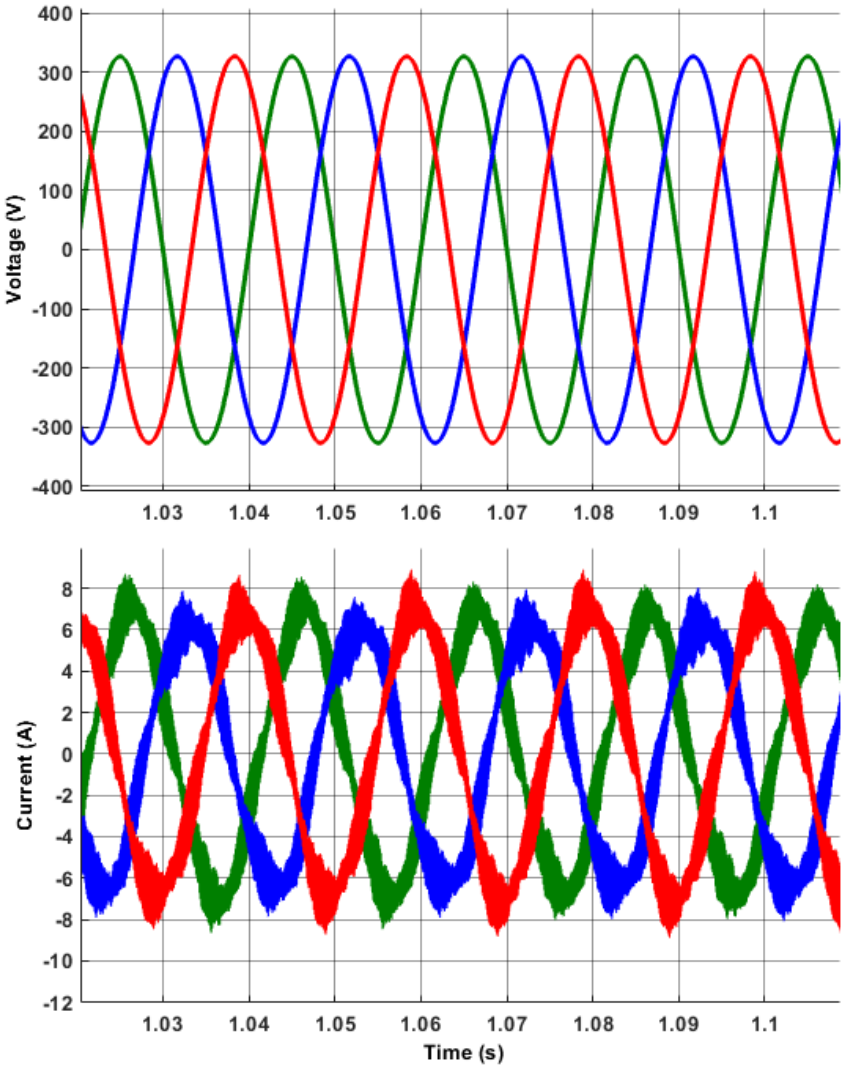

Figure 4.14. The voltage and current of inverter output at charging mode with P&O at 500 W/m^2

It is observed that the oscillation is more than 1000 W/m^2 by looking at the current graph in Figure 4.14. The THD graph of the system is also shown in Figure 4.15.

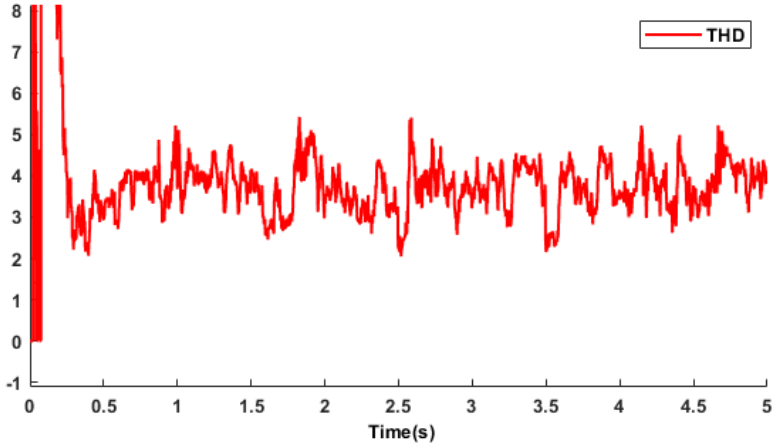

Figure 4.15. The THD of the system at charging mode with P&O at 500 W/m^2

The efficiency of the generated power for 500 W/m^2 is given in Figure 4.16. Efficiency is around 84%.

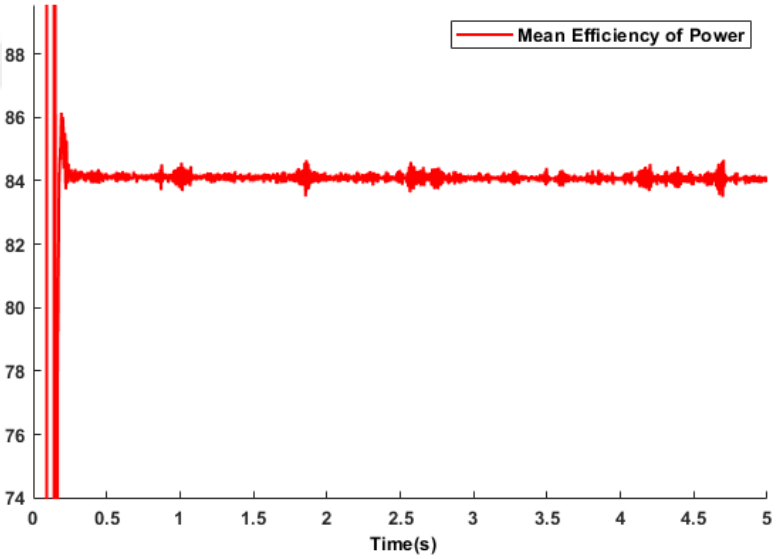

Figure 4.16. The efficiency of produced power at charging mode with P&O at 500 W/m^2

The DC-link voltage oscillates around 710 V, it is given in Figure 4.17 and Figure 4.18.

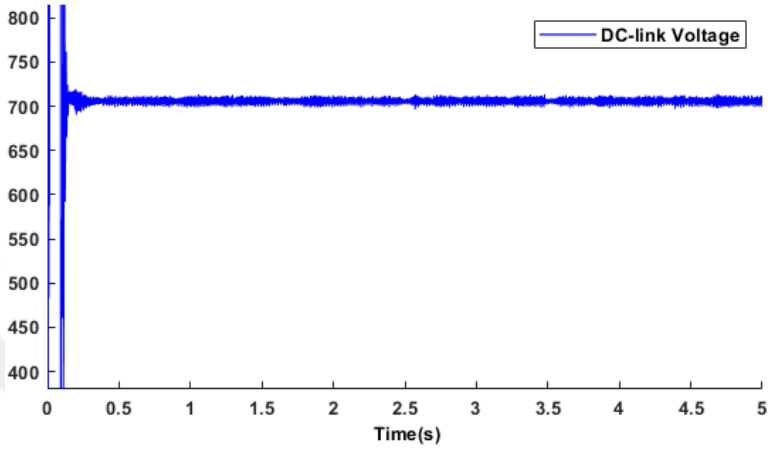

Figure 4.17. The DC-link voltage at charging mode with P&O at 500 W/m^2

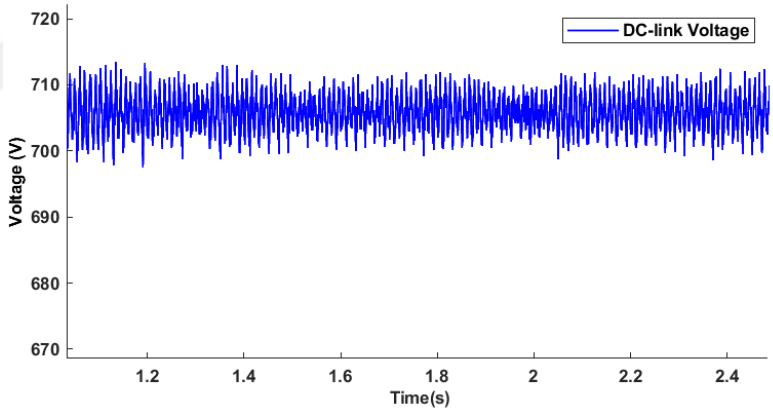

Figure 4.18. The DC-link voltage at charging mode with P&O at 500 W/m^2

4.1.2. PV to Grid Mode

4.1.2.1. 1000 W/m^2 at 25 ˚C

The PV to grid mode of the system is simulated for 1000 W/m^2 irradiation and 25 ˚C temperature values for P&O method, and graphic results are given in this section. For this situation to occur, the SOC of the battery must be above or equal to

90%. In this case all the power produced by the PV is transferred to the grid. The inverter voltage and current graph is shown in the Figure 4.19 for 1000 W/m^2. As seen in Figure 4.19 the pf value is zero, the current and voltage graphs have the same phase angle, the maximum phase voltage value is 325 V and the current value per phase is maximum 25 A.

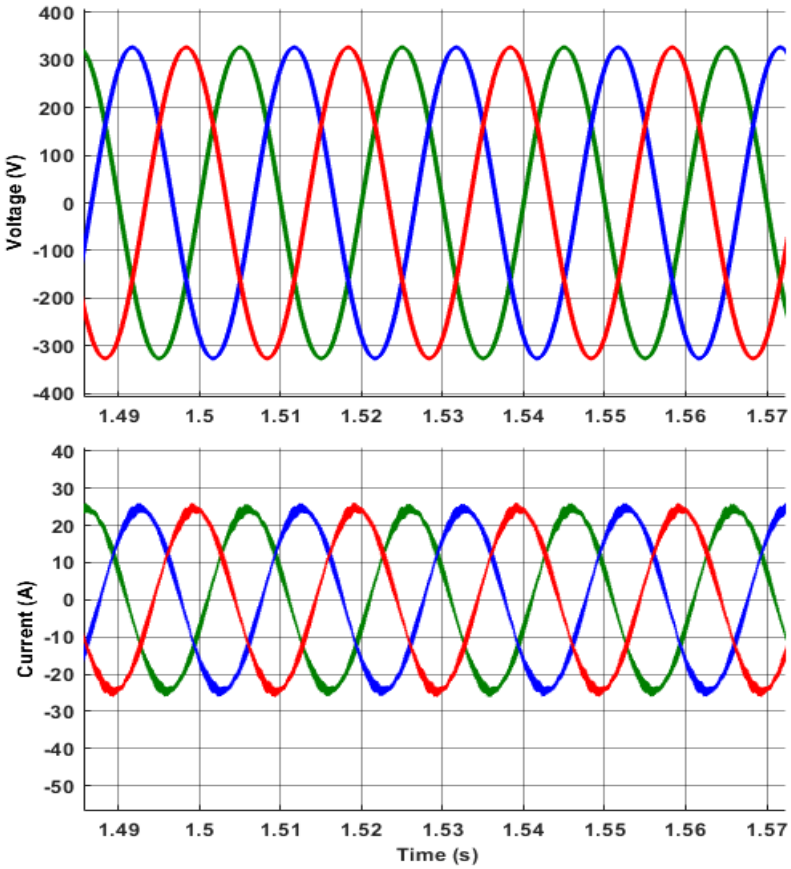

Figure 4.19. The voltage and current of inverter output at PV to grid mode with P&O at 1000 W/m^2

The produced PV power is shown in Figure 4.20. With the P&O method, it is seen that the power produced by the PV is at the level is between 12.45 kW and 12.46 kW.

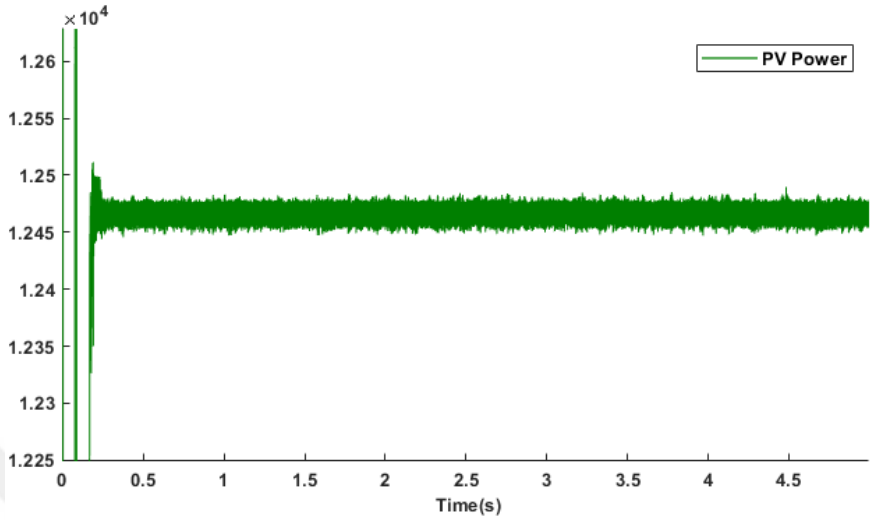

Figure 4.20. The produced PV power with P&O for PV to grid mode at 1000 W/m^2

The power transferred to the grid from this generated power is shown in the Figure 4.21.

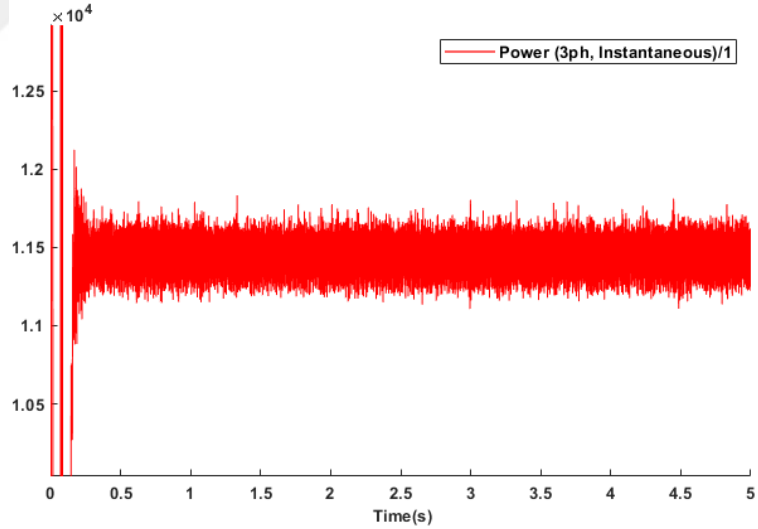

Figure 4.21. The power transferred to the grid with P&O for PV to grid mode at 1000 W/m^2

In this case, as the SOC value of the battery is given as 90%, as seen in Figure 4.22, the battery has never been charged. The battery voltage is stable at 455 V, the battery current is zero.

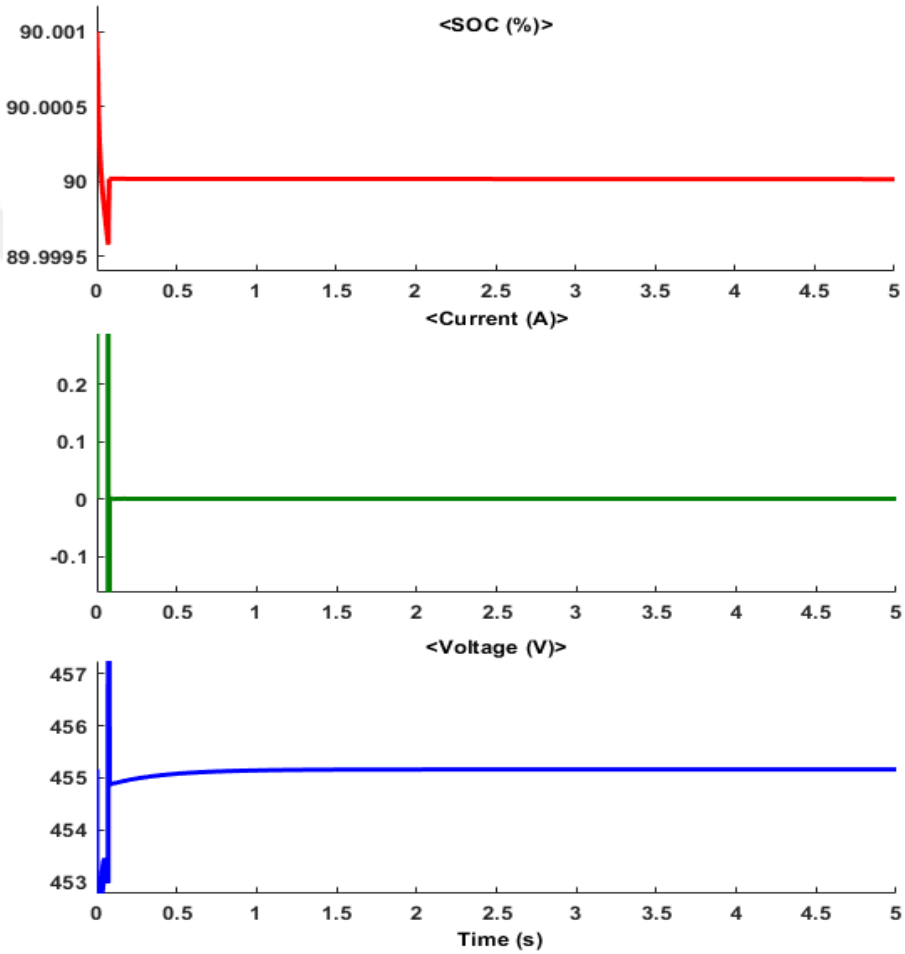

Figure 4.22. The SOC, voltage and current of the battery for PV to grid mode with P&O at 1000 W/m^2

The DC-link voltage is oscillating between 705 V and 715 V as seen in Figure 4.23 and 4.24.

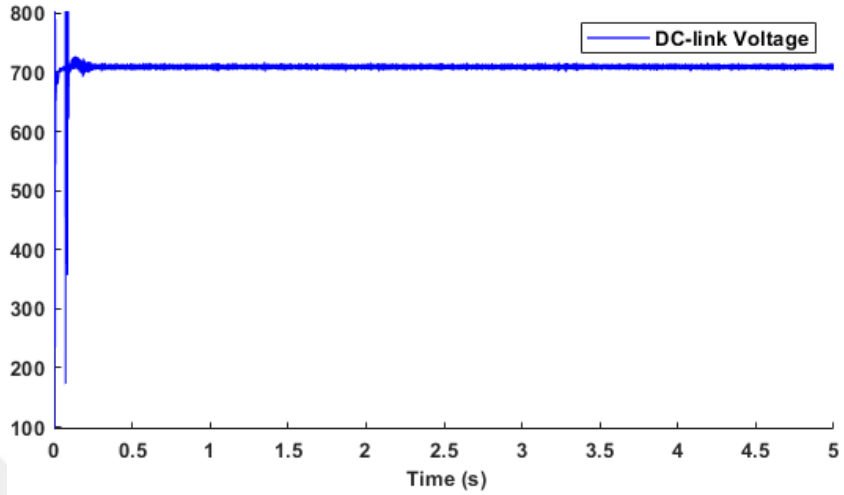

Figure 4.23. DC-link voltage for PV to grid mode with P&O at 1000 W/m^2

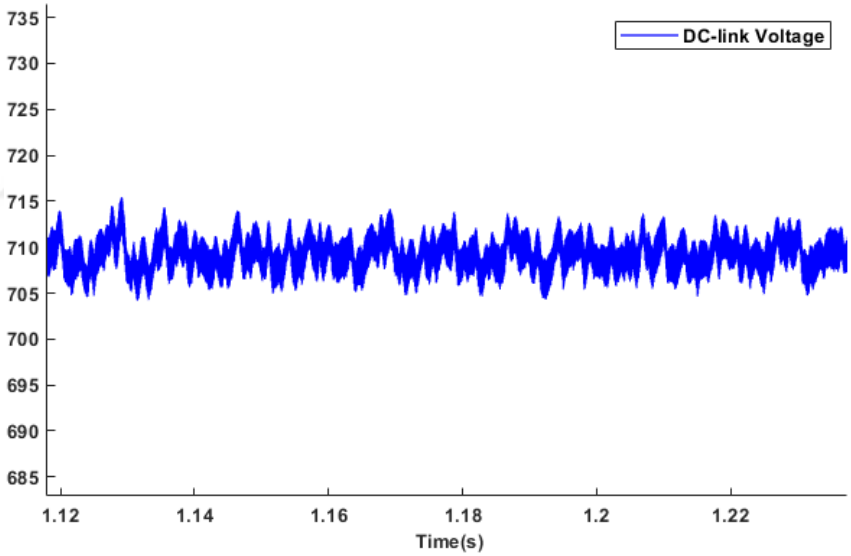

Figure 4.24. DC-link voltage for PV to grid mode with P&O at 1000 W/m^2

The efficiency of the power produced in the system is close to 92% in Figure 4.25 for the PV to grid mode.

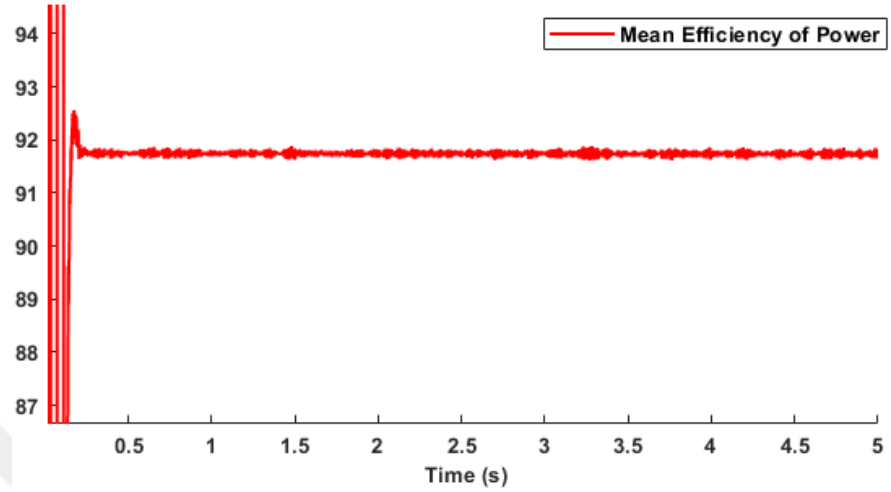

Figure 4.25. The efficiency of produced power

It is seen from the Figure 4.26 that the THD decreases and increases by around 1% while transferring power from PV to the grid.

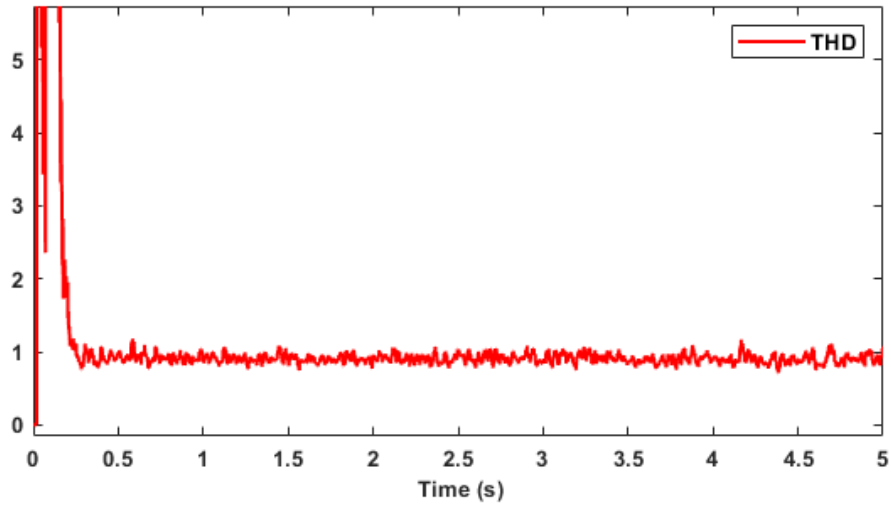

Figure 4.26. The THD of system for PV to grid mode with P&O at 1000 W/m^2

4.1.2.2. 500 W/m^2 at 25 ˚C

The PV to grid mode of the system is simulated for 500 W/m^2 irradiation and 25 ˚C temperature values for P&O method, and graphic results are given in this section. For this situation to occur, the SOC of the battery must be above or equal to 90%. In this case all the power produced by the PV is transferred to the grid. The inverter voltage and current graph is shown in the Figure 4.27 for 500 W/m^2. As seen in Figure 4.27 the pf value is zero, the current and voltage graphs have the same phase angle, the maximum phase voltage value is 325 V and the current value per phase is maximum 12.5 A.

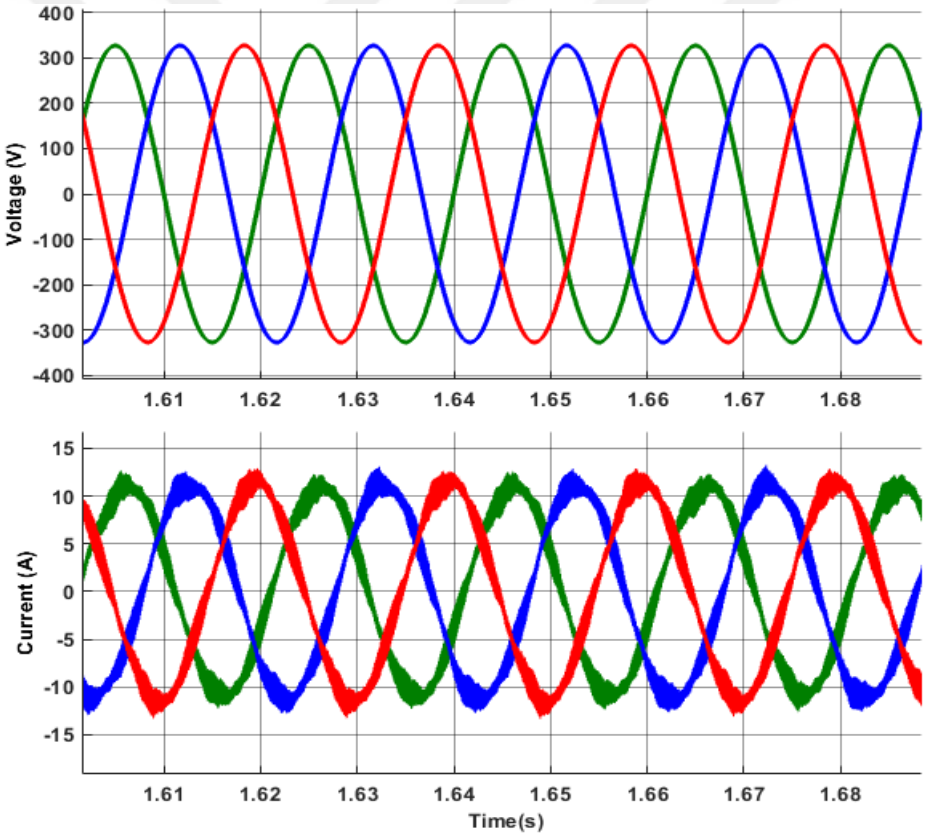

Figure 4.27. The voltage and current of inverter output for PV to grid mode with P&O at 500 W/m^2

The produced PV power is shown in Figure 4.28. With the P&O method, it is seen that the power produced by the PV is at the level of 6.3 kW.

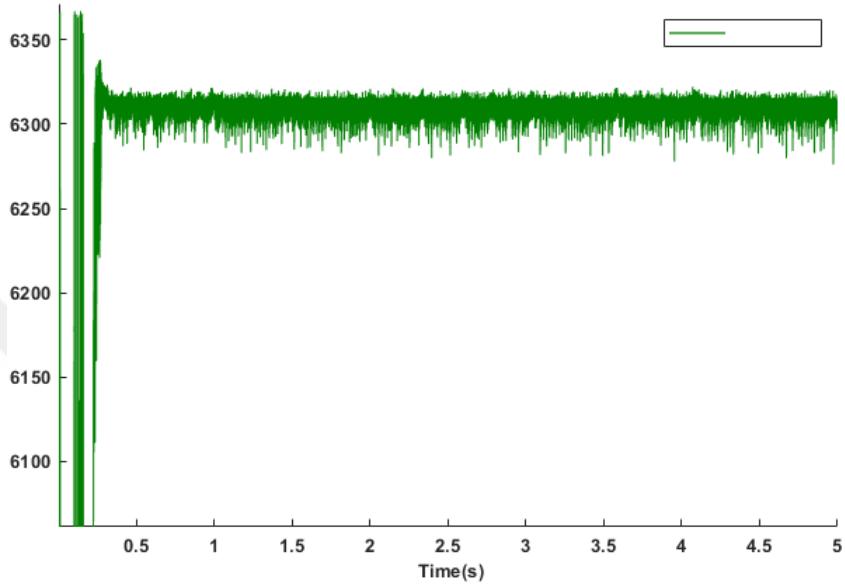

Figure 4.28. The produced PV power with P&O for PV to grid mode at 500 W/m^2

The power transferred to the grid from this generated power is shown in the Figure 4.29.

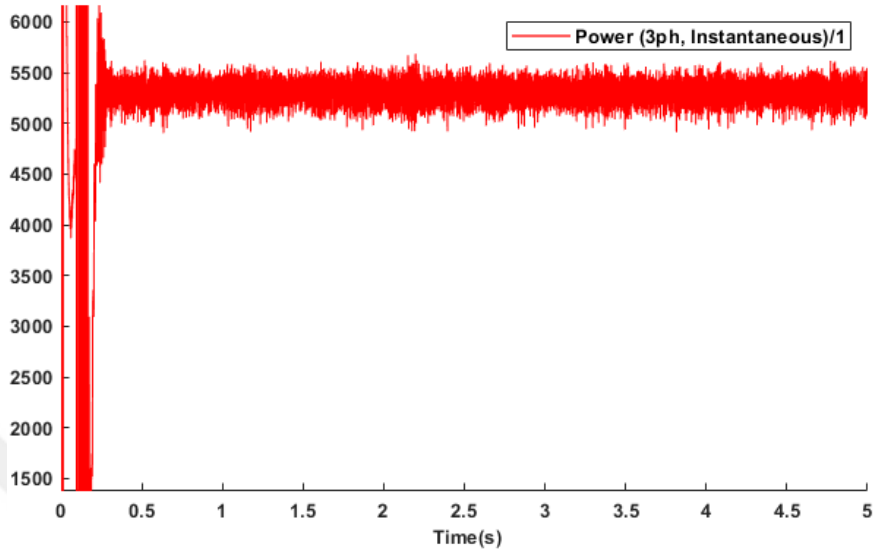

Figure 4.29. The power transferred to the grid with P&O for PV to grid mode at 500 W/m^2

In this case, as the SOC value of the battery is given as 90%, as seen in Figure 4.30, the battery has never been charged. The battery voltage is stable at 455 V, the battery current is zero.

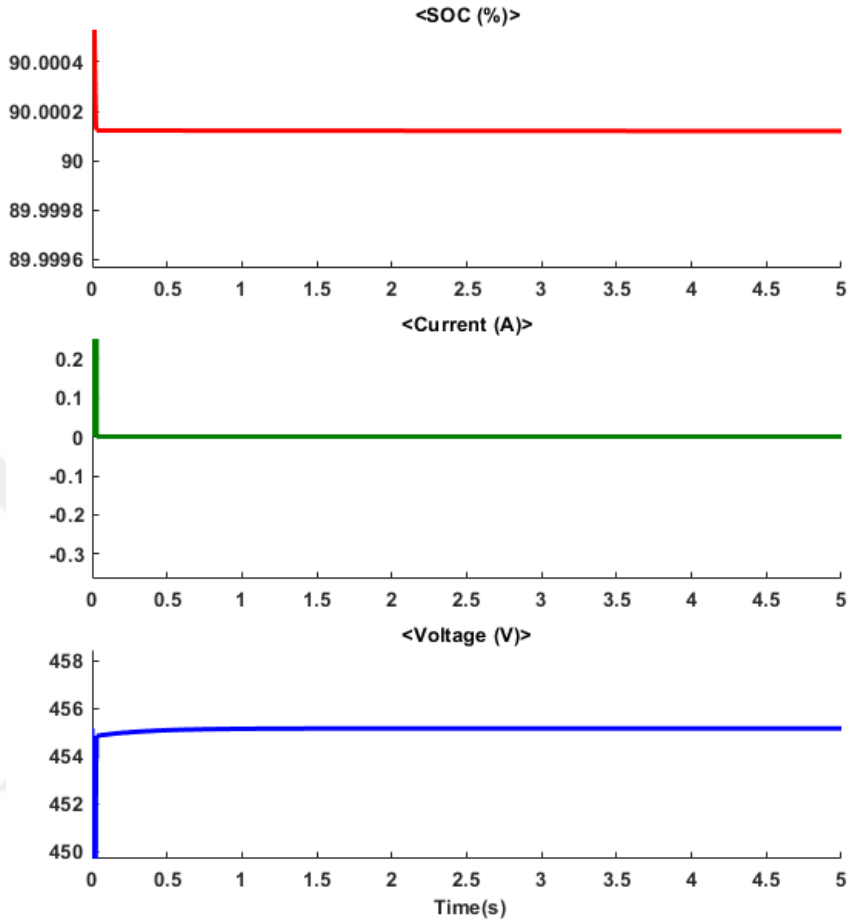

Figure 4.30. The SOC, current and voltage of battery for PV to grid mode with P&O at 500 W/m^2

The Dc-link voltage is oscillating between 700 V and 715 V as seen in Figure 4.31 and Figure 4.32.

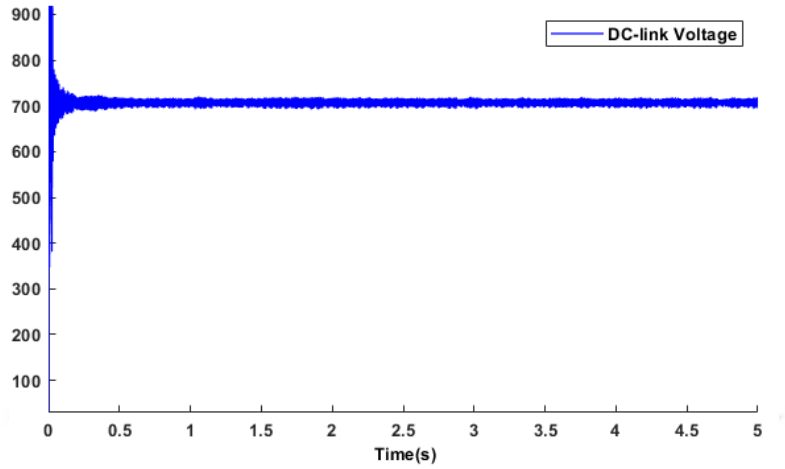

Figure 4.31. DC-link voltage for PV to grid mode with P&O at 500 W/m^2

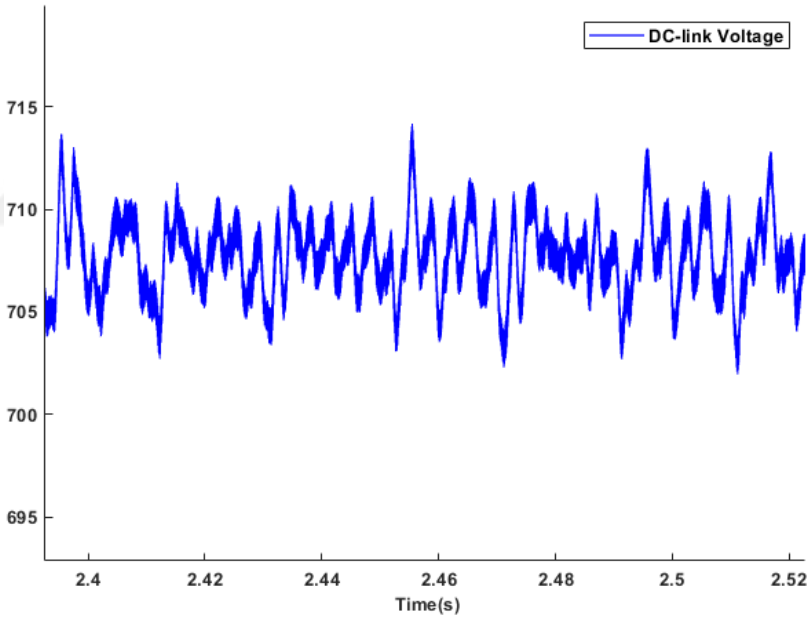

Figure 4.32. DC-link voltage for PV to grid mode with P&O at 500 W/m^2

The efficiency of the power produced in the system is 84% in Figure 4.33 for the PV to grid mode at 500 W/m^2.

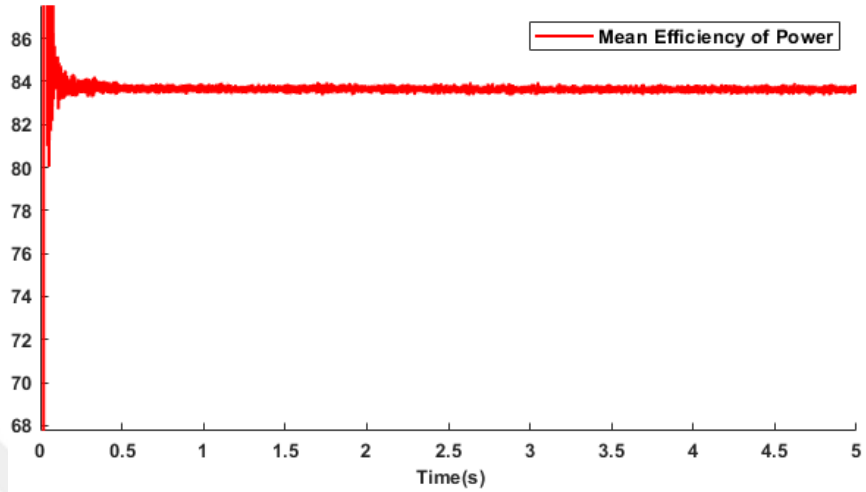

Figure 4.33. The efficiency of produced power for PV to grid mode with P&O at 500 W/m^2

It is seen in Figure 4.34 THD varies between 2% and 4% when transferring power from PV to grid.

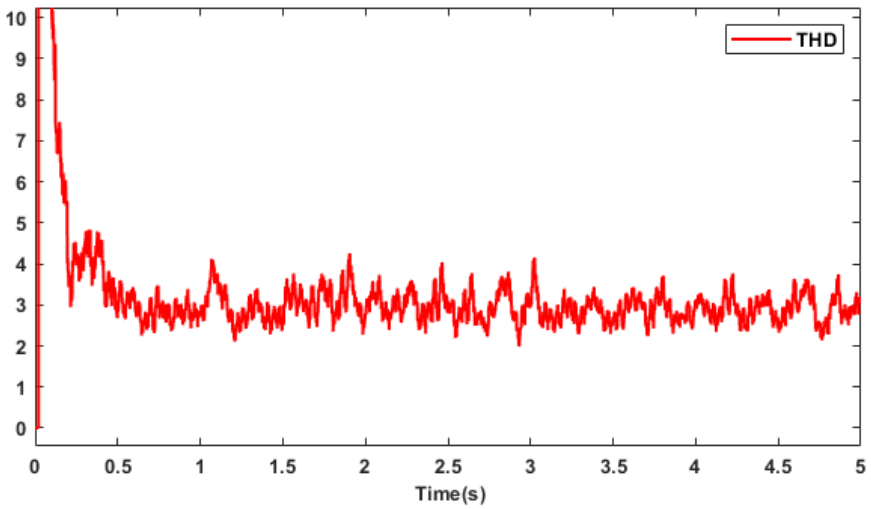

Figure 4.34. The THD of system for PV to grid mode with P&O at 500 W/m^2

4.1.3. Discharging Mode Battery to Grid

The results of discharging mode for P&O method are shown in this part. The discharging mode occurs when the SOC is above %50 and P_{PV} is lower than 620 W. The battery is assumed to be fully charged before discharging. The SOC of the battery is 90%. The battery discharge current ranges from a maximum of 10.43 A to a minimum of 8.5 A. SOC, voltage, and current graphs for the discharge mode of the battery are shown in the Figure 4.35. As seen in Figure 4.35 the battery is in discharging mode. The power in the battery is transferred to the grid.

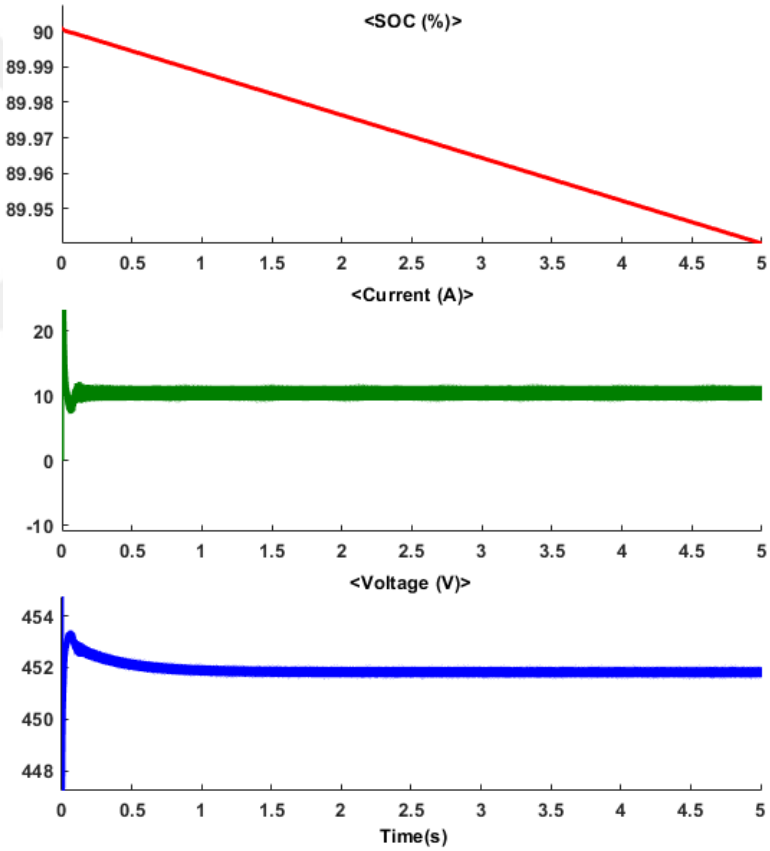

Figure 4.35. The SOC, current and voltage of battery for discharging mode

The battery power is seen in Figure 4.36 when the battery is discharging mode.

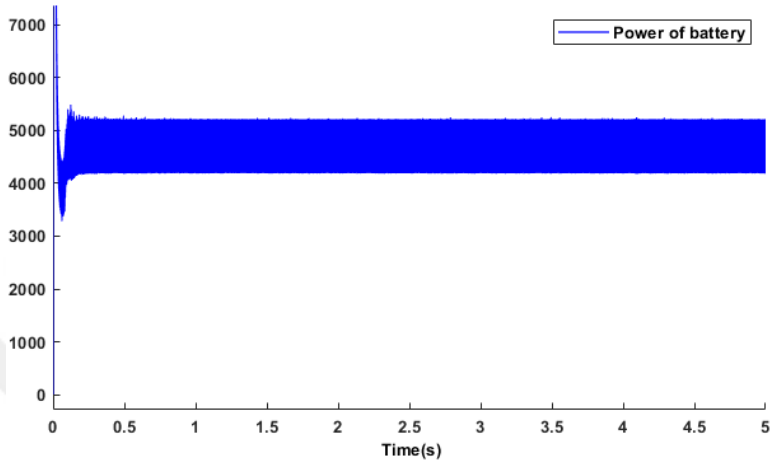

Figure 4.36. The battery power for discharging mode

The power transferred from the battery to the grid is displayed in Figure 4.37.

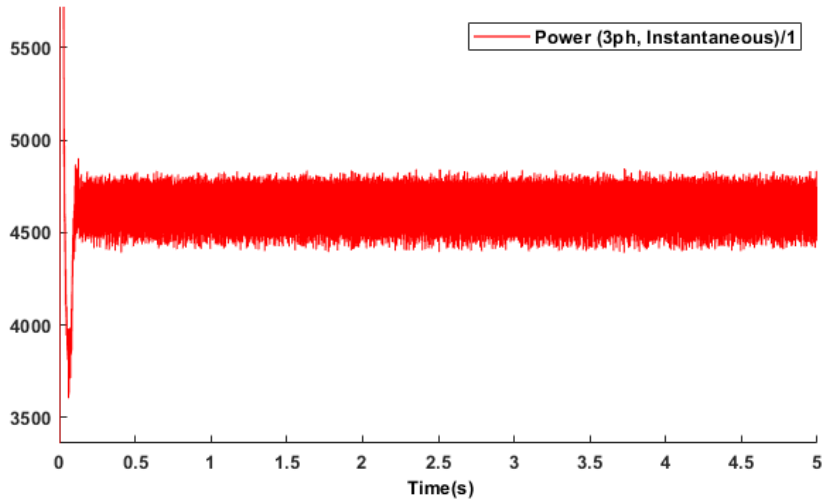

Figure 4.37. The power transferred to grid at discharging mode

The inverter output voltage and current graph is seen in Figure 4.38. It is seen from the graphs that the pf is zero.

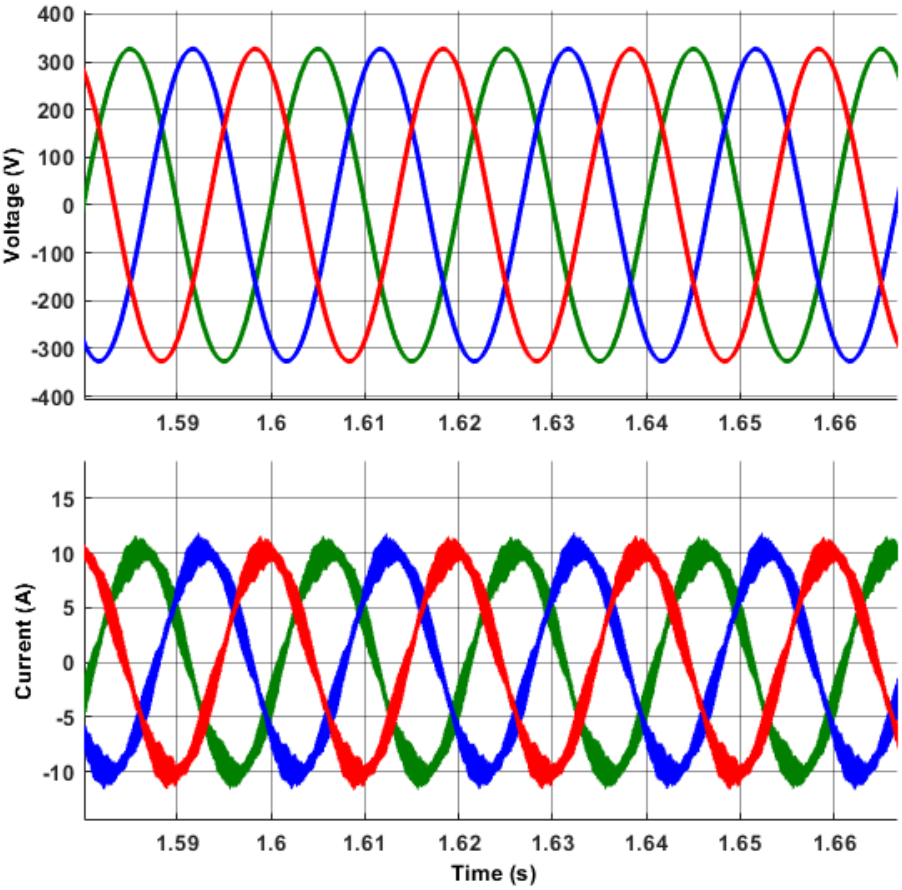

Figure 4.38. The voltage and current of inverter output for discharging mode

The power transfer from the battery to the grid is carried out via the DC-link. In this case, it is seen that the DC-link voltage oscillates between 705 V and 710 V in Figure 4.39 and 4.40.

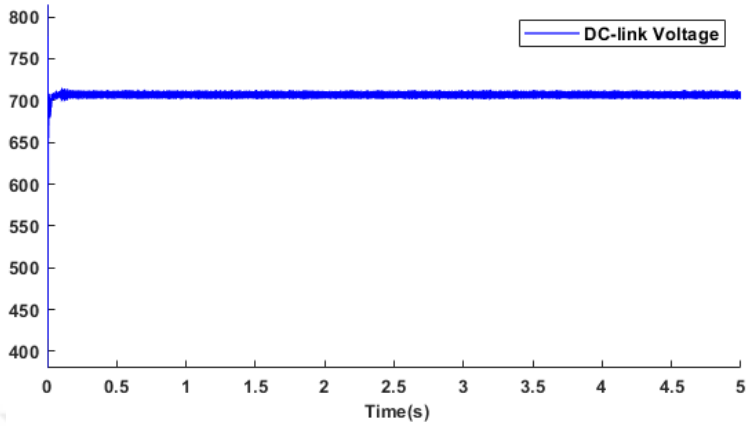

Figure 4.39. The DC-link voltage for discharging mode

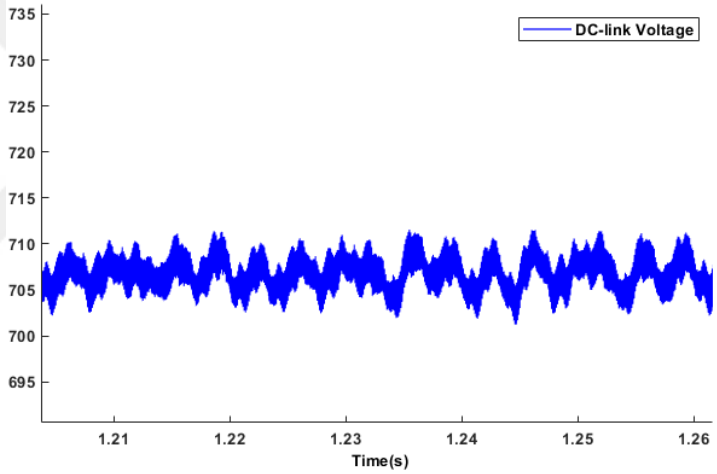

Figure 4.40. The DC-link voltage for discharging mode

It is seen from the Figure 4.41 that the THD decreases and increases by around 2% when the power is transferred from battery to grid.

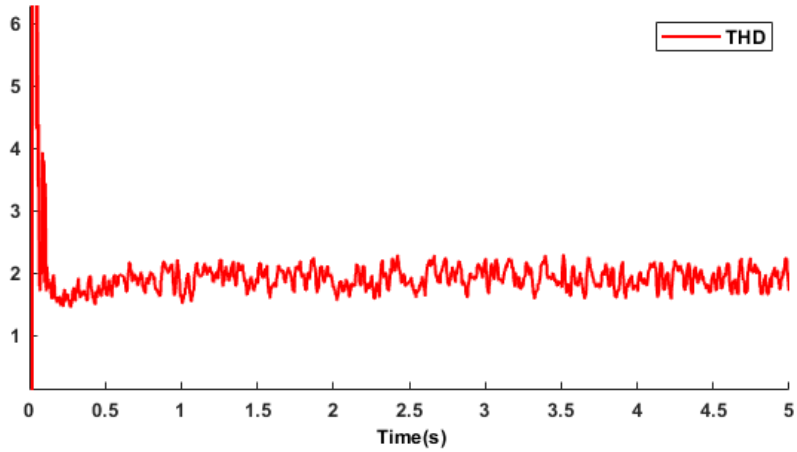

Figure 4.41. The THD of system for discharging mode

4.2. Incremental Conductance

4.2.1. Charging Mode

4.2.1.1. 1000 W/m^2 at 25 ˚C

The charging mode of the battery is simulated for 1000 W/m^2 irradiation at 25 ˚C temperature for the INC method, and graphic results are given in this section. For this situation to occur, the SOC of the battery must be below 90%. The maximum and minimum charging current is determined as 10. 43 A, 8.5 A respectively, for this situation. Figure 4.42 shows the SOC, current and voltage states when the battery is charging at 1000 W/m^2. The initial SOC value of the battery is given as 50% and it is observed on the graph that it increases. The battery is charged with a voltage value varying between 454 V and 456 V. The current value is between the maximum and minimum current values that we have mentioned before.

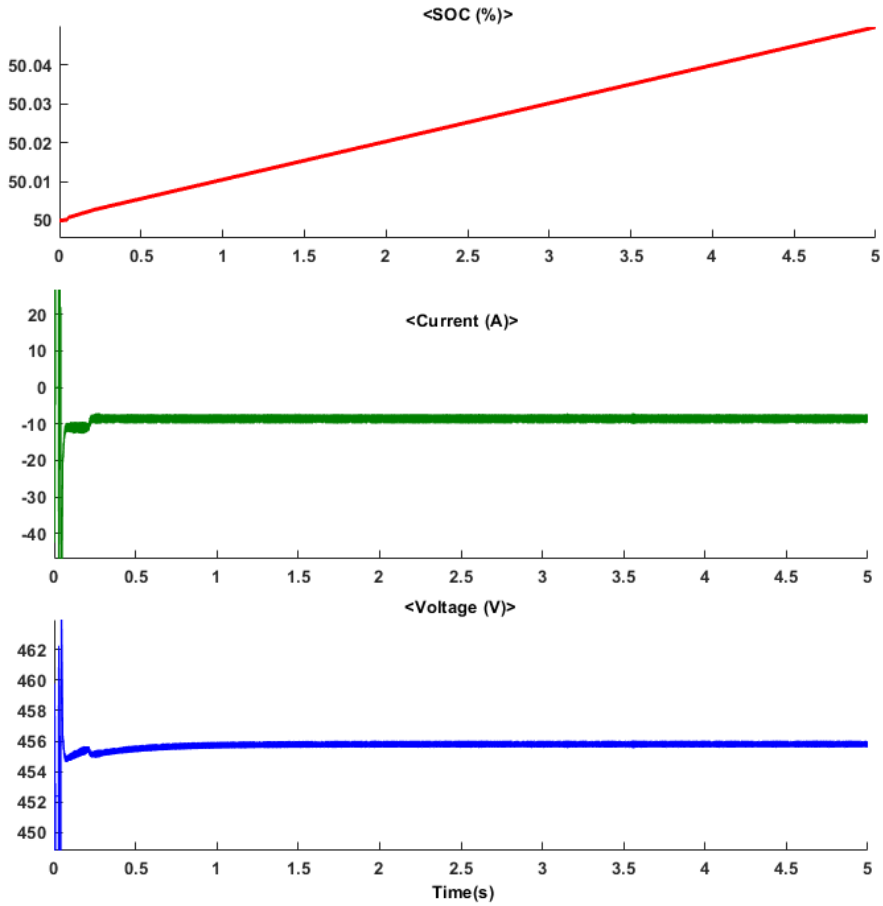

Figure 4.42. The SOC, current and voltage of the battery at charging process with INC at 1000 W/m^2

The produced PV power is shown in Figure 4.43. With the INC method, it is seen that the power produced by the PV is at the level of 12.45 kW.

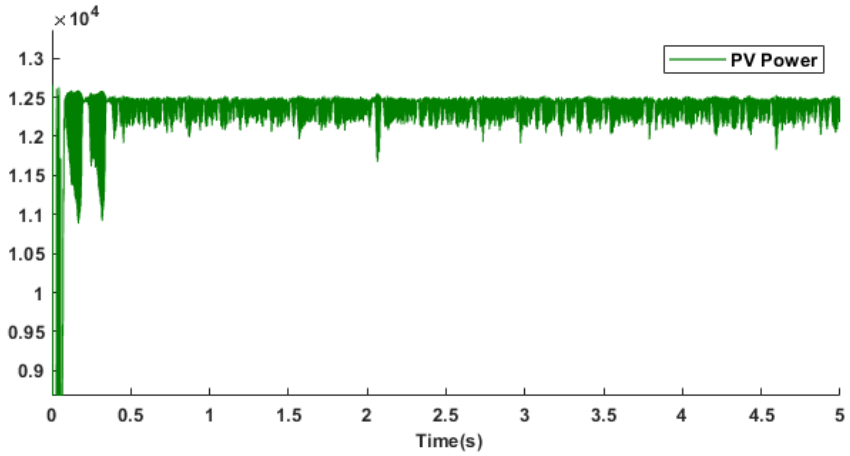

Figure 4.43. The produced PV power with INC for charging mode at 1000 W/m^2

The power transferred to the battery from this generated power is shown in the Figure 4.44.

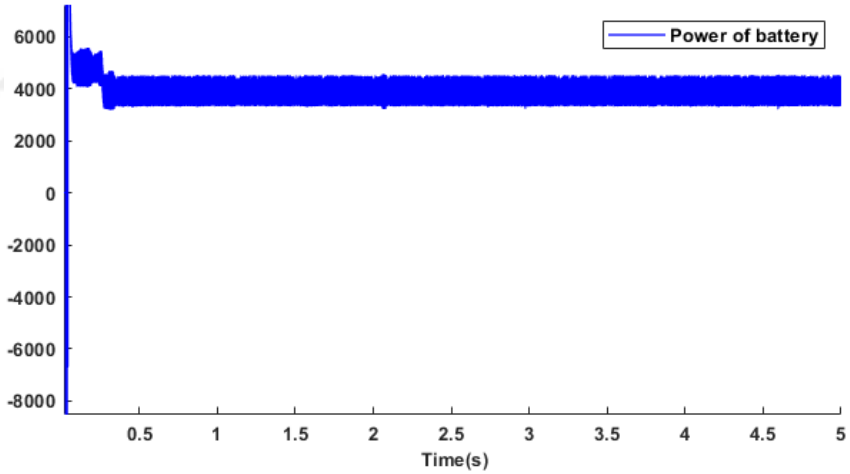

Figure 4.44. The power transferred to battery for charging mode with INC at 1000 W/m^2

The power transferred to the grid from this generated power is shown in the Figure 4.45.

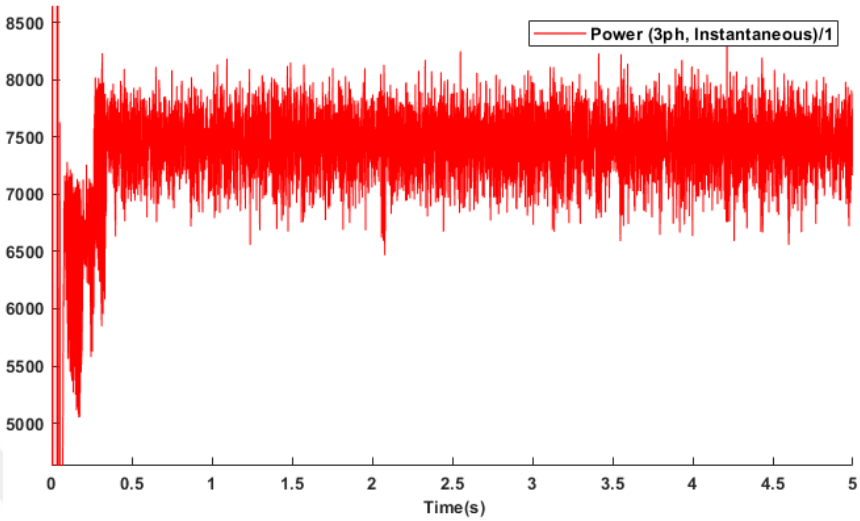

Figure 4.45. The power transferred to grid for charging mode with INC at 1000 W/m^2

In the charging state of the battery the inverter voltage and current graphs are shown in Figure 4.46. As can be seen from the graphs, the pf value is zero, the current and voltage graphs have the same phase angle.

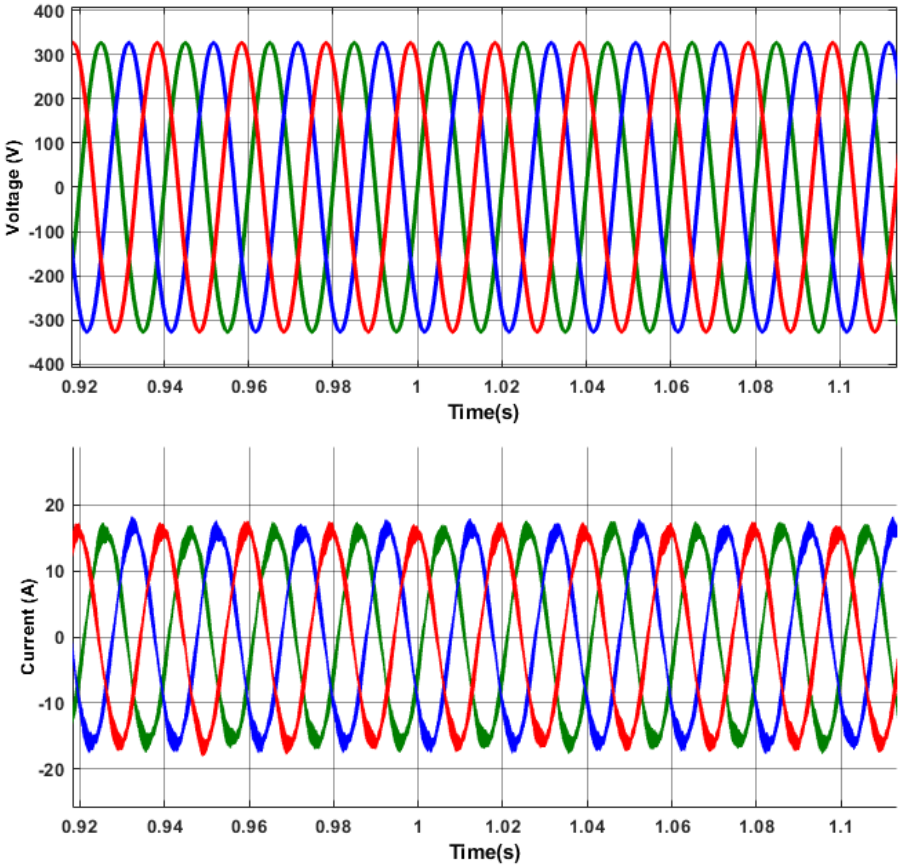

Figure 4.46. The voltage and current of inverter for charging mode with INC at 1000 W/m^2

While power transfer is provided from PV system to both the battery and the grid, the DC-link voltage should be at the specified level. Figure 4.47 and Figure 4.48 shows that this voltage varies between 700 V and 715 V.

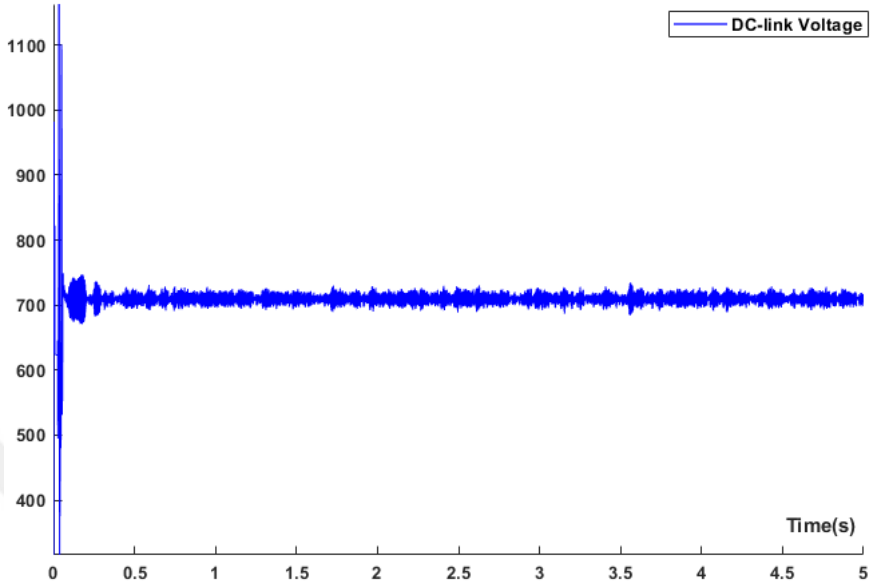

Figure 4.47. The DC-link voltage for charging mode with INC at 1000 W/m^2

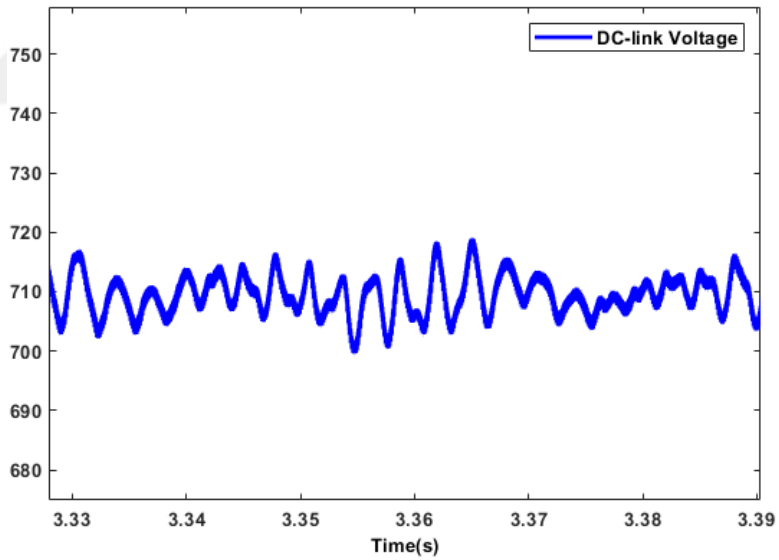

Figure 4.48. The DC-link voltage for charging mode with INC at 1000 W/m^2

The measurement of power efficiency in simulation studies is constantly changing due to small step size values, so efficiency is measured using the 'mean'

block, which is averaged power efficiency over the simulation period. The power efficiency graph is seen in Figure 4.49.

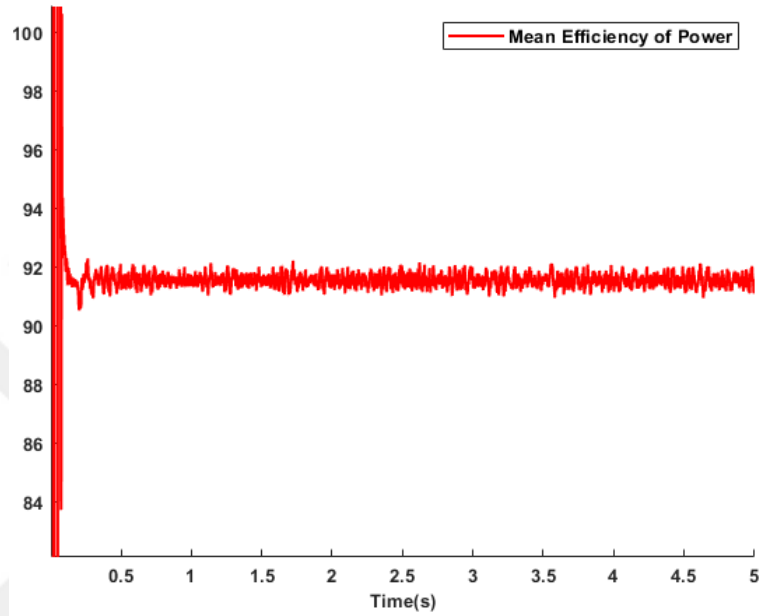

Figure 4.49. The efficiency of produced power for charging mode with INC at 1000 W/m^2

The THD for charging state is shown in Figure 4.50. THD of the system varies between 2% and 4%.

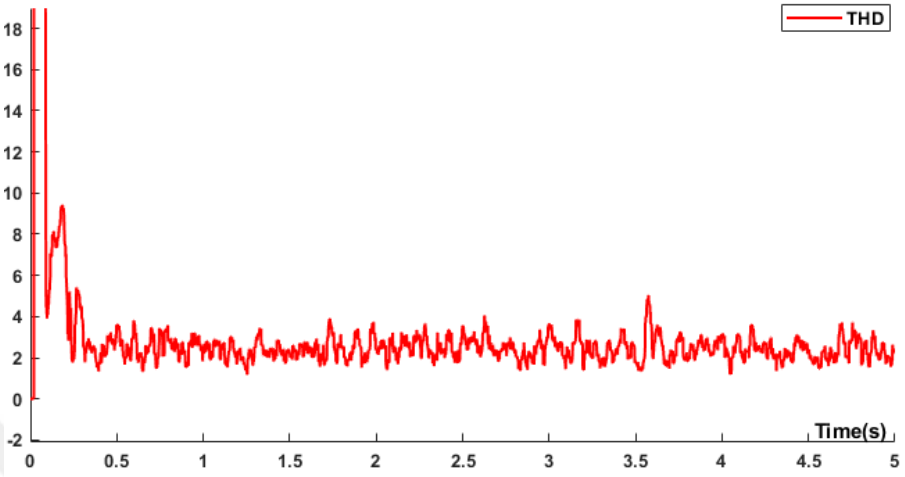

Figure 4.50. The THD of system for charging mode with INC at 1000 W/m^2

4.2.1.2. 500 W/m^2 at 25 ˚C

The charging mode for Inc Con method is analyzed for 500 W/m^2 irradiance at 25 ˚**C** temperature. The power generated from the PV system is transferred to both the battery and the grid. While examining this situation, the charging current of the battery is re-evaluated by calculating the power that the irradiation value can produce. While this transmission is taking place, the power produced must be balanced distributed. Large filters should be used for the inverter while the battery stores power with maximum current. To avoid this situation, the charging current is determined as 5 A for 500 W/m^2 irradiation, as shown in the Figure 4.51.

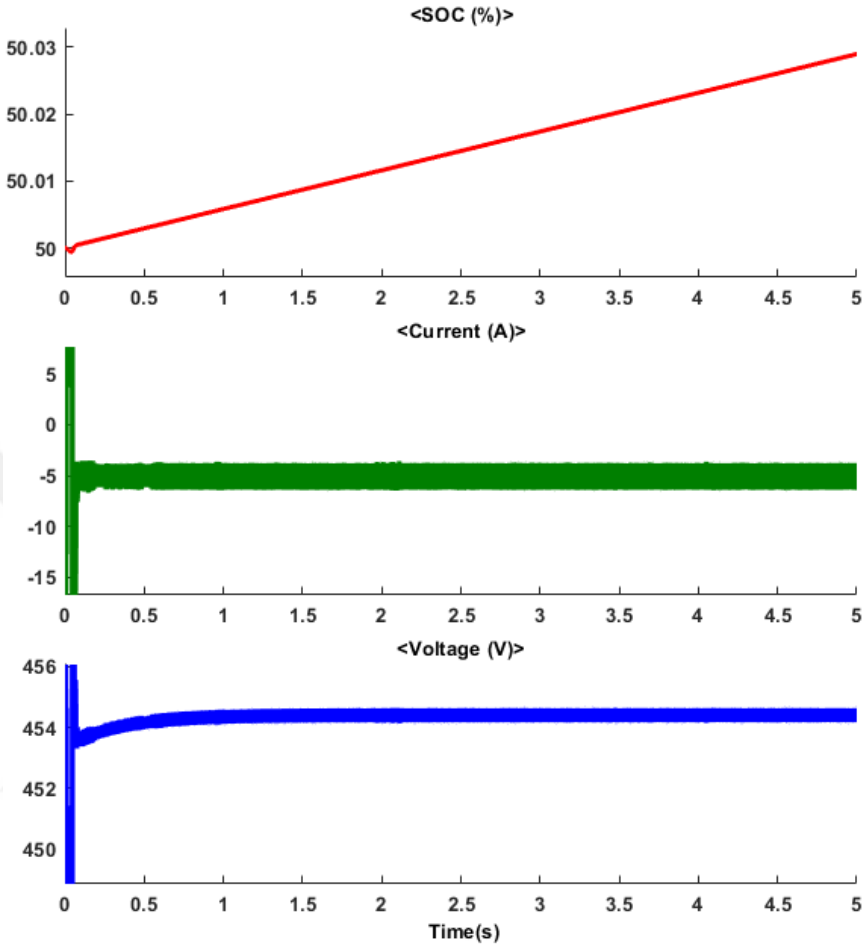

Figure 4.51. The SOC, voltage and current of the battery for charging mode with INC at 500 W/m^2

The produced PV power is shown in Figure 4.52. With the INC method, it is seen that the power produced by the PV oscillates around of 6.2 kW.

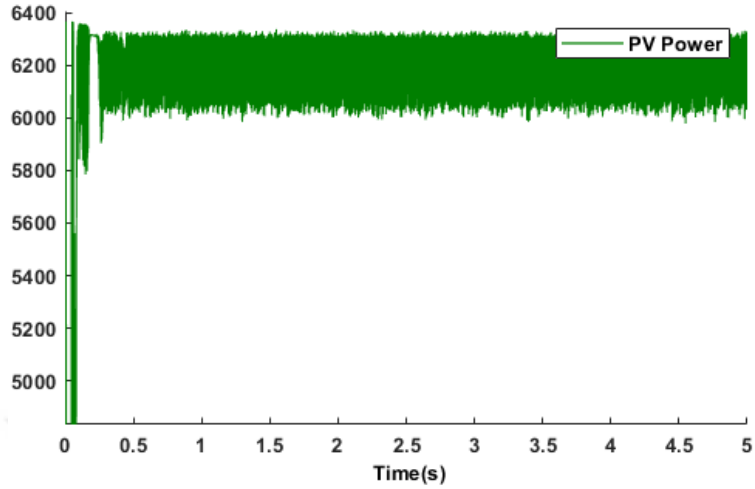

Figure 4.52. The produced PV power for charging mode with INC at 500 W/m^2

The power transferred to the battery from this generated power is shown in the Figure 4.53.

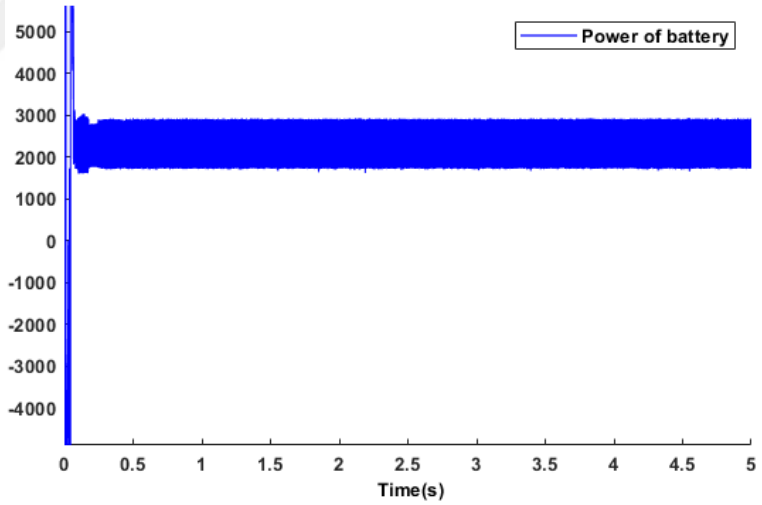

Figure 4.53. The power transferred to battery for charging mode with INC at 500 W/m^2

The power transferred to the grid from this generated power is shown in the Figure 4.54.

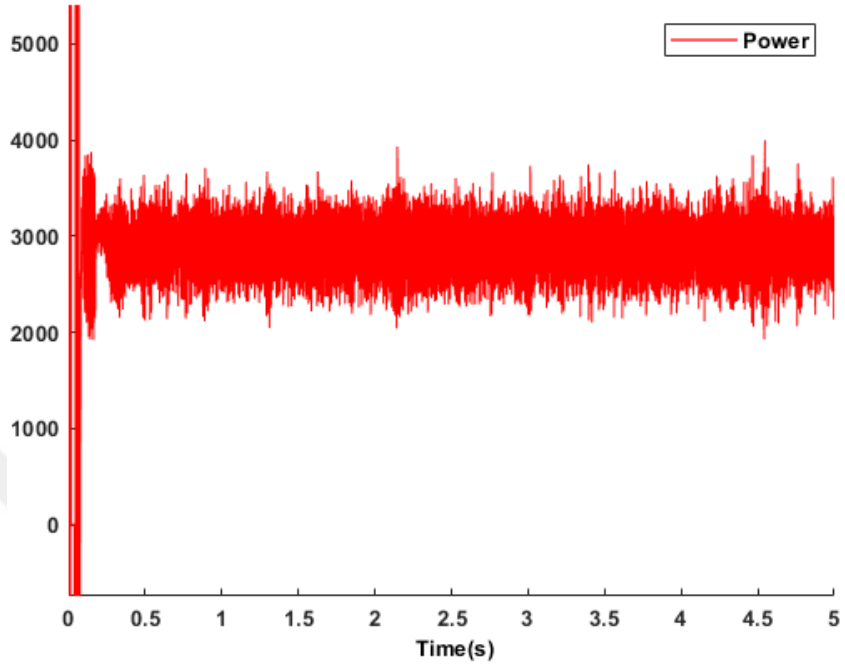

Figure 4.54. The power transferred to grid for charging mode with INC at 500 W/m^2

The inverter output voltage and current graphs are shown in Figure 4.55. It is seen that there is no phase difference between current and voltage and pf is zero.

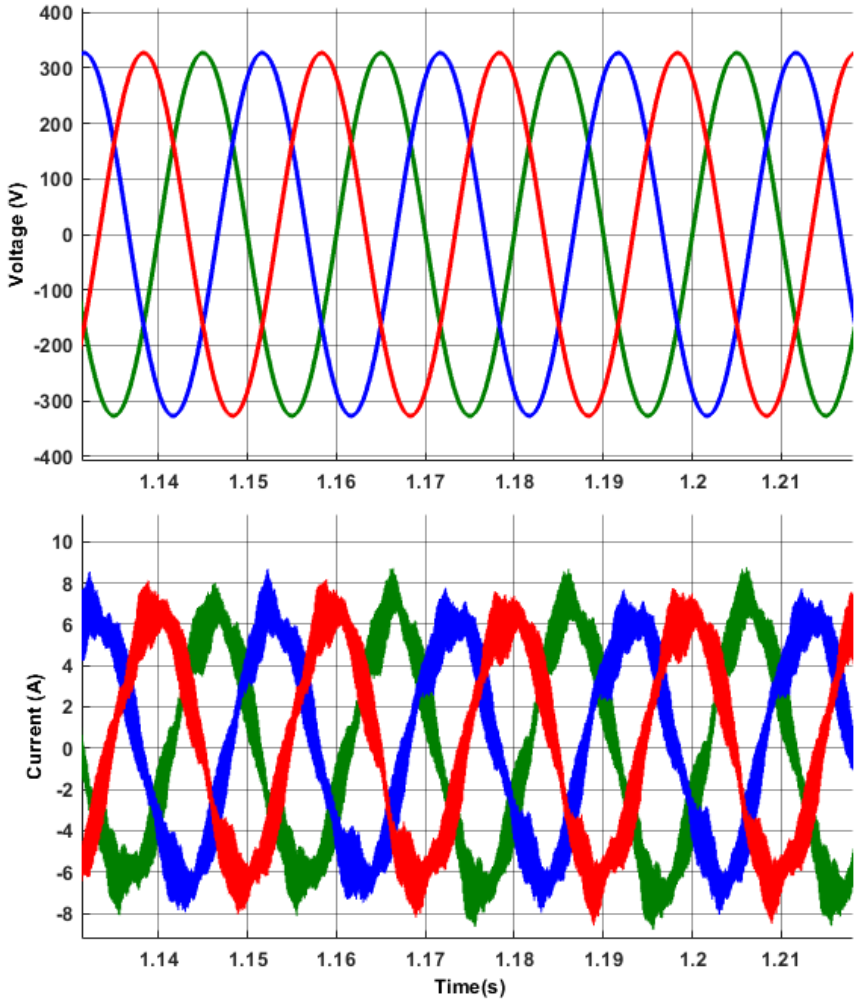

Figure 4.55. The voltage and current of inverter output for charging mode with INC at 500 W/m^2

It is observed that the oscillation is more than 1000 W/m^2 by looking at the current graph in Figure 4.55. The THD of the system is also shown in Figure 4.56. It is observed that the THD of the system increases at low irradiance.

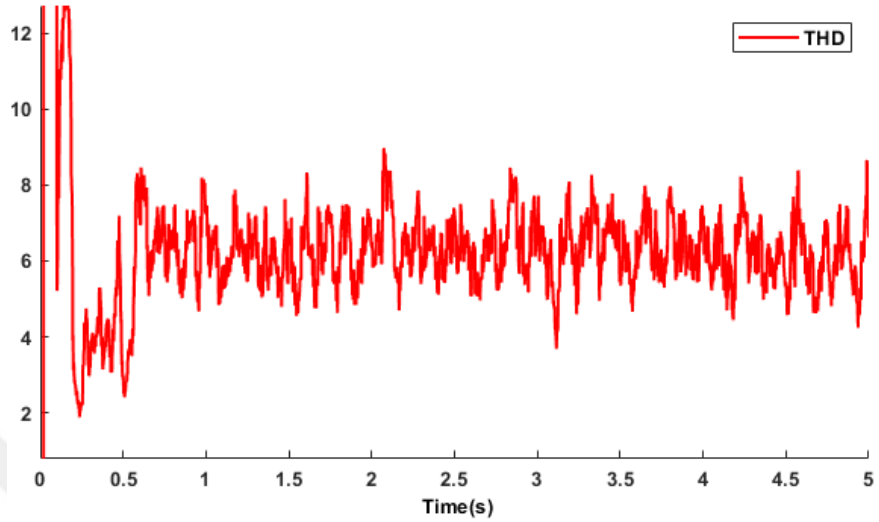

Figure 4.56. The THD of the system for charging mode with INC at 500 W/m^2

The THD of the system oscillates between 6% and 8% as seen in Figure 4.56. The power transfer takes place via the DC-link. The DC-link voltage oscillates between 705 V and 710 V. The graphic showing the DC-link voltage is seen in the Figure 4.57 and Figure 4.58.

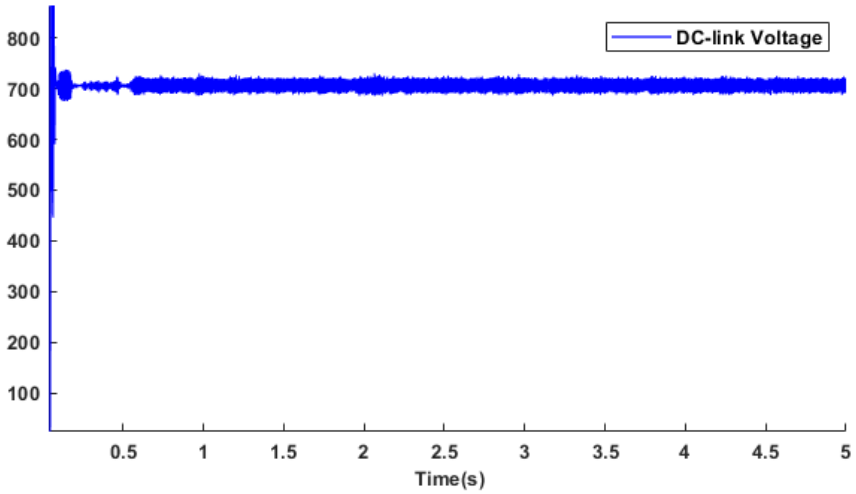

Figure 4.57. DC-link voltage for charging mode with INC at 500 W/m^2

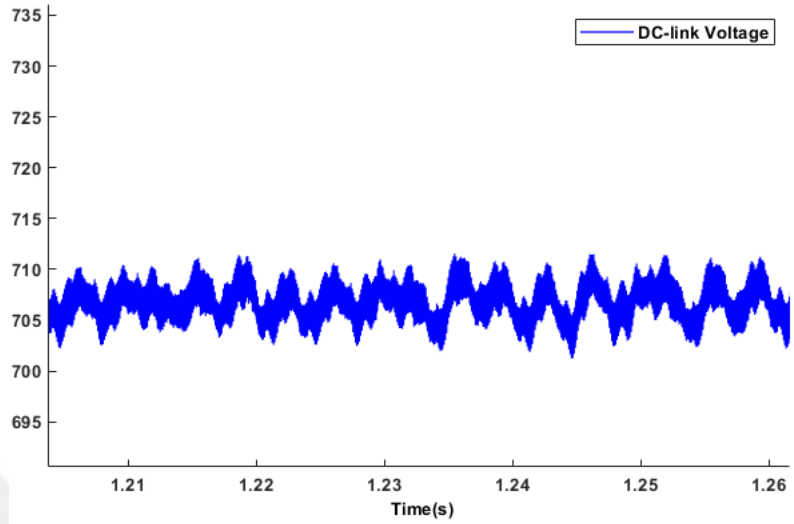

Figure 4.58. The DC-link voltage for charging mode with INC at 500 W/m^2

The efficiency of the generated power for 500 W/m^2 is given in Figure 4.59. Efficiency is between 83% and 84%.

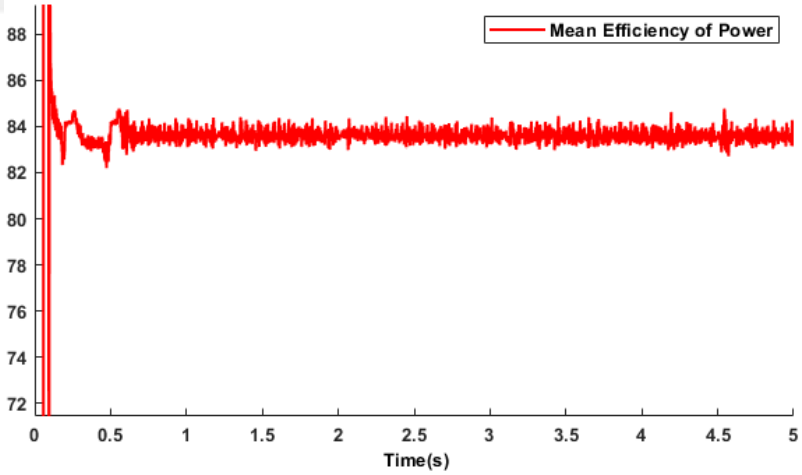

Figure 4.59. The efficiency of produced power for charging mode with INC at 500 W/m^2

4.2.2. PV to Grid Mode

4.2.2.1. 1000 W/m^2 at 25 ˚C

The PV to grid mode of the system is simulated for 1000 W/m^2 irradiation and 25 ˚C temperature values for the INC method, and graphic results are given in this section. For this situation to occur, the SOC of the battery must be above or equal to 90%. In this case all the power produced by the PV is transferred to the grid. The inverter output voltage and current graph is shown in the Figure 4.60 for 1000 W/m^2. As seen in Figure 4.60 the pf value is zero, the current and voltage graphs have the same phase angle. As seen in Figure 4.60, the maximum phase voltage value is 325 V, and the current value is maximum 25 A. This value is the maximum value of the current per phase.

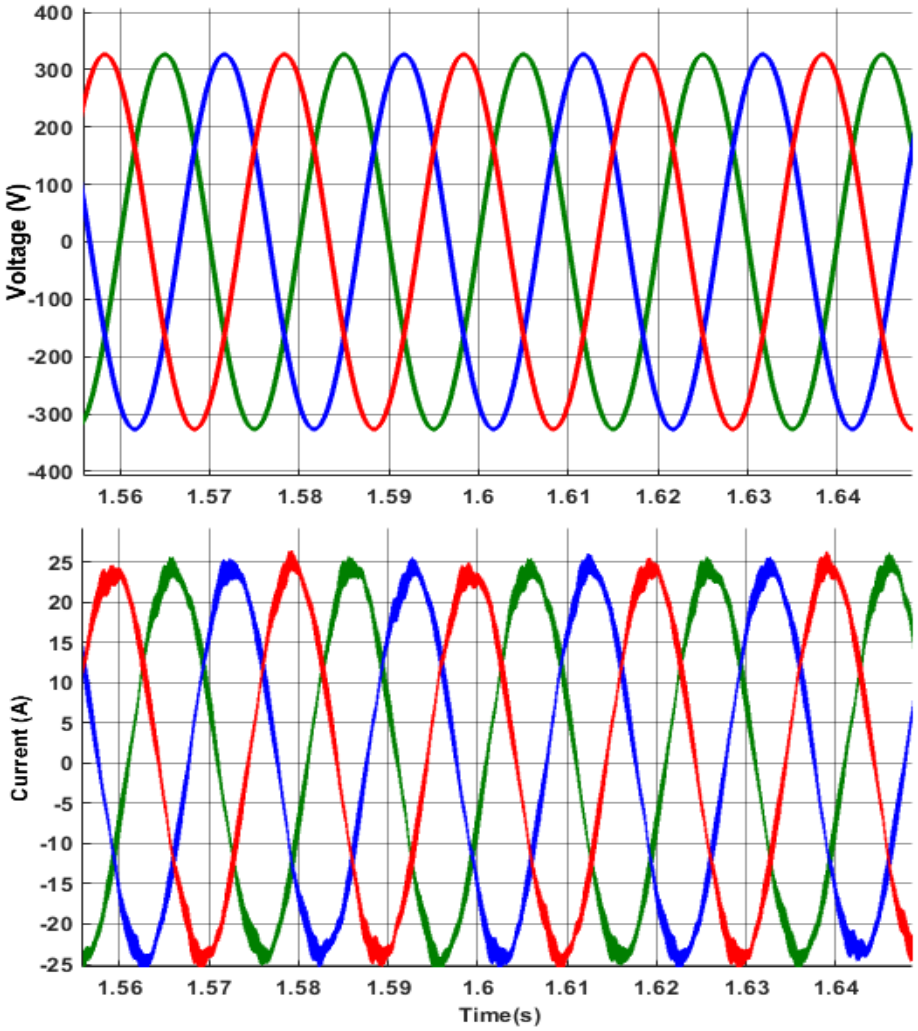

Figure 4.60. The voltage and current of inverter output for PV to grid mode with INC at 1000 W/m^2

The produced PV power is shown in Figure 4.61. With the INC method, it is seen that the power produced by the PV is at the level is between 12.4 kW and 12.45 kW.

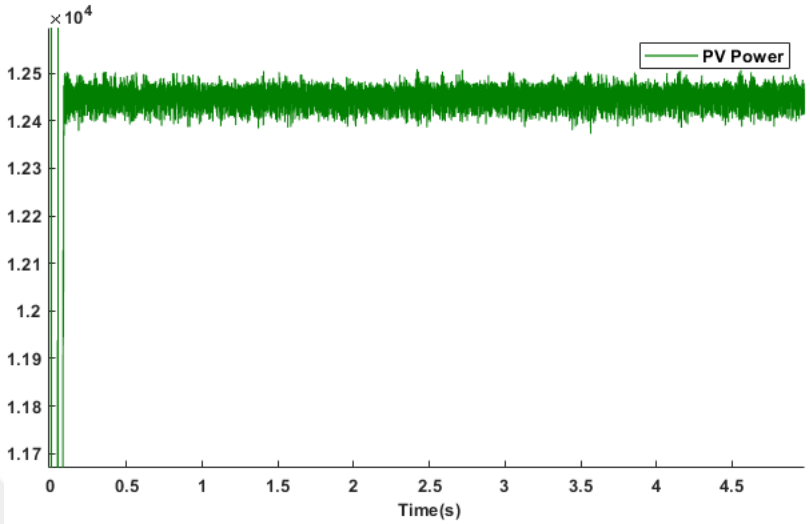

Figure 4.61. The produced PV power with INC for PV to grid mode at 1000 W/m^2

The power transferred to the grid from this generated power is shown in the Figure 4.62.

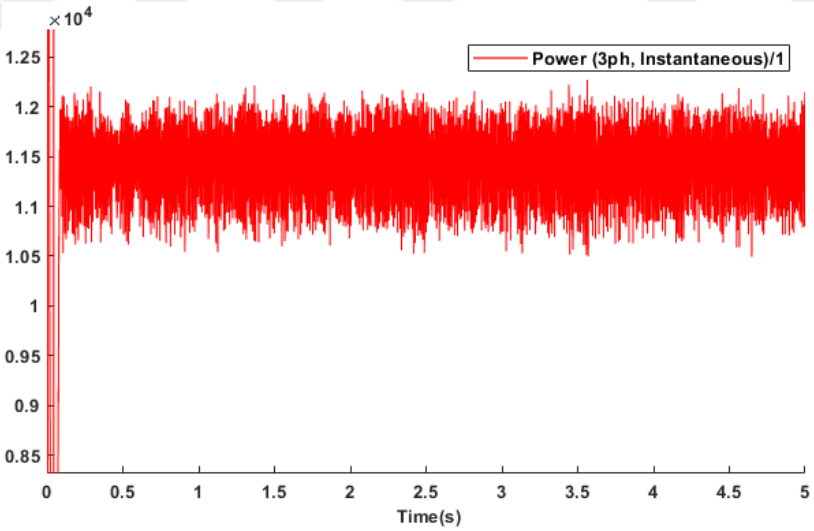

Figure 4.62. The power transferred to the grid with INC for PV to grid mode at 1000 W/m^2

In this case, as the SOC value of the battery is given as 90%, as seen in Figure 4.63, the battery should not be charged at all.

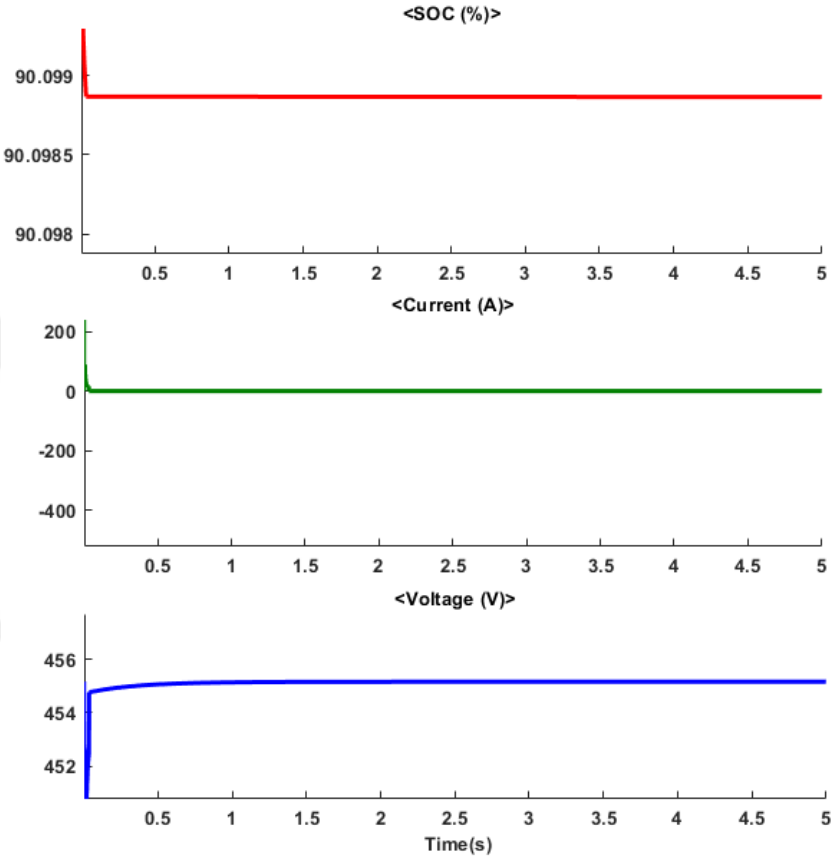

Figure 4.63. The SOC, voltage and current of the battery for PV to grid mode with INC at 1000 W/m^2

In Figure 4.64 and Figure 4.65, it is seen that the DC-link voltage oscillates between 705 V and 715 V.

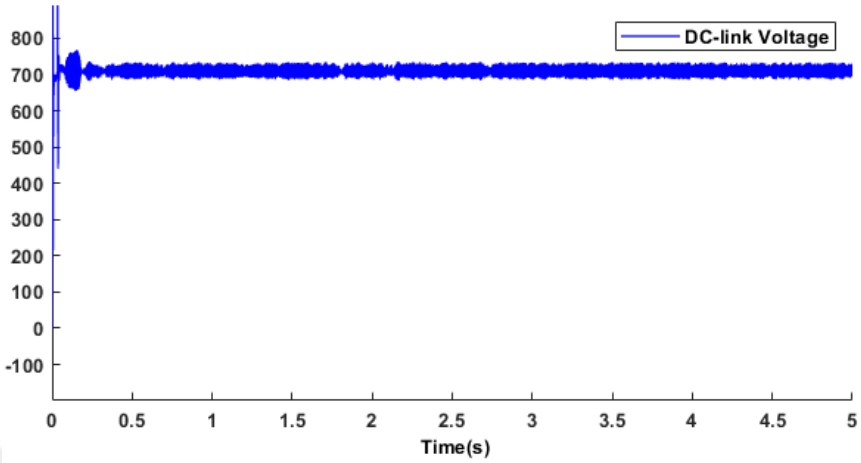

Figure 4.64. The DC-link voltage for PV to grid mode with INC at 1000 W/m^2

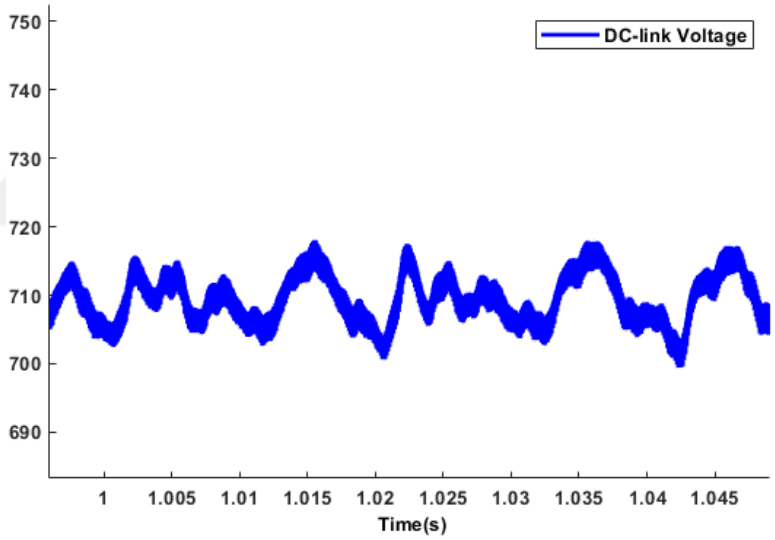

Figure 4.65. The DC-link voltage for PV to grid mode with INC at 1000 W/m^2

The power efficiency of the system for PV to grid mode is seen in Figure 4.66 as 92%.

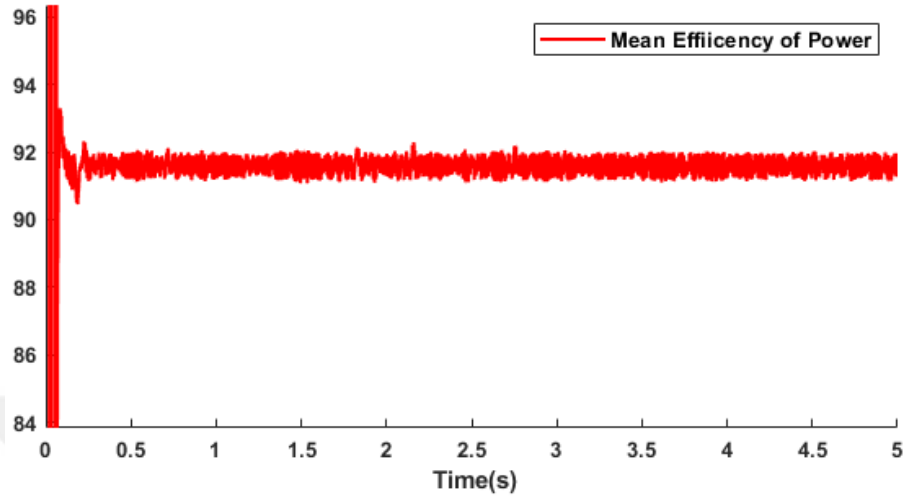

Figure 4.66. The efficiency of produced power for PV to grid mode with INC at 1000 W/m^2

The THD of the system is seen in Figure 4.67. The THD varies between 1% and 3%.

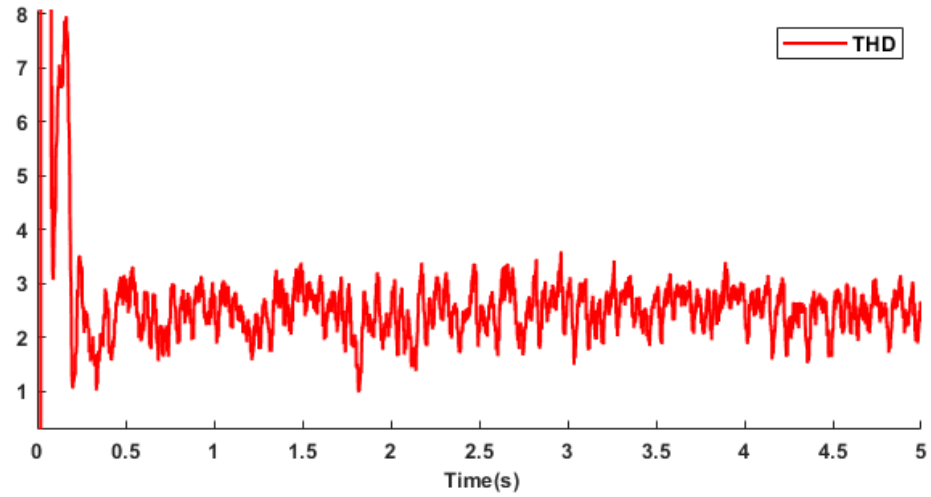

Figure 4.67. The THD of system for PV to grid mode with INC at 1000 W/m^2

4.2.2.2. 500 W/m^2 at 25 ˚C

The PV to grid mode of the system is simulated for 500 W/m^2 irradiation and 25 ˚C temperature values for the INC method, and graphic results are given in this section. For this situation to occur, the SOC of the battery must be above or equal to 90%. In this case all the power produced by the PV is transferred to the grid. The inverter output voltage and current graph is shown in the Figure 4.68 for 500 W/m^2. As seen in Figure 4.68 the pf value is zero, the current and voltage graphs have the same phase angle. As seen in Figure 4.68, the maximum phase voltage value is 325 V, and the current value is maximum 12.5 A. This value is the maximum value of the current per phase.

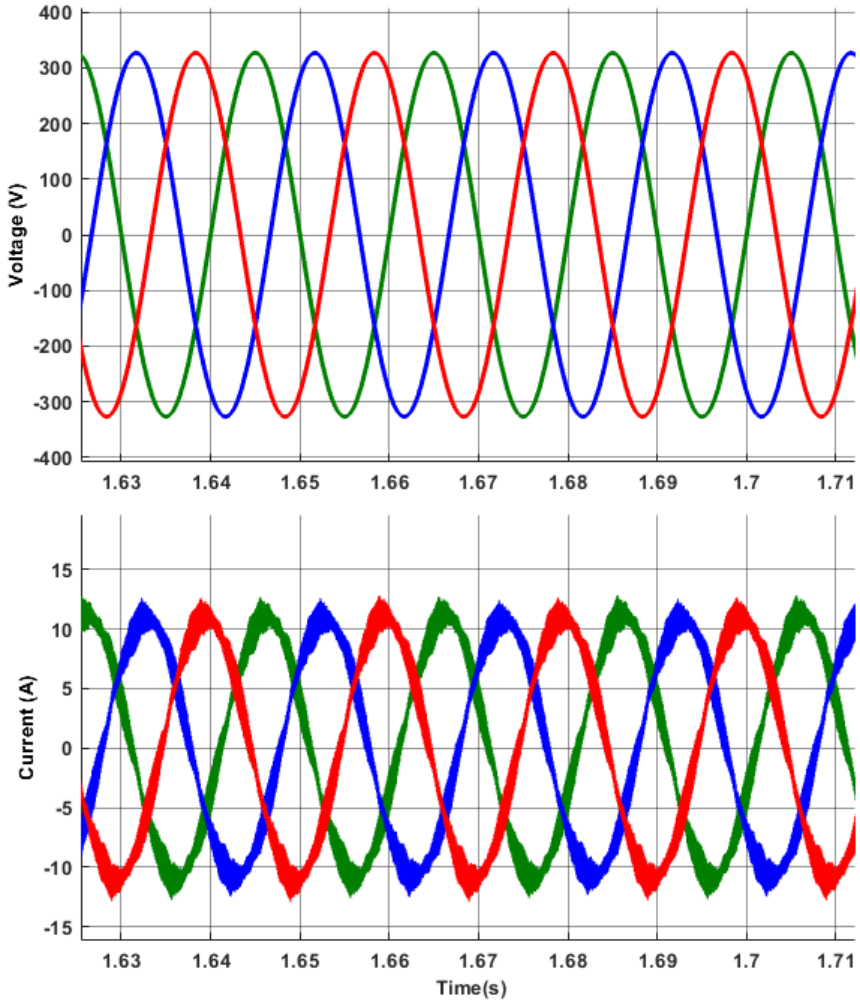

Figure 4.68. The voltage and current of inverter output for PV to grid mode with INC at 500 W/m^2

The produced PV power is shown in Figure 4.69. With the INC method, it is seen that the power produced by the PV is at the level is between 6 kW and 6.2 kW.

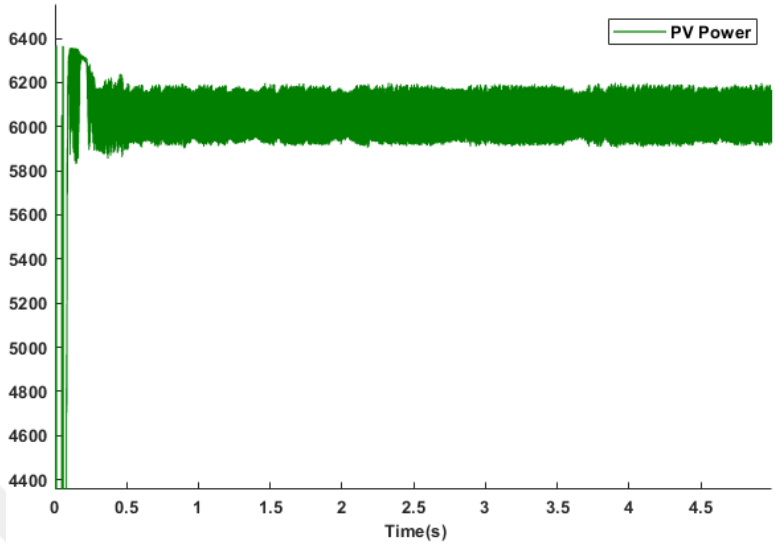

Figure 4.69. The produced PV power with INC for PV to grid mode at 500 W/m^2

The power transferred to the grid from this generated power is shown in the Figure 4.70.

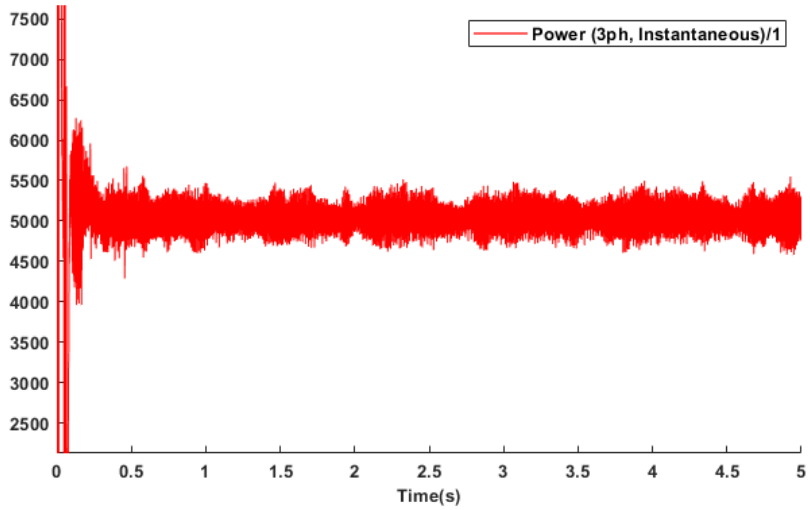

Figure 4.70. The power transferred to the grid with INC for PV to grid mode at 500 W/m^2

In this case, as the SOC value of the battery is given as 90%, as seen in Figure 4.71, the battery should not be charged at all.

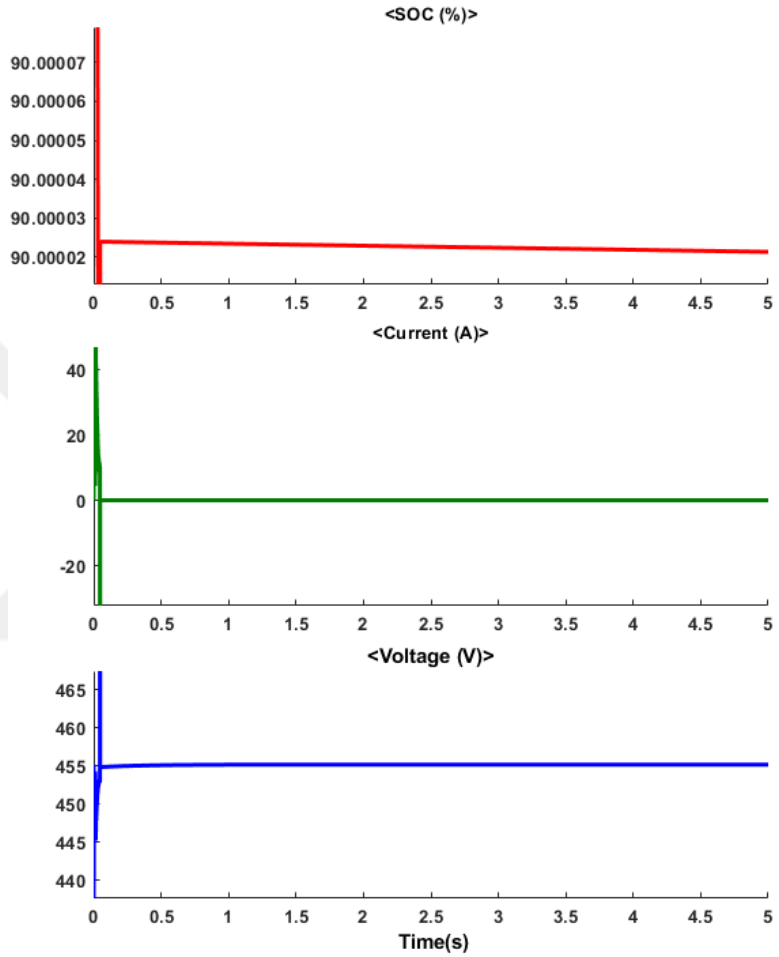

Figure 4.71. The SOC, current and voltage of battery for PV to grid mode with INC at 500 W/m^2

In Figure 4.72 and Figure 4.73, it is seen that the DC-link voltage oscillates around 700 V and 715 V.

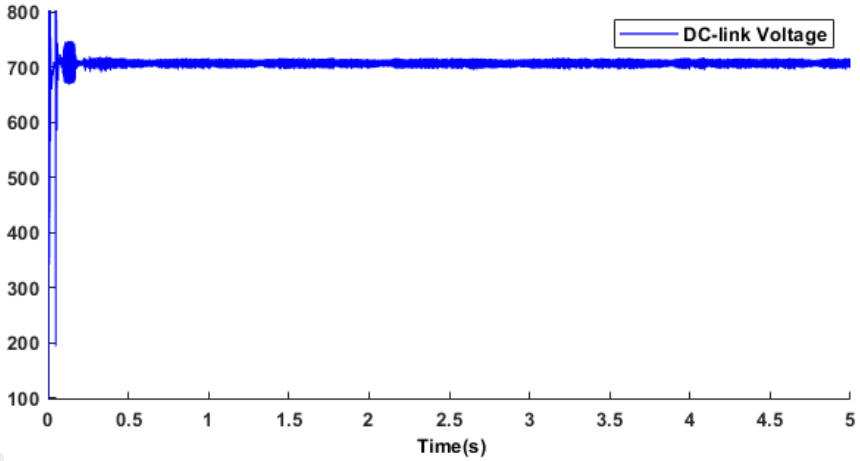

Figure 4.72. DC-link voltage for PV to grid mode with INC at 500 W/m^2

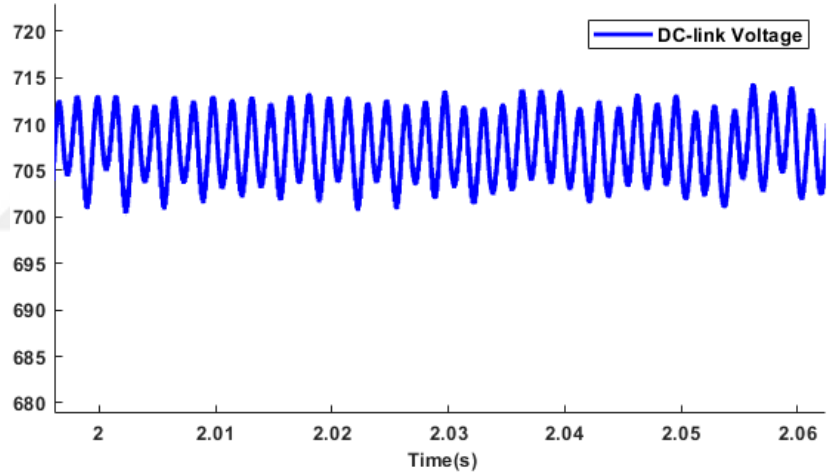

Figure 4.73. DC-link voltage for PV to grid mode with INC at 500 W/m^2

The power efficiency for the PV-to-grid mode of the system is seen in Figure 4.74 as close to 83%.

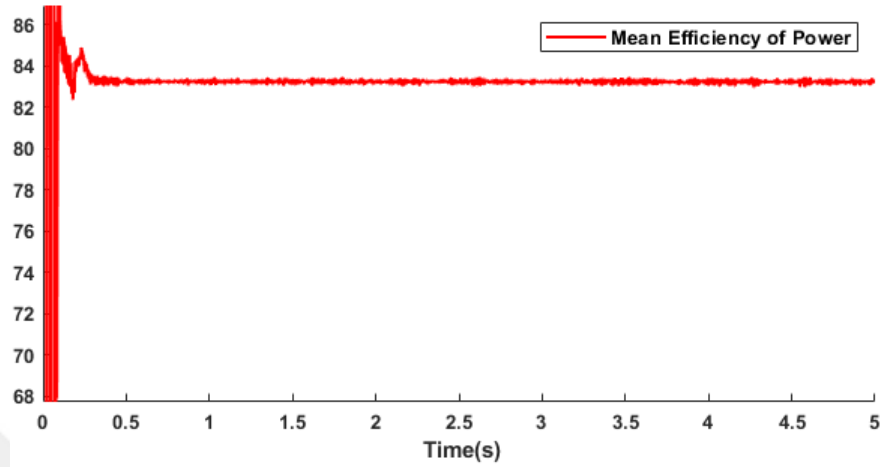

Figure 4.74. The efficiency of produced power for PV to grid mode with INC at 500 W/m^2

The THD of the system is seen in Figure 4.75. The THD varies between 2% and 4%.

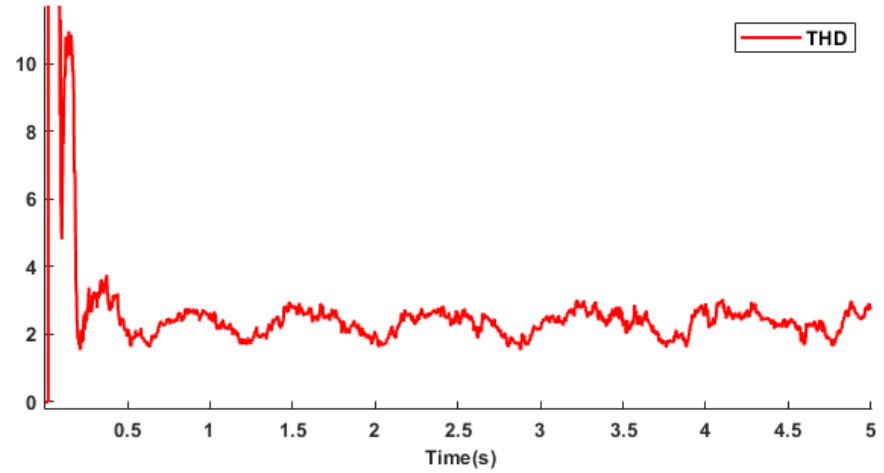

Figure 4.75. The THD of system for PV to grid mode with INC at 500 W/m^2

4.2.3. Discharging Mode Battery to Grid

The results of discharging mode for Inc Con method are shown in this part. The discharging mode occurs when the SOC is above %50 and P_{PV} is lower than 620

W. The battery is assumed to be fully charged before discharging. The SOC of the battery is 90%. The battery discharge current ranges from a maximum of 10.43 A to a minimum of 8.5 A. SOC, voltage, and current graphs for the discharge mode of the battery are shown in the Figure 4.76.

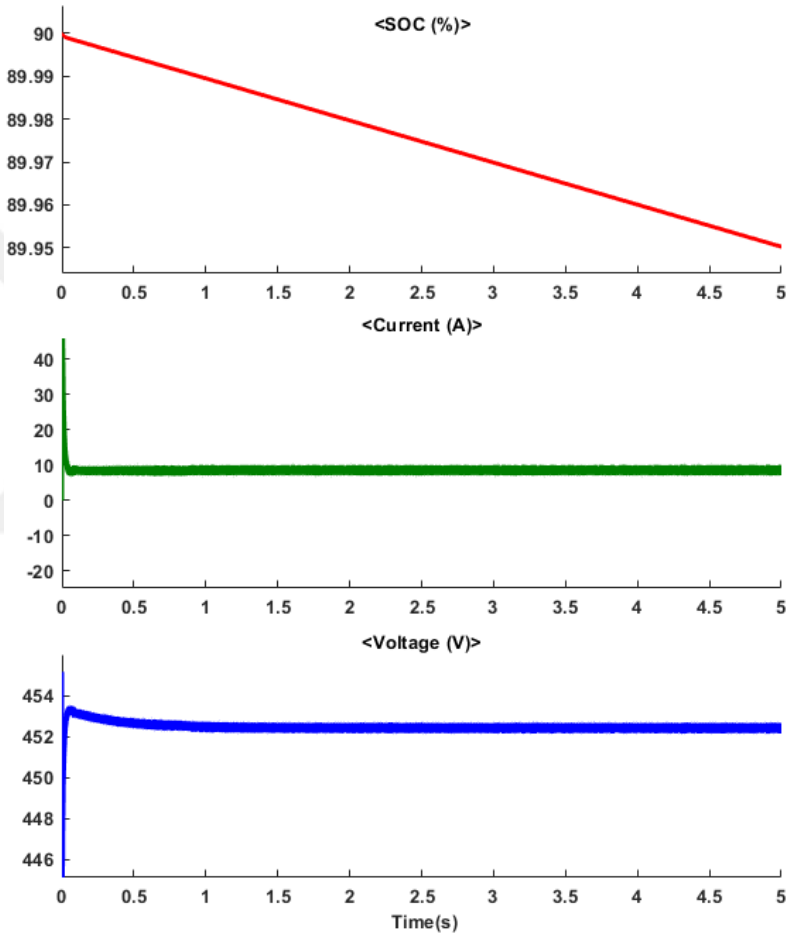

Figure 4.76. Discharging mode of the battery

The battery power is seen in Figure 4.77 when the battery is discharging mode.

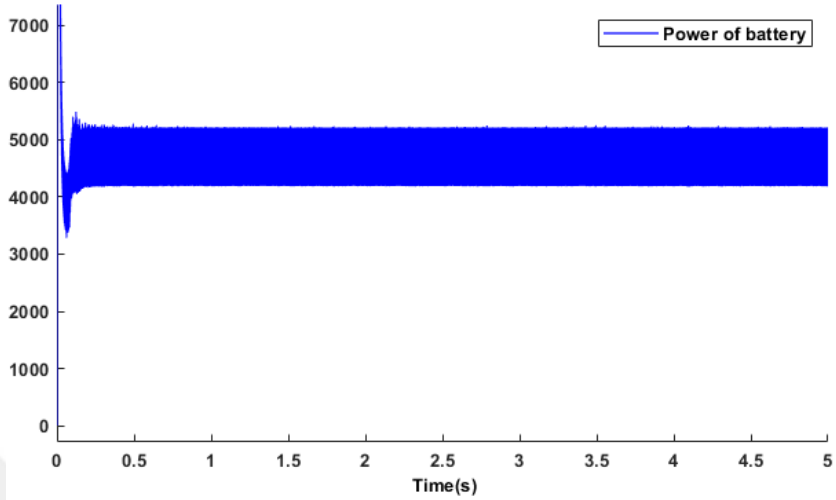

Figure 4.77. The battery power for discharging mode

The power transferred from the battery to the grid is displayed in Figure 4.78.

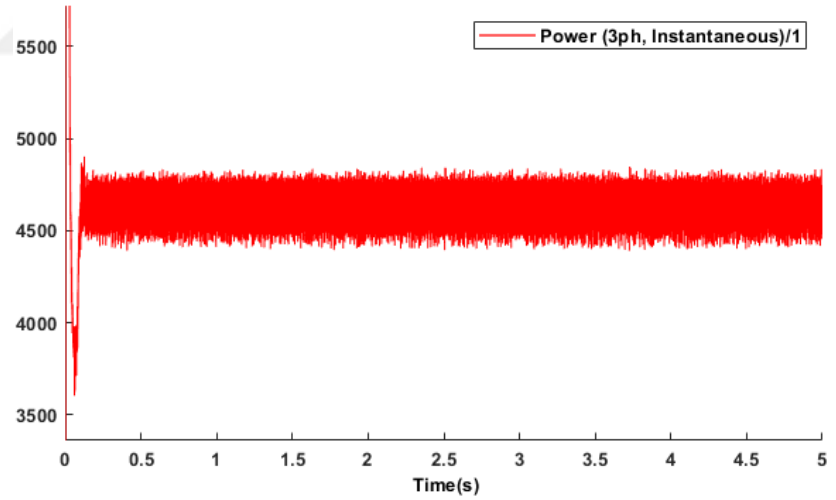

Figure 4.78. The power transferred to grid at discharging mode

The power transfer from the battery to the grid is carried out via the DC-link. In this case, it is seen that the DC-link voltage oscillates between 705 V and 710 Vdc in Figure 4.79 and Figure 4.80.

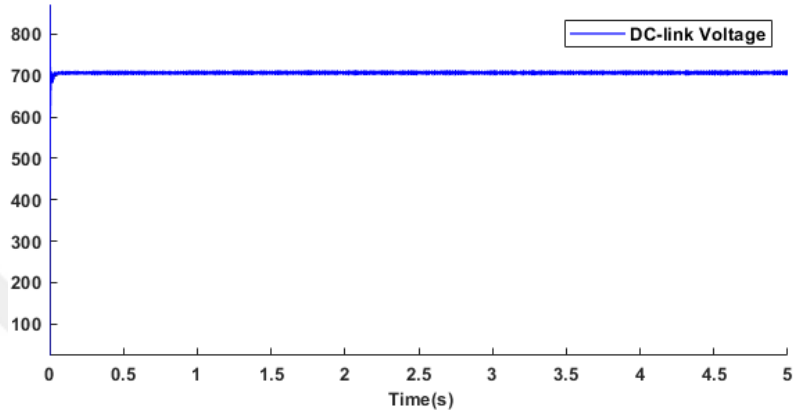

Figure 4.79. The DC-link voltage for discharging mode

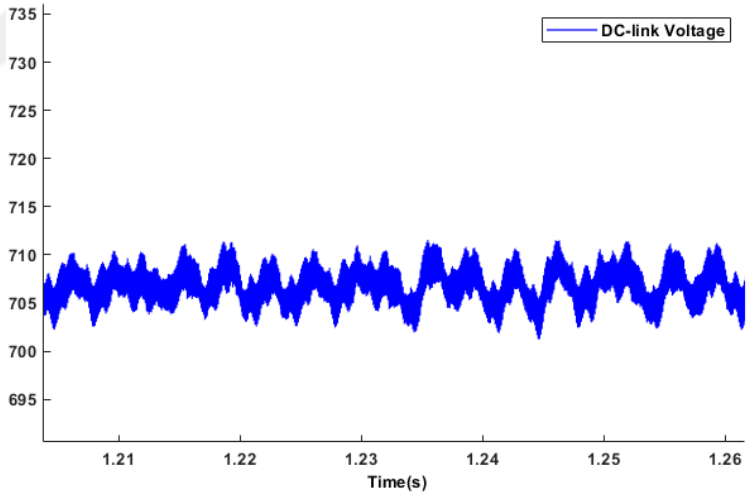

Figure 4.80. The DC-link voltage for discharging mode

The inverter output voltage current graph for the discharge mode is shown in the Figure 4.81.

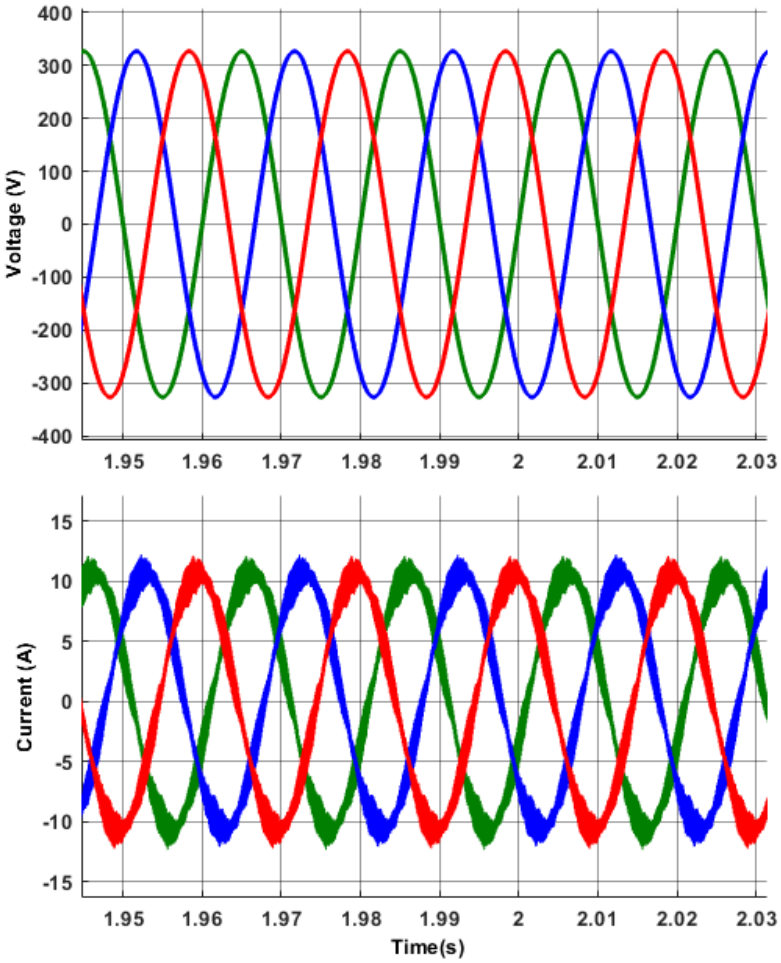

Figure 4.81. The voltage and current of inverter output for discharging mode

System THD is seen as close to 2% while the battery is being discharged. Figure 4.82 is given.

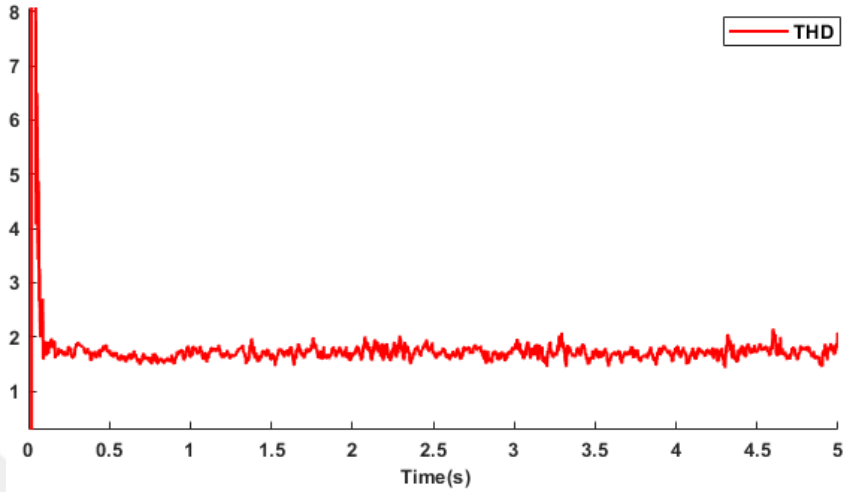

Figure 4.82. The THD of the system for discharging mode

4.3. Proposed ANN-based MPPT method

4.3.1. Charging Mode

4.3.1.1. 1000 W/m^2 at 25 ˚C

The charging mode of the battery is simulated for 1000 W/m^2 irradiation at 25 ˚C temperature for the ANN method, and graphic results are given in this section. For this situation to occur, the SOC of the battery must be below 90%. The maximum and minimum charging current is determined as 10. 43 A, 8.5 A respectively, for this situation. Figure 4.83 shows the SOC, current and voltage graphs when the battery is charging at 1000 W/m^2 from PV system. The initial SOC value of the battery is given as 50% and it is observed on the graph that SOC increases. The battery is charged with a voltage value varying between 454 V and 456 V. The current value is between the maximum and minimum current values.

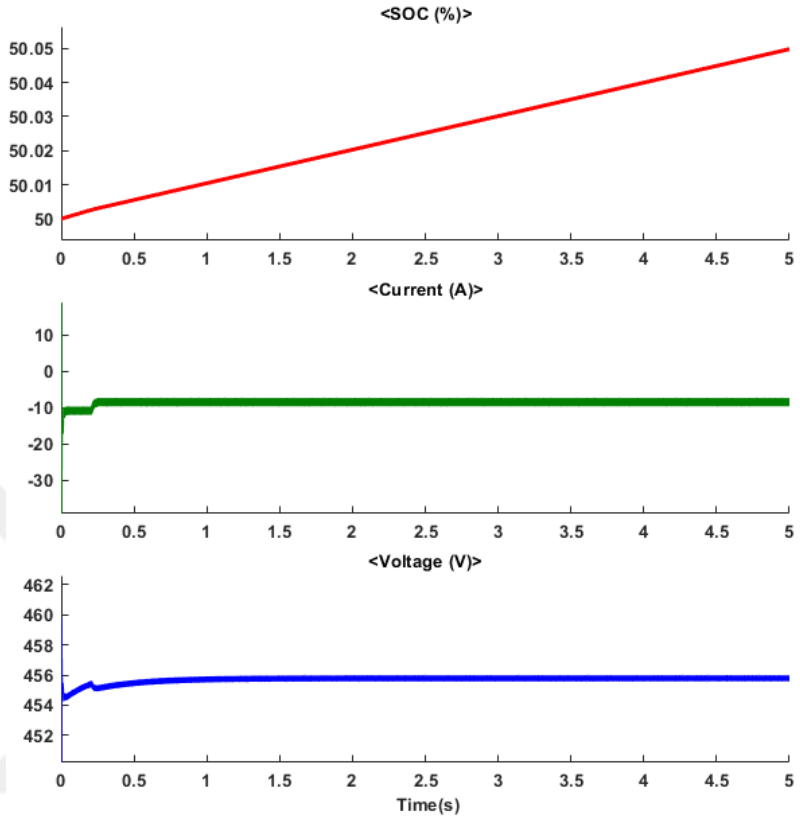

Figure 4.83. The SOC, current and voltage of battery for charging mode with ANN-based method at 1000 W/m^2

The produced PV power is shown in Figure 4.84. With the ANN-based method, it is seen that the power produced by the PV is at the level of 12.48 kW.

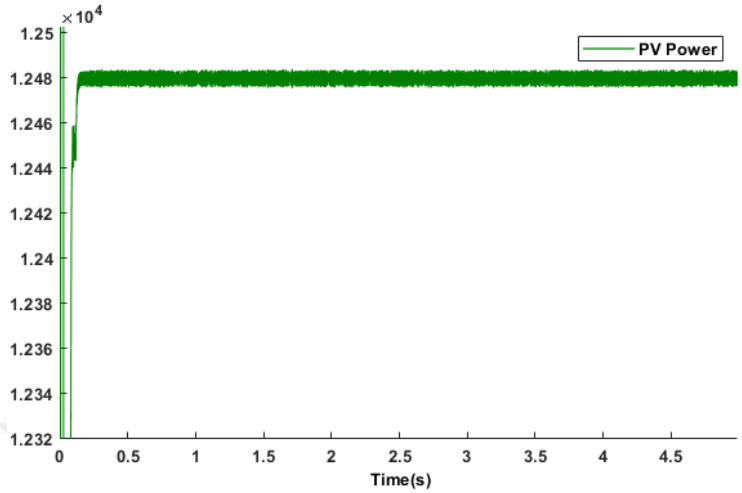

Figure 4.84. The produced PV power with ANN-based method for charging mode at 1000 W/m^2

The power transferred to the battery from this generated power is shown in the Figure 4.85.

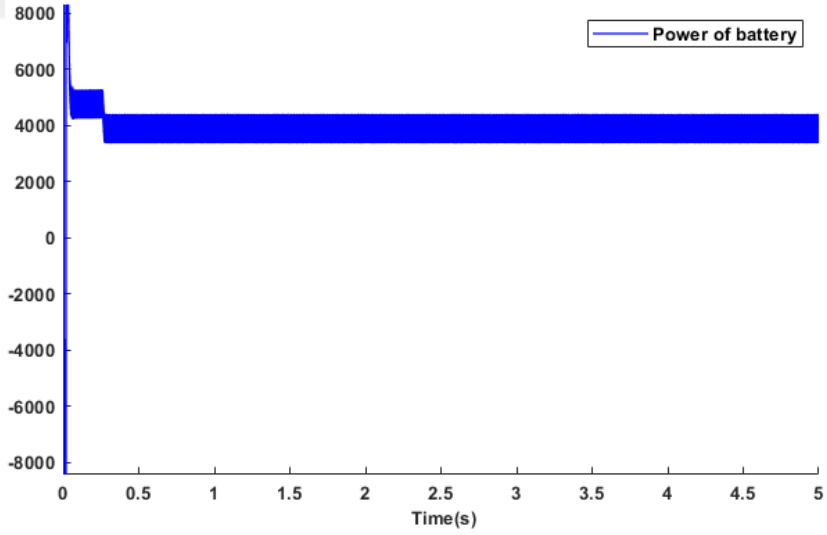

Figure 4.85. The power transferred to battery for charging mode with ANN-based method at 1000 W/m^2

The power transferred to the grid from this generated power is shown in the Figure 4.86.

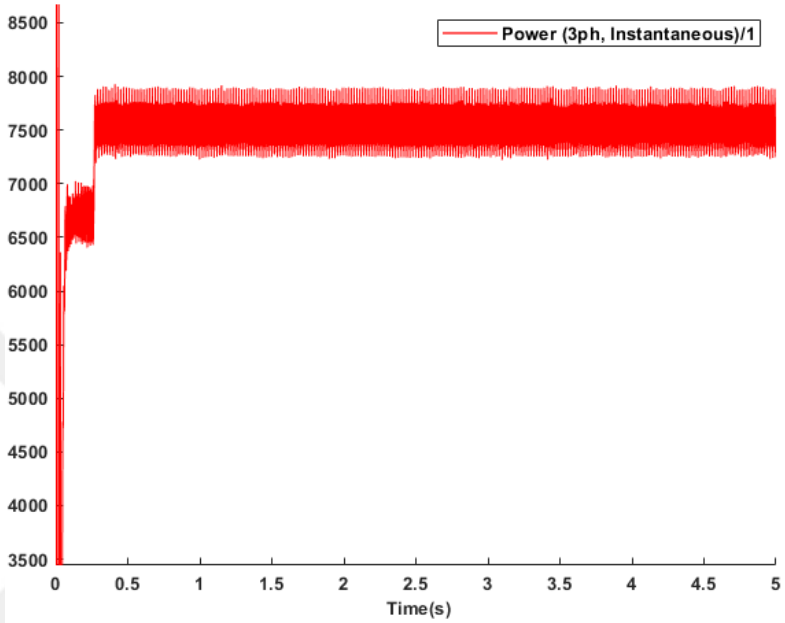

Figure 4.86. The power transferred to grid for charging mode with ANN-based method at 1000 W/m^2

In the charging state of the battery the inverter output voltage and current graphs are shown in Figure 4.87. As can be seen from the graphs, the pf value is zero, the current and voltage graphs have the same phase angle.

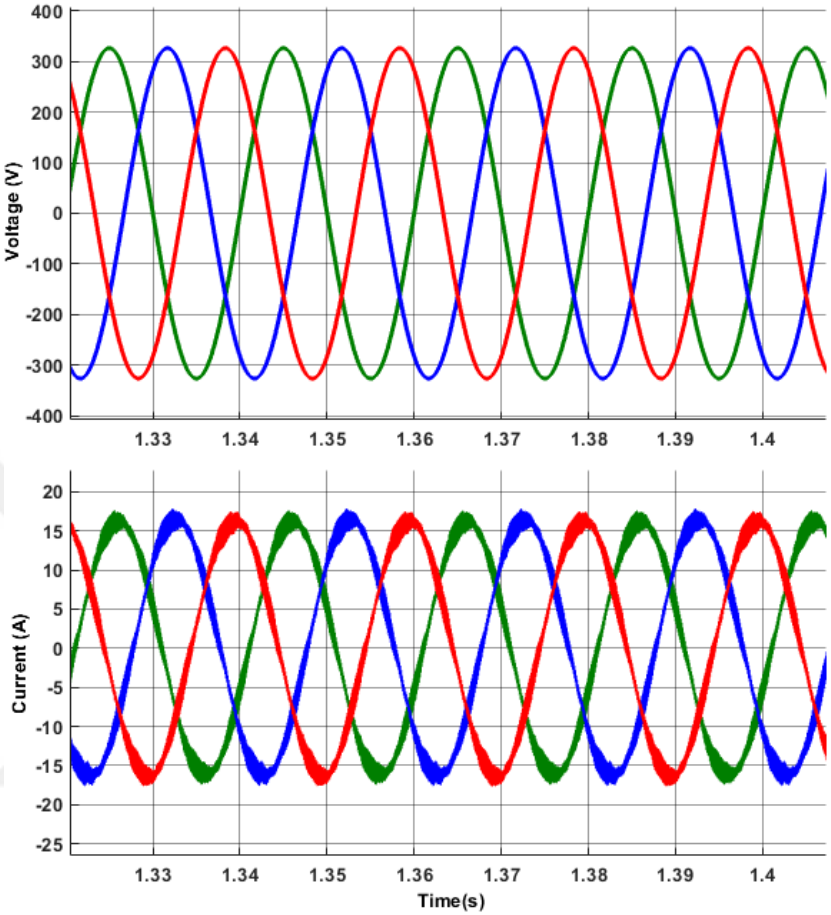

Figure 4.87. The voltage and current of inverter output for charging mode with ANN-based method at 1000 W/m^2

While power transfer is provided from PV system to both the battery and the grid, the DC-link voltage should be at the specified level. Figure 4.88 and Figure 4.89 shows that this voltage is around 710 V.

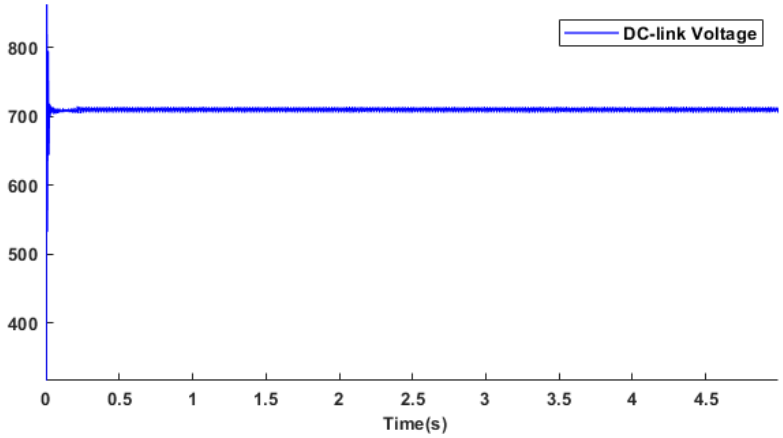

Figure 4.88. The DC-link voltage for charging mode with ANN-based method at 1000 W/m^2

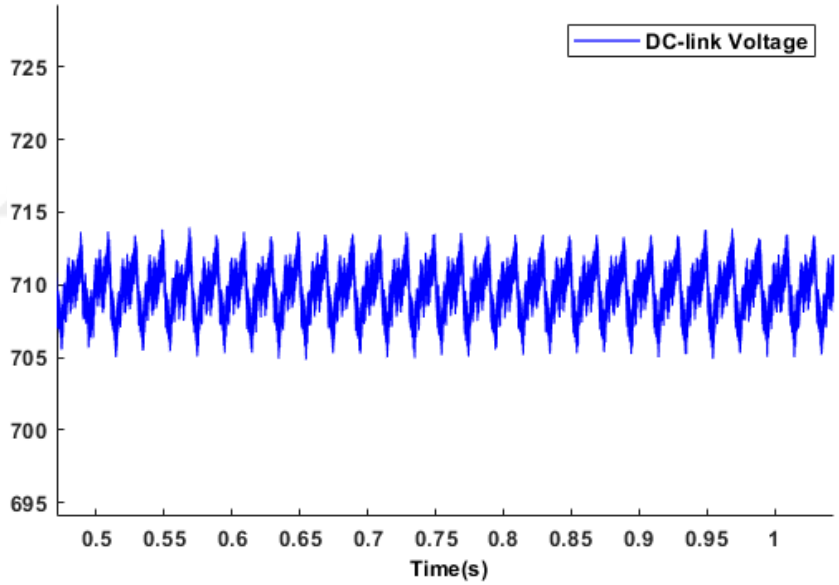

Figure 4.89. The DC-link voltage for charging mode with ANN-based method at 1000 W/m^2

The efficiency of produced power is shown in Figure 4.90. It is seen around 92%.

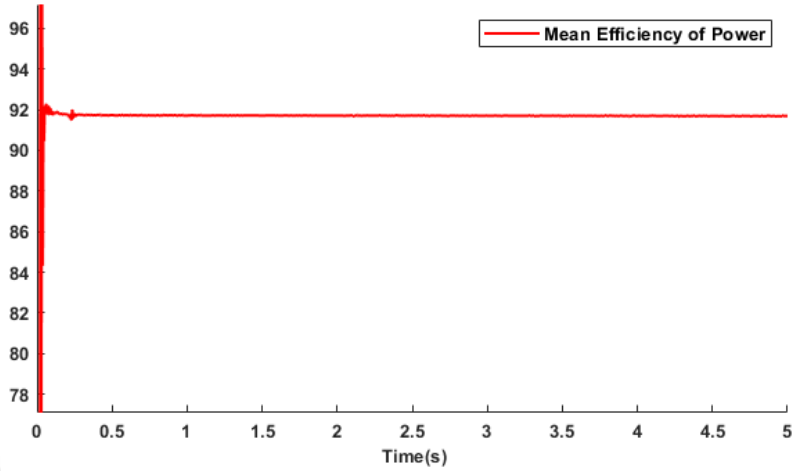

Figure 4.90. The efficiency of produced power for charging mode with ANN-based method at 1000 W/m^2

The THD of the proposed ANN-based method system gives lower results than the P&O and INC methods. Compared to the results for the 1000 W/m^2 charge mode of other MPPT methods, the THD of the proposed method is between 1.3% and 1.4%, the THD for P&O is between 1.5% and 2%, and the INC is between 2% and 4% The Figure 4.91 and Figure 4.92 shows the THD for proposed ANN-based method.

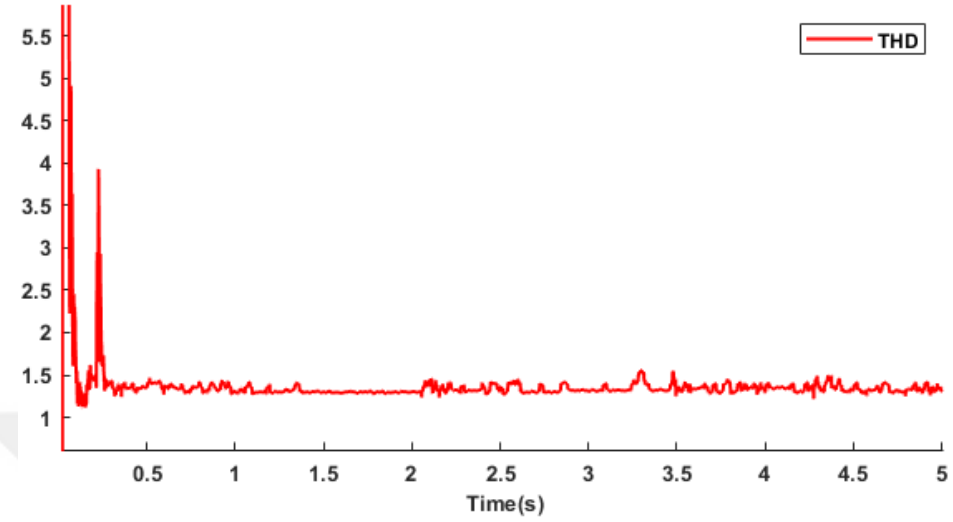

Figure 4.91. The THD of system for charging mode with ANN-based method at 1000 W/m^2

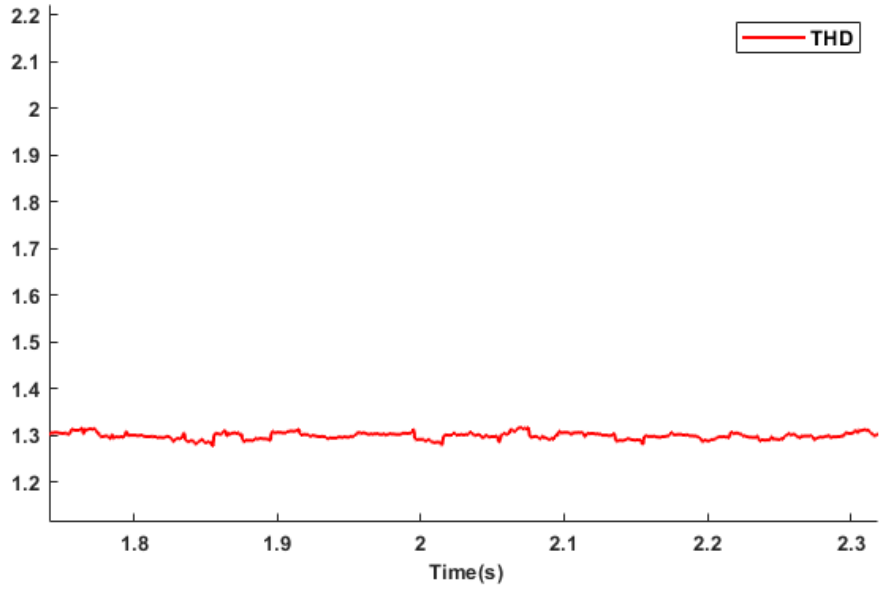

Figure 4.92. The THD of system for charging mode with ANN-based method at 1000 W/m^2

4.3.1.2. 500 W/m^2 at 25 ˚C

The charging mode for ANN-based method is analyzed for 500 W/m^2 irradiance at 25 ˚C temperature. The power generated from the PV system is transferred to both the battery and the grid. While examining this situation, the charging current of the battery is re-evaluated by calculating the power that the irradiation value can produce. While this transmission is taking place, the power produced must be balanced distributed. Large filters should be used for the inverter while the battery stores power with maximum current. To avoid this situation, the charging current is determined as 5 A for 500 W/m^2 irradiation, as shown in the Figure 4.93.

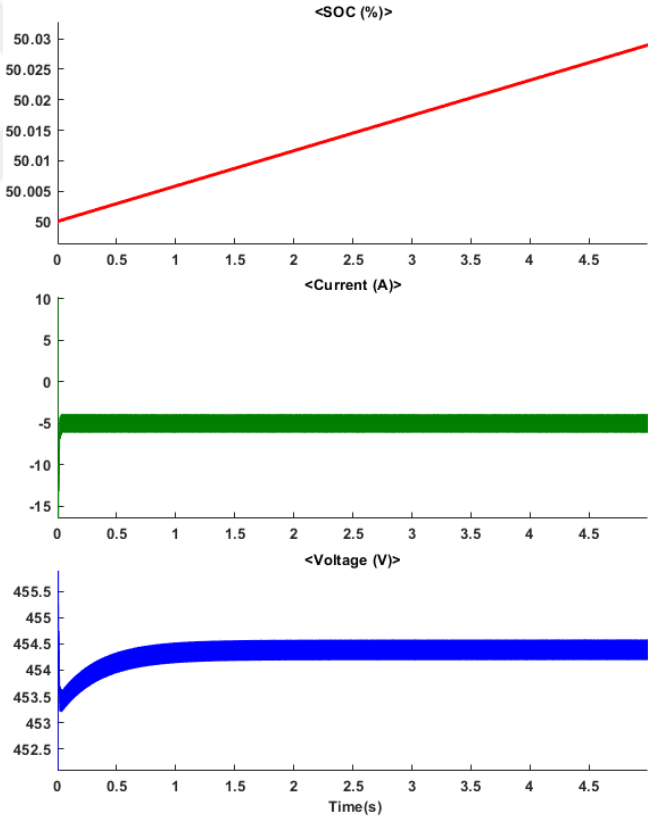

Figure 4.93. The SOC, current and voltage of battery for charging mode with ANN-based method at 500 W/m^2

The produced PV power is shown in Figure 4.94. With the INC method, it is seen that the power produced by the PV oscillates around of 6.2 kW.

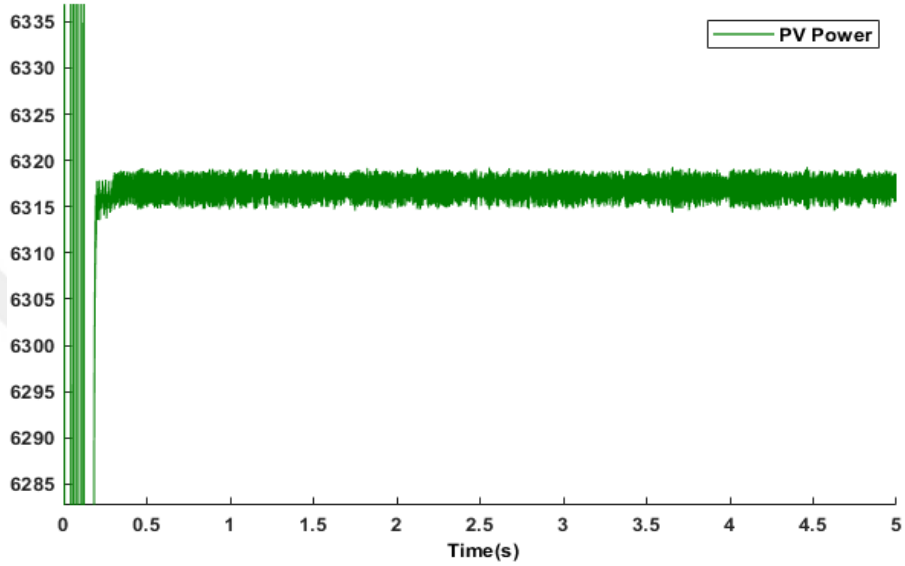

Figure 4.94. The produced PV power for charging mode with ANN-based method at 500 W/m^2

The power transferred to the battery from this generated power is shown in the Figure 4.95.

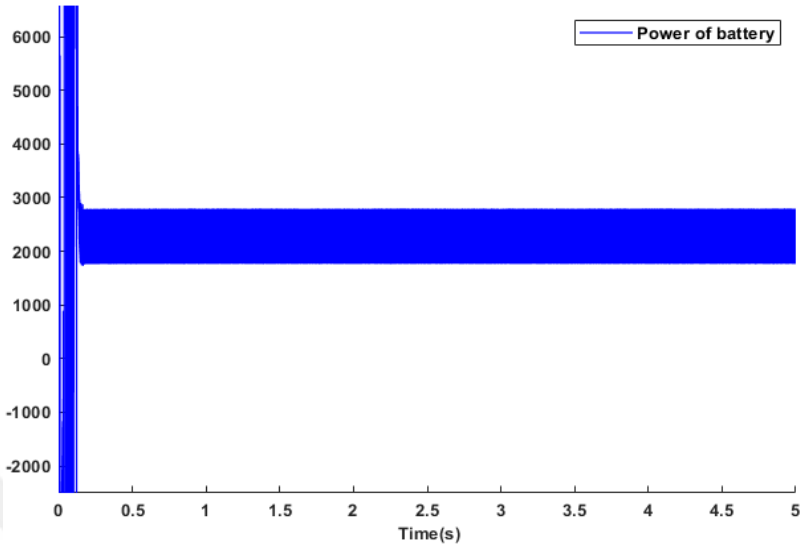

Figure 4.95. The power transferred to battery for charging mode with ANN-based method at 500 W/m^2

The power transferred to the grid from this generated power is shown in the Figure 4.96.

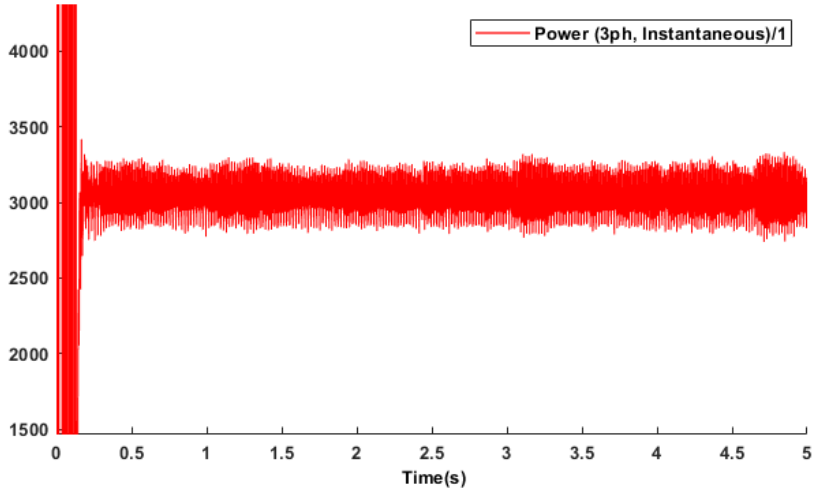

Figure 4.96. The power transferred to grid for charging mode with ANN-based method at 500 W/m^2

The inverter output voltage and current graphs are shown in Figure 4.97. It is seen that there is no phase difference between current and voltage and pf is zero. It is observed that the oscillation is more than 500 W/m^2 by looking at the current graph in Figure 4.97.

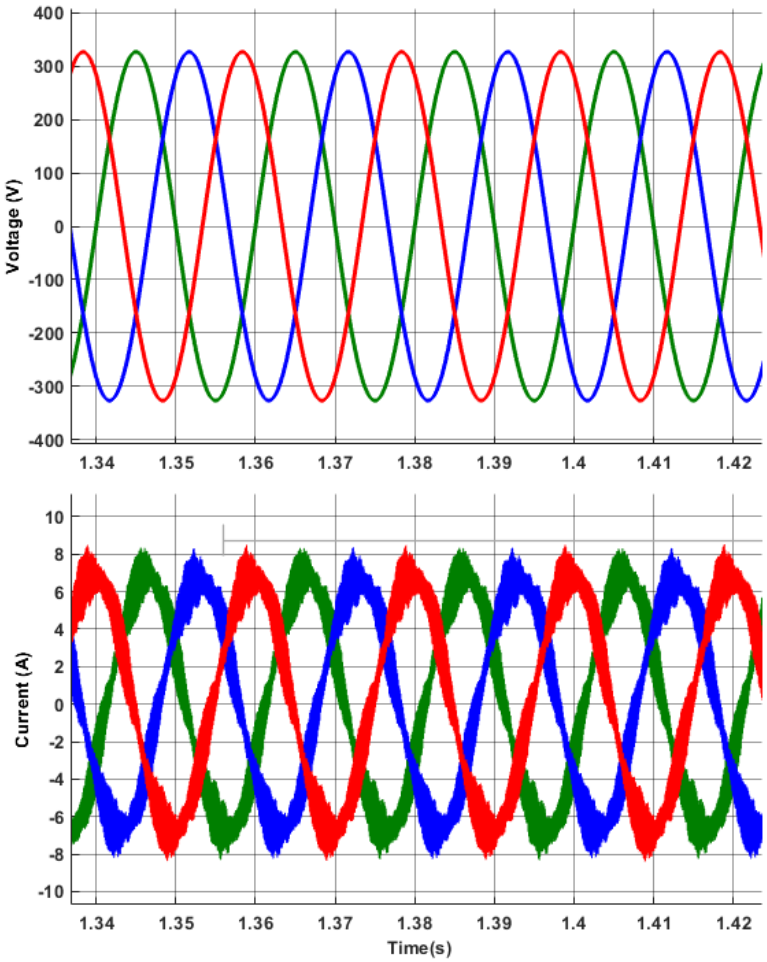

Figure 4.97. The voltage and current of inverter output for charging mode with ANN-based method at 500 W/m^2

The power transfer takes place via the DC-link. The DC-link voltage oscillates around 705 V. The graphic showing the DC-link voltage is seen in the Figure 4.98 and Figure 4.99.

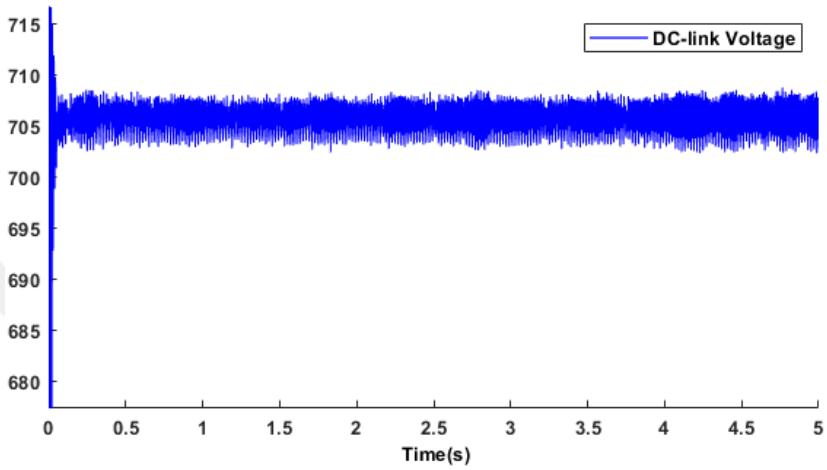

Figure 4.98. The DC-link voltage for charging mode with ANN-based method at 500 W/m^2

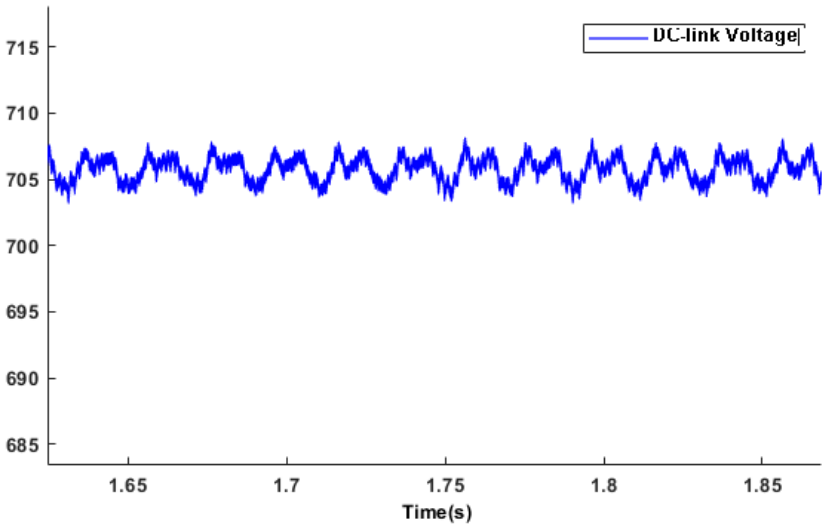

Figure 4.99. The DC-link voltage for charging mode with ANN-based method at 500 W/m^2

The THD of the system is shown in Figure 4.100. The THD of the proposed ANN-based MPPT system gives better results than the P&O and INC methods. Compared to the results for the 500 W/m^2 charge mode of other MPPT methods, the THD of the proposed method is between 2% and 3%, the THD for P&O is between 2% and 4%, and the THD for INC is between 6% and 8%.

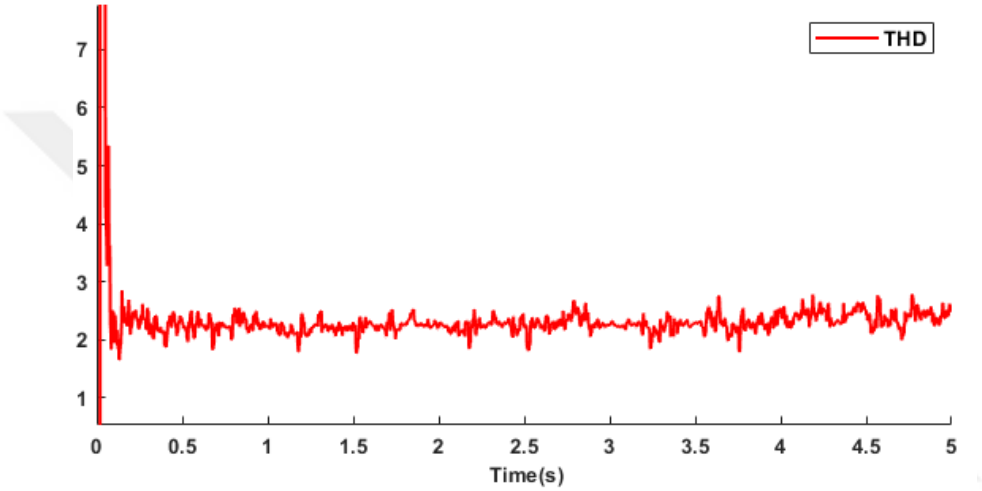

Figure 4.100. The THD of system for charging mode with ANN-based method at 500 W/m^2

The proposed ANN-based MPPT method increases the efficiency of the produced power in the system for low irradiance values. It is seen from the Figure 4.101 that the efficiency is 84.5%.

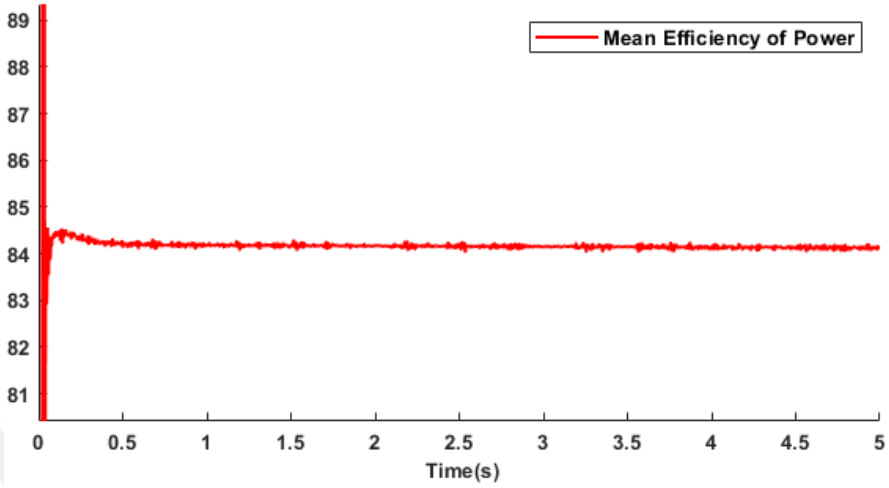

Figure 4.101. The efficiency of produced power for charging mode with ANN-based method at 500 W/m^2

4.3.2. PV to Grid Mode

4.3.2.1. 1000 W/m^2 at 25 ˚C

The PV to grid mode of the system is simulated for 1000 W/m^2 irradiation and 25 ˚C temperature values for proposed ANN-based method, and graphic results are given in this section. For this situation to occur, the SOC of the battery must be above or equal to 90%. In this case all the power produced by the PV is transferred to the grid. The inverter output voltage and current graph is shown in the Figure 4.102 for 1000 W/m^2. As seen in Figure 4.102 the pf value is zero, the current and voltage graphs have the same phase angle. As seen in Figure 4.102, the maximum phase voltage value is 325 V, and the current value is maximum 25 A. This value is the maximum value of the current per phase.

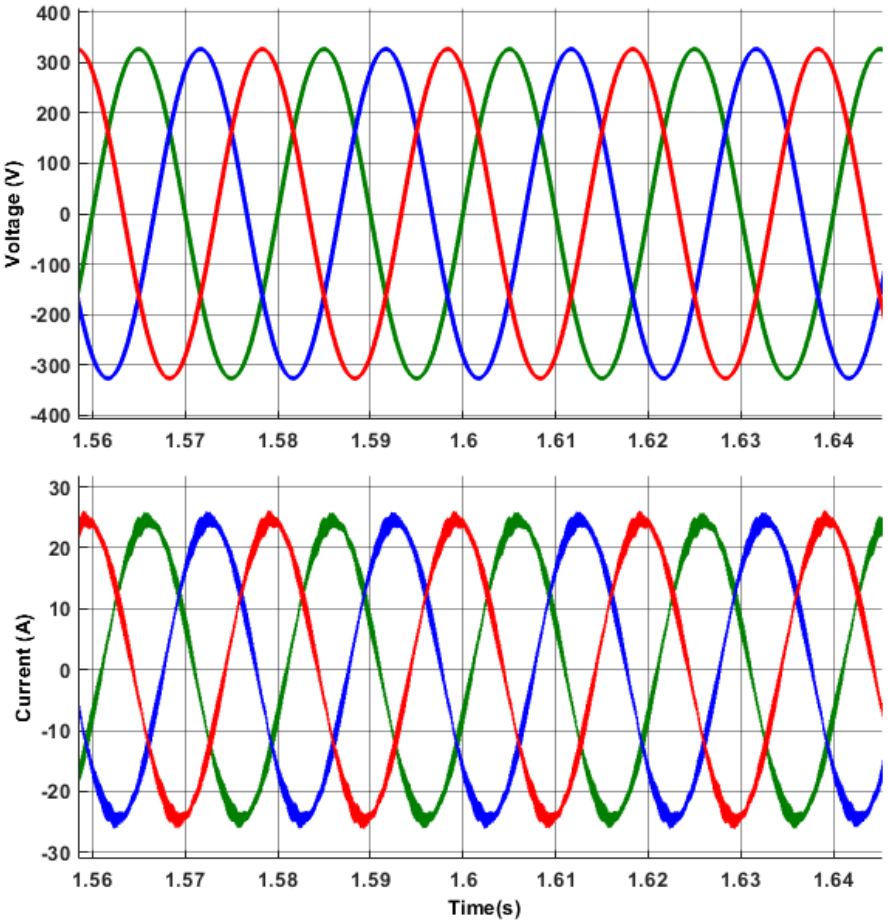

Figure 4.102. The voltage and current of inverter output for PV to grid mode with ANN-based method

The produced PV power is shown in Figure 4.103. With the ANN-based method, it is seen that the power produced by the PV is at the level is between 12.48 kW.

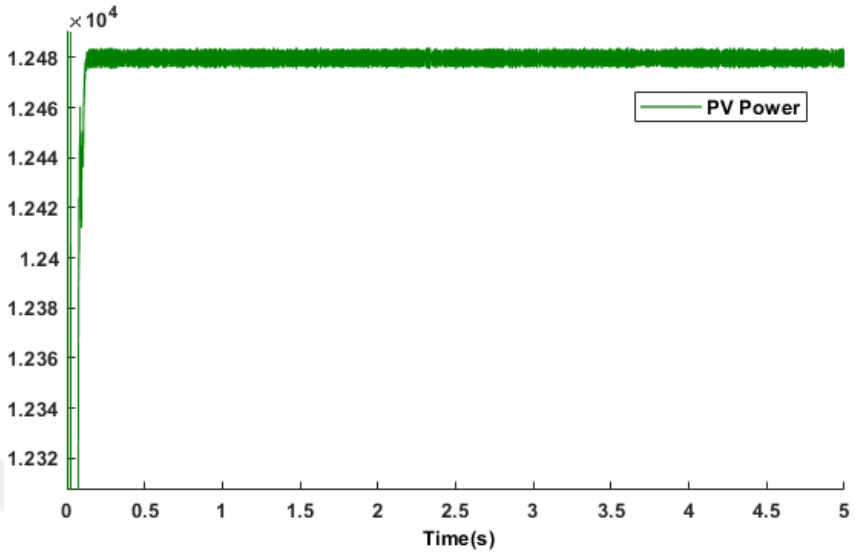

Figure 4.103. The produced PV power with ANN-based method for PV to grid mode at 1000 W/m^2

The power transferred to the grid from this generated power is shown in the Figure 4.104.

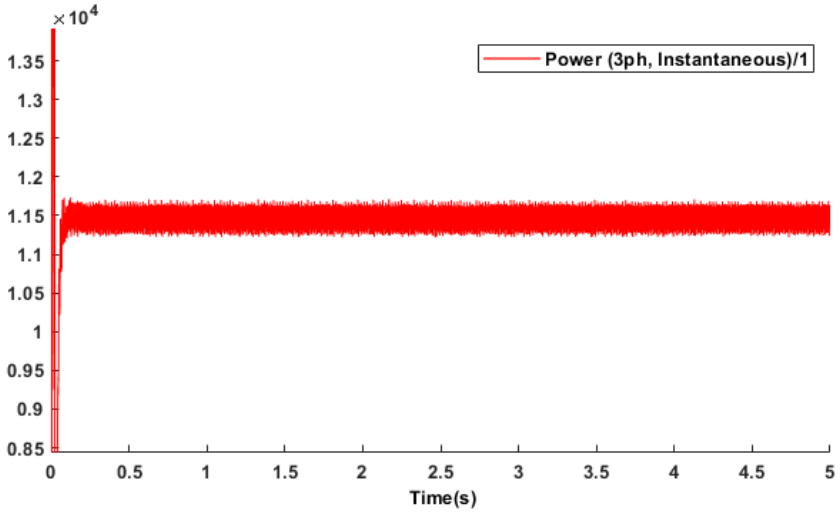

Figure 4.104. The power transferred to the grid with ANN-based method for PV to grid mode at 1000 W/m^2

In this case, as the SOC value of the battery is given as 90%, as seen in Figure 4.105, the battery should not be charged at all.

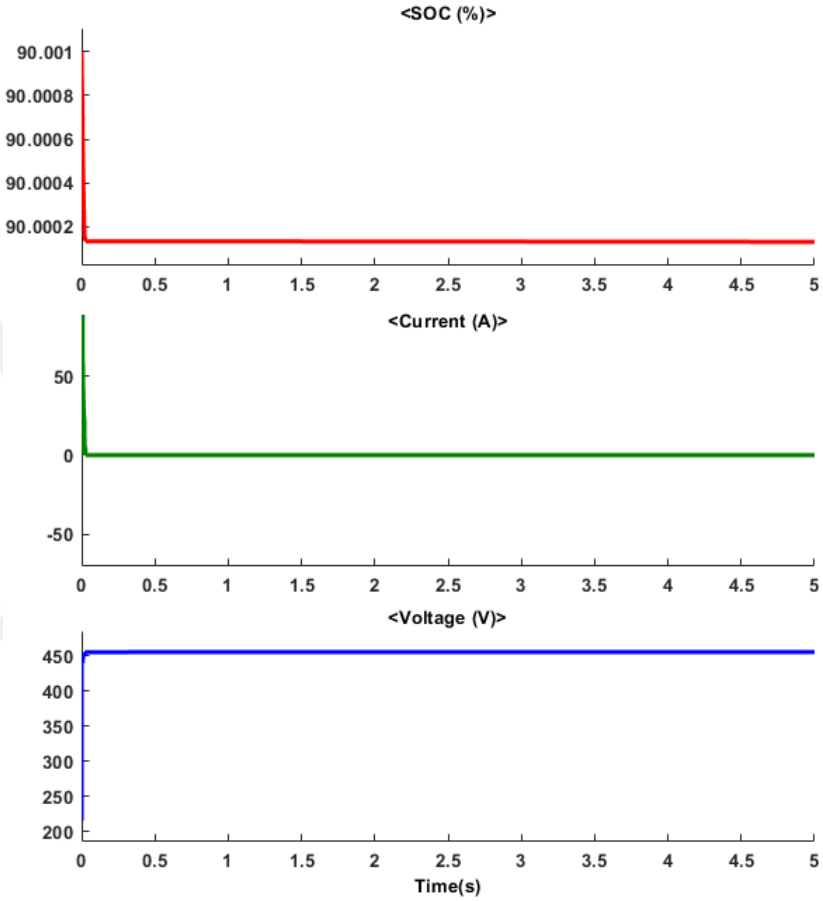

Figure 4.105. The SOC, current and voltage of battery

In Figure 4.106 and Figure 4.107, it is seen that the DC-link voltage oscillates between 705 V and 710 V.

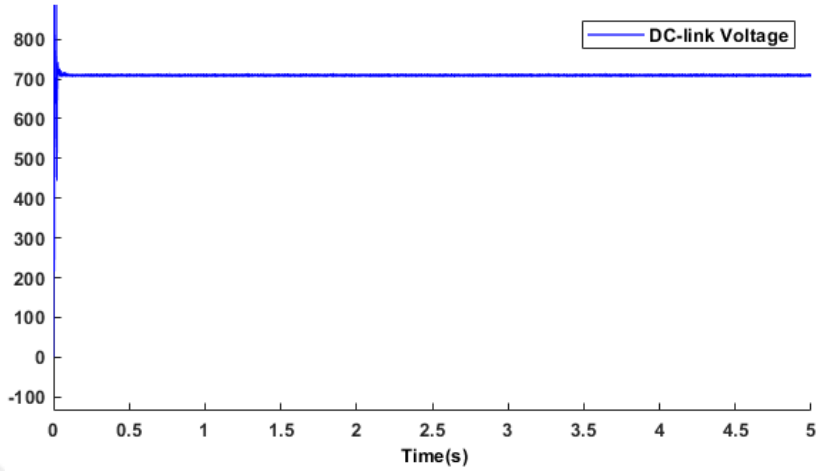

Figure 4.106. The DC-link voltage for PV to grid mode at 1000 W/m^2

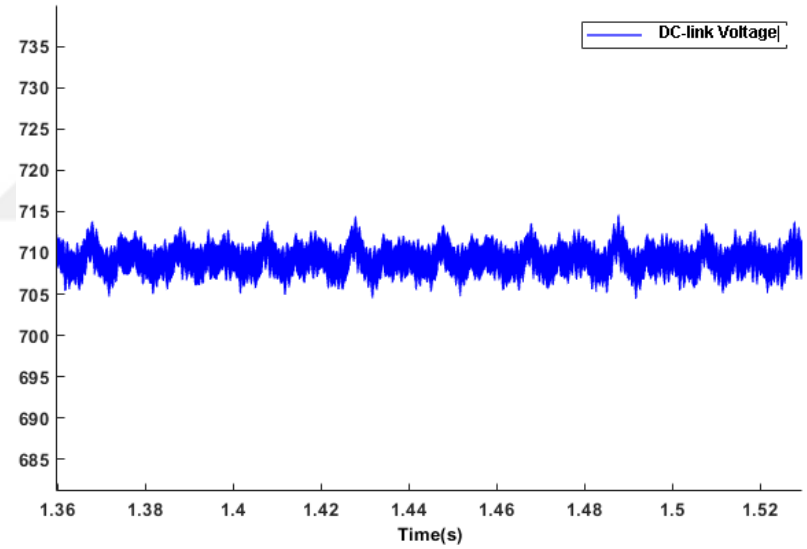

Figure 4.107. The DC-link voltage for PV to grid mode at 1000 W/m^2

The power efficiency of the system for PV to grid mode is seen in Figure 4.108 as 92%.

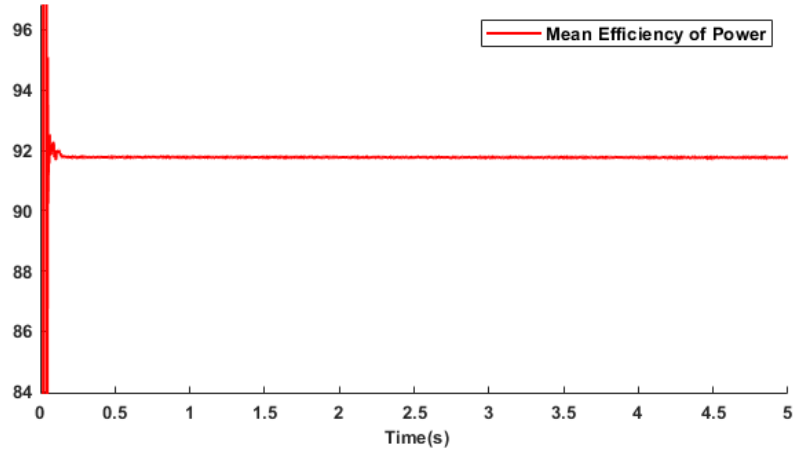

Figure 4.108. The efficiency of produced power for PV to grid mode with ANN-based method at 1000 W/m^2

The THD of the proposed ANN-based MPPT system gives lower results than the P&O and INC methods. Compared to the results for the 1000 W/m^2 PV to grid mode of other MPPT methods, the THD of the proposed method is under 1 % around 0.85%, the THD for P&O oscillates around 1% and the THD for INC is between 1% and 3%. The Figure 4.109 shows the THD for proposed ANN-based method.

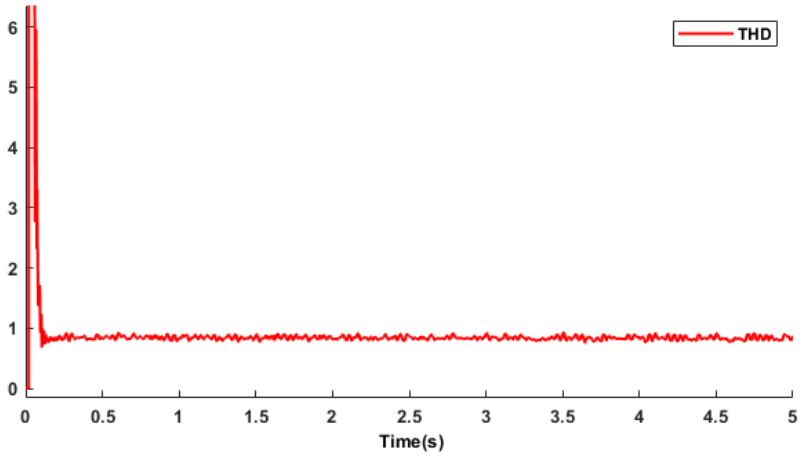

Figure 4.109. The THD of system for PV to grid mode with ANN-based method at 1000 W/m^2

4.3.2.2. 500 W/m^2 at 25 ˚C

The PV to grid mode of the system is simulated for 500 W/m^2 irradiation and 25 ˚C temperature values for ANN-based method, and graphic results are given in this section. For this situation to occur, the SOC of the battery must be above or equal to 90%. In this case all the power produced by the PV is transferred to the grid. The inverter output voltage and current graph is shown in the Figure 4.110 for 500 W/m^2. As seen in Figure 4.110 the pf value is zero, the current and voltage graphs have the same phase angle. As seen in Figure 4.110, the maximum phase voltage value is 325 V, and the current value is maximum 12.5 A. This value is the maximum value of the current per phase.

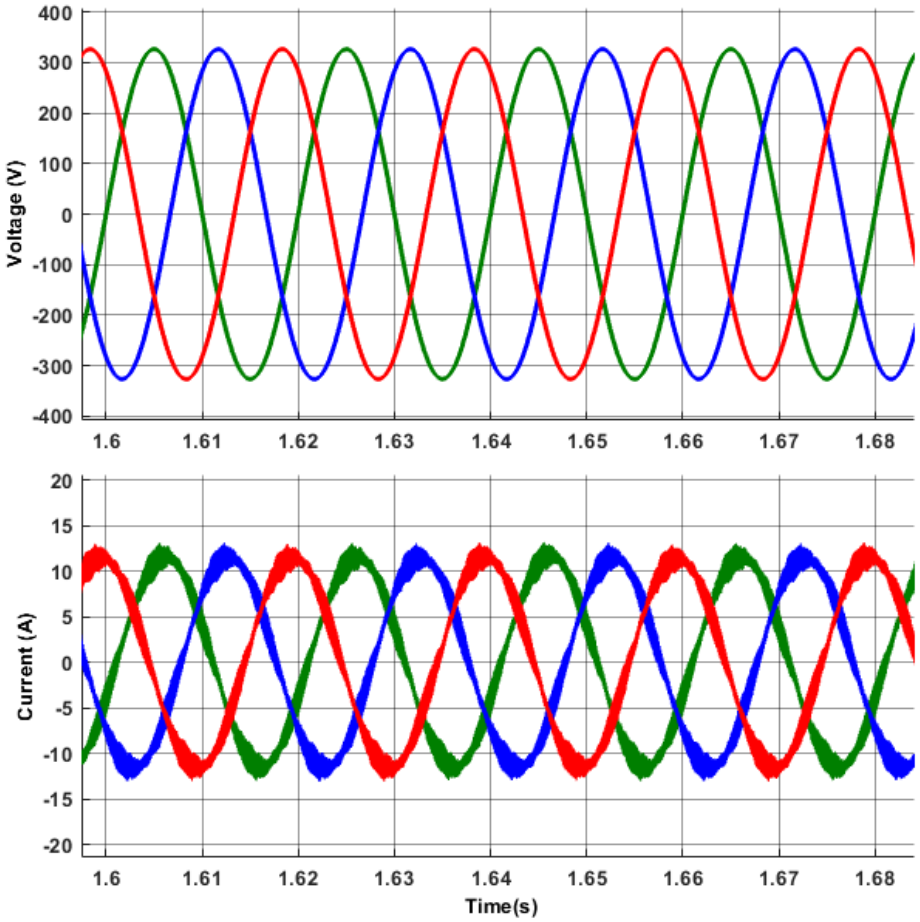

Figure 4.110. The voltage and current of inverter output for PV to grid mode with ANN-based method at 500 W/m^2

The produced PV power is shown in Figure 4.111. With the ANN-based method, it is seen that the power produced by the PV is at the level of 6.32 kW.

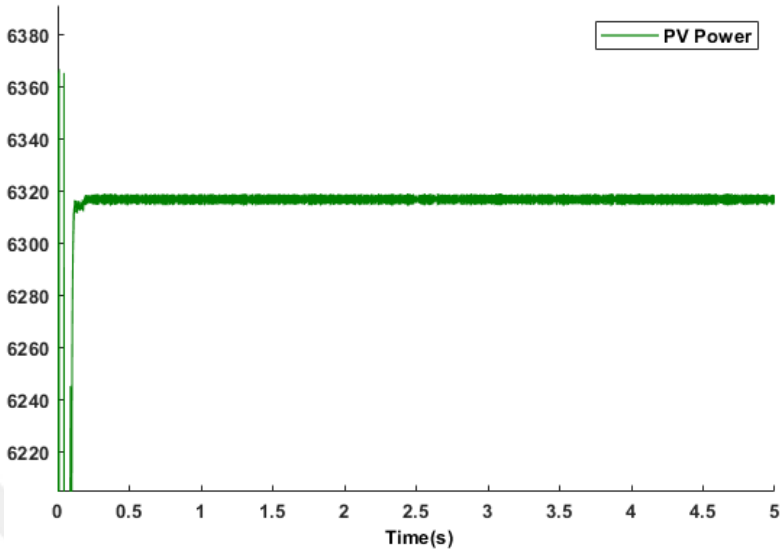

Figure 4.111. The produced PV power with ANN-based method for PV to grid mode at 500 W/m^2

The power transferred to the grid from this generated power is shown in the Figure 4.112.

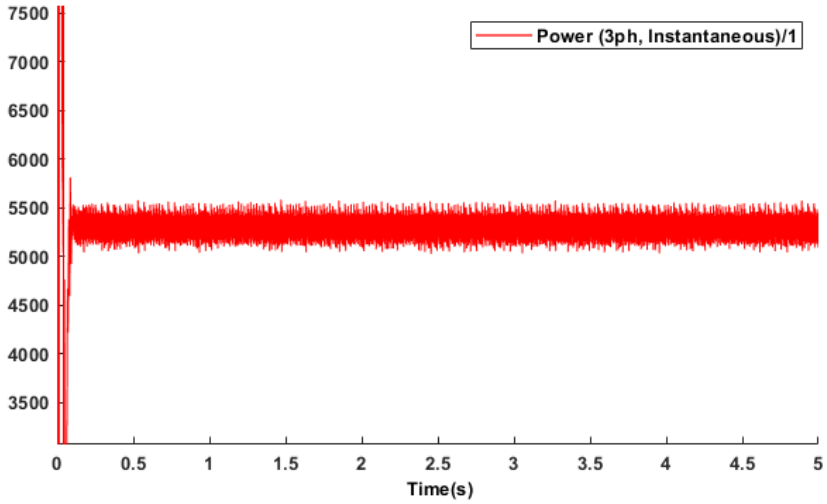

Figure 4.112. The power transferred to grid with ANN-based method for PV to grid mode at 500 W/m^2

In this case, as the SOC value of the battery is given as 90%, as seen in Figure 4.113, the battery should not be charged at all.

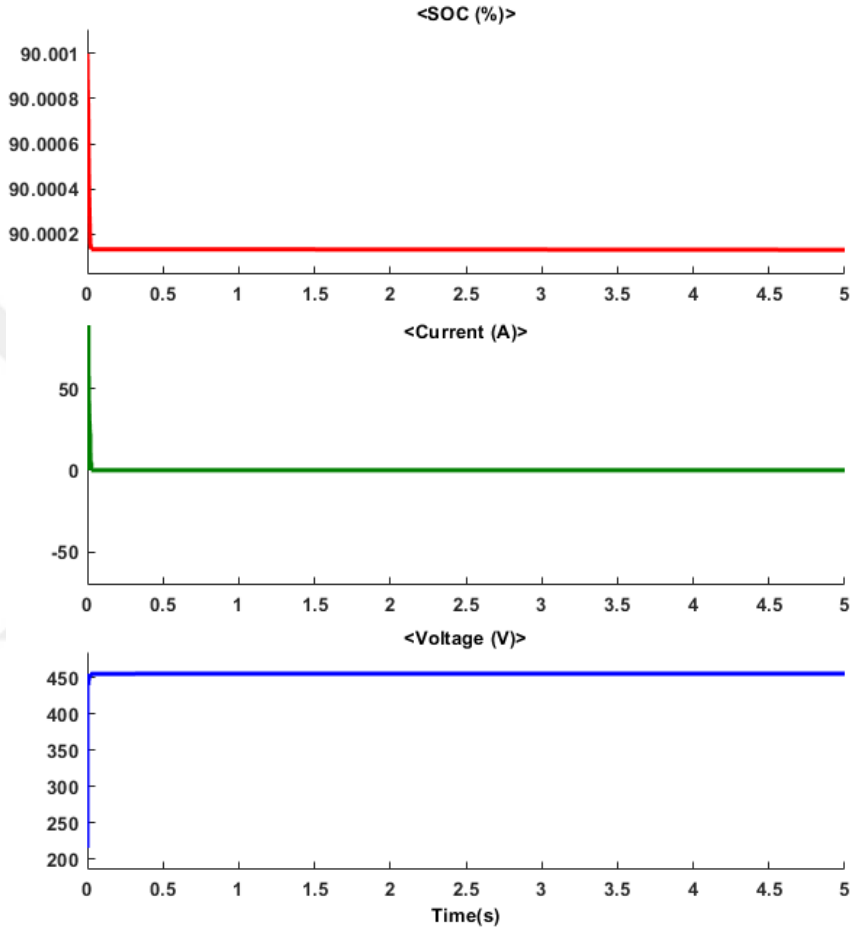

Figure 4.113. The SOC, current and voltage of battery for PV to grid mode with ANN-based method at 500 W/m^2

In Figure 4.114 and Figure 4.115, it is seen that the DC-link voltage oscillates between 705 V and 710 V.

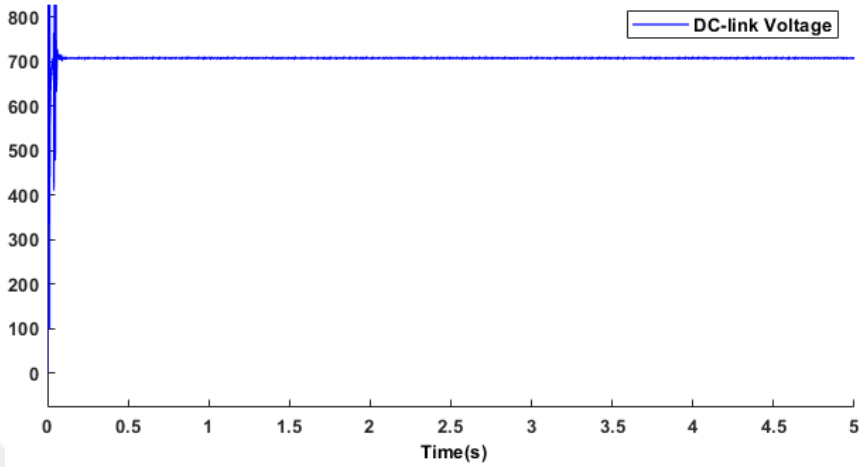

Figure 4.114. The DC-link voltage for PV to grid mode with ANN at 500 W/m^2

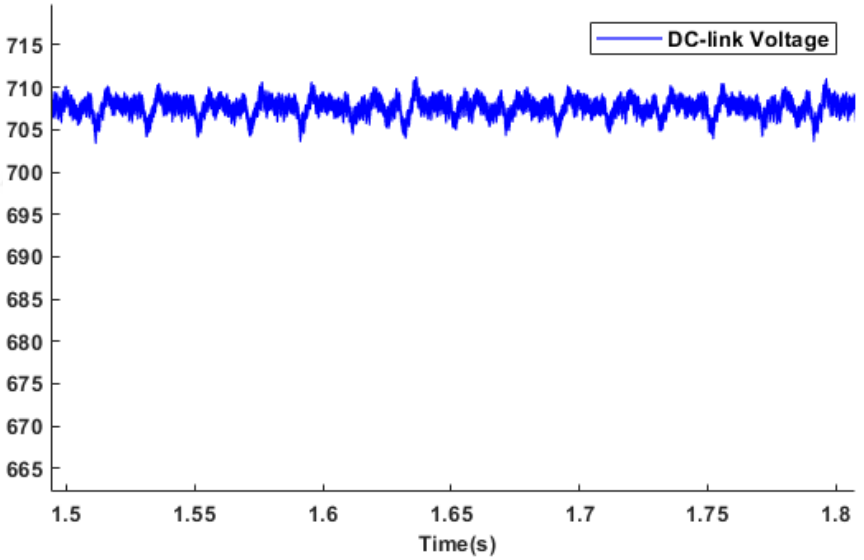

Figure 4.115. The DC-link voltage for PV to grid mode with ANN at 500 W/m^2

The power efficiency for the PV-to-grid mode of the system is seen in Figure 4.116 as close to 84.3%.

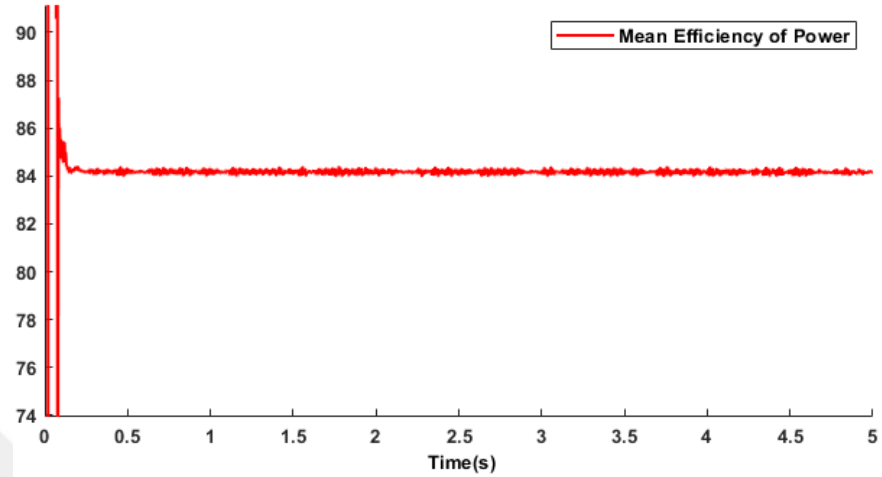

Figure 4.116. The efficiency of produced power for PV to grid mode with ANN-based method at 500 W/m^2

The THD of the proposed ANN-based MPPT system gives better results than the P&O and Inc methods. Compared to the results for the 500 W/m^2 PV-to-grid mode of other MPPT methods, the THD of the proposed method is between 1% and 2%, the THD for P&O is between 2% and 4%, and the THD for INC is between 2% and 4%. The Figure 4.117 shows the THD for proposed ANN-based method.

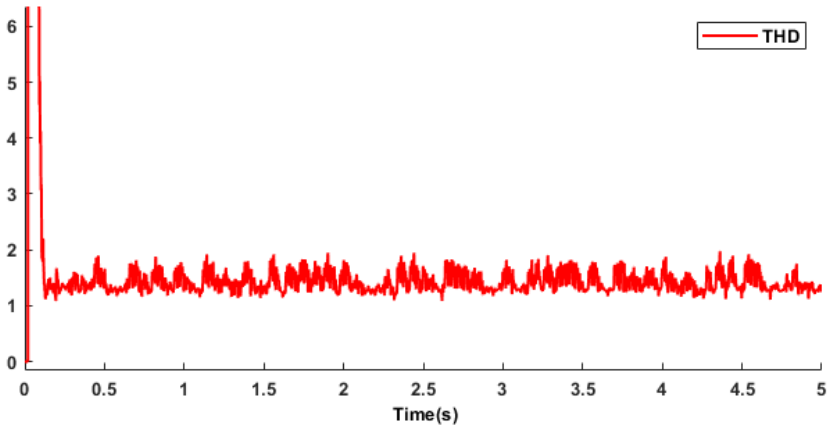

Figure 4.117. The THD of system for PV to grid mode with ANN-based method at 500 W/m^2

4.3.3. Discharging Mode Battery to Grid

The results of discharging mode for ANN-based method are shown in this part. The discharging mode occurs when the SOC is above %50 and P_{PV} is lower than 620 W. The battery is assumed to be fully charged before discharging. The SOC of the battery is 90%. The battery discharge current ranges from a maximum of 10.43 A to a minimum of 8.5 A. SOC, voltage, and current graphs for the discharge mode of the battery are shown in the Figure 4.118. As seen in Figure 4.118 the battery is in discharging mode. The power in the battery is transferred to the grid.

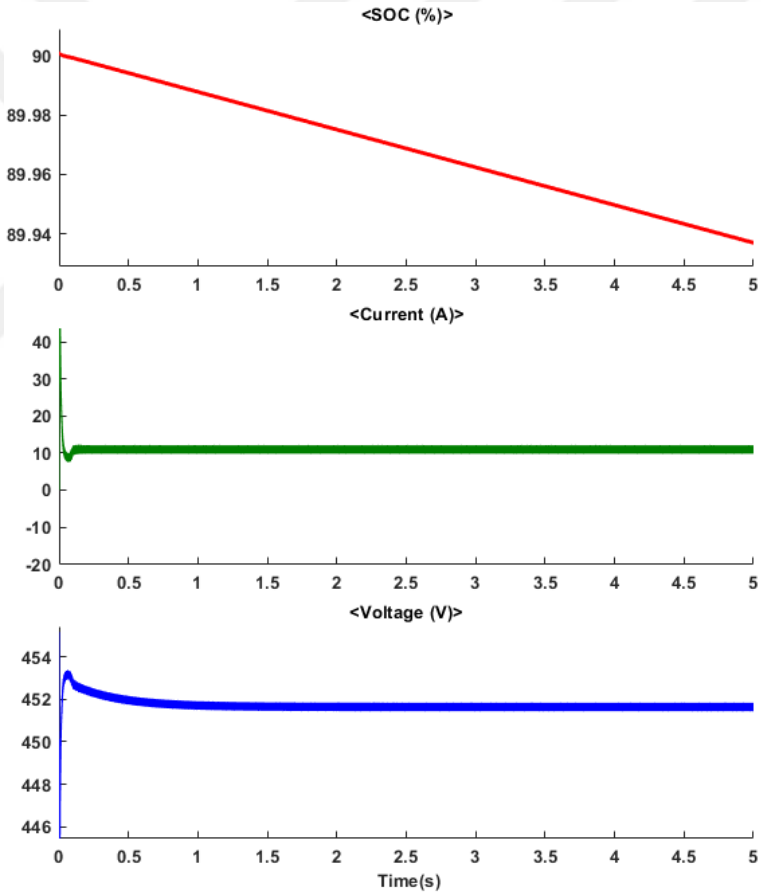

Figure 4.118. The SOC, current and voltage of battery for discharging mode

The battery power is seen in Figure 4.119 when the battery is discharging mode.

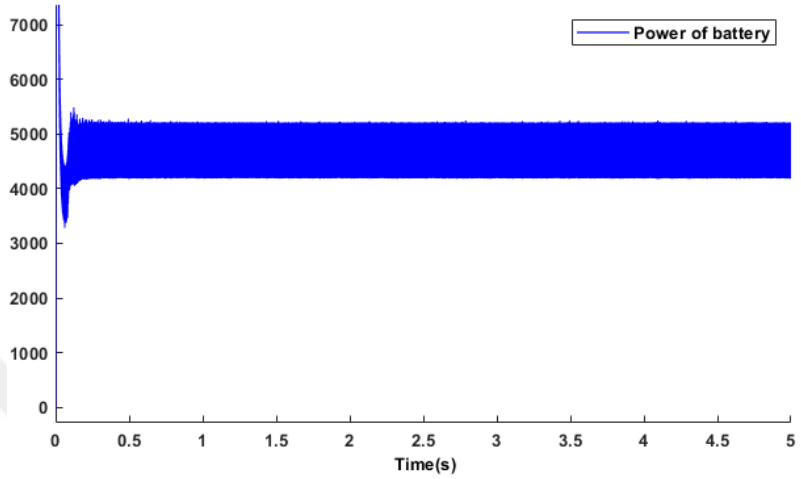

Figure 4.119. The battery power for discharging mode

The power transferred from the battery to the grid is displayed in Figure 4.120.

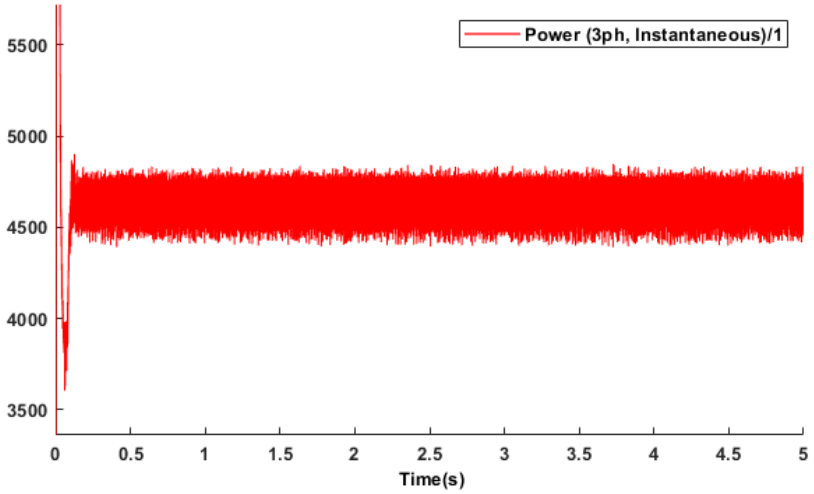

Figure 4.120. The power transferred to grid at discharging mode

The power transfer from the battery to the grid is carried out via the DC-link. In this case, it is seen that the DC-link voltage oscillates between 705 V and 710 Vdc in Figure 4.121 and Figure 4.122.

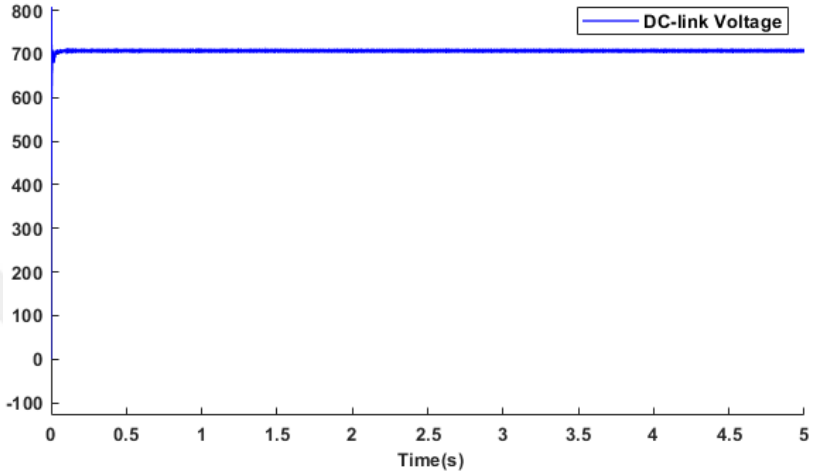

Figure 4.121. The DC-link voltage for discharging mode

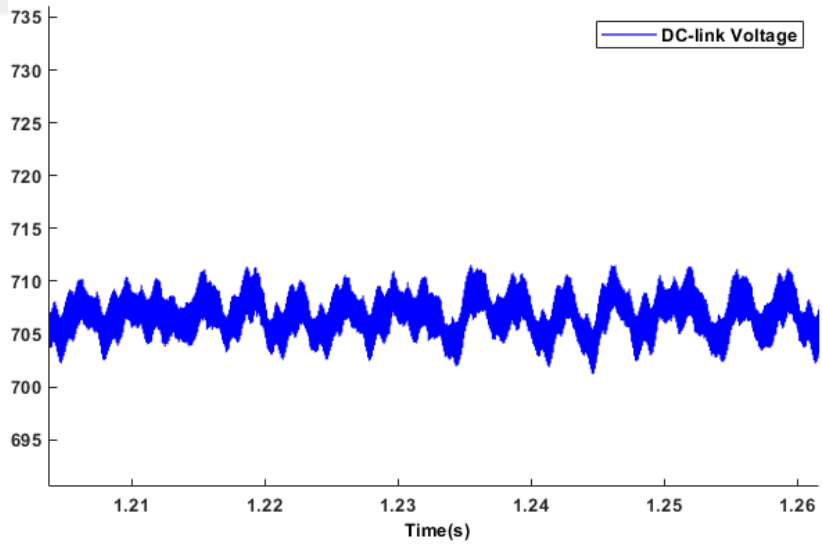

Figure 4.122. The DC-link voltage for discharging mode

The inverter output voltage and current graph is shown in the Figure 4.123 for discharging mode of battery. As seen in Figure 4.123 the pf value is zero, the current and voltage graphs have the same phase angle.

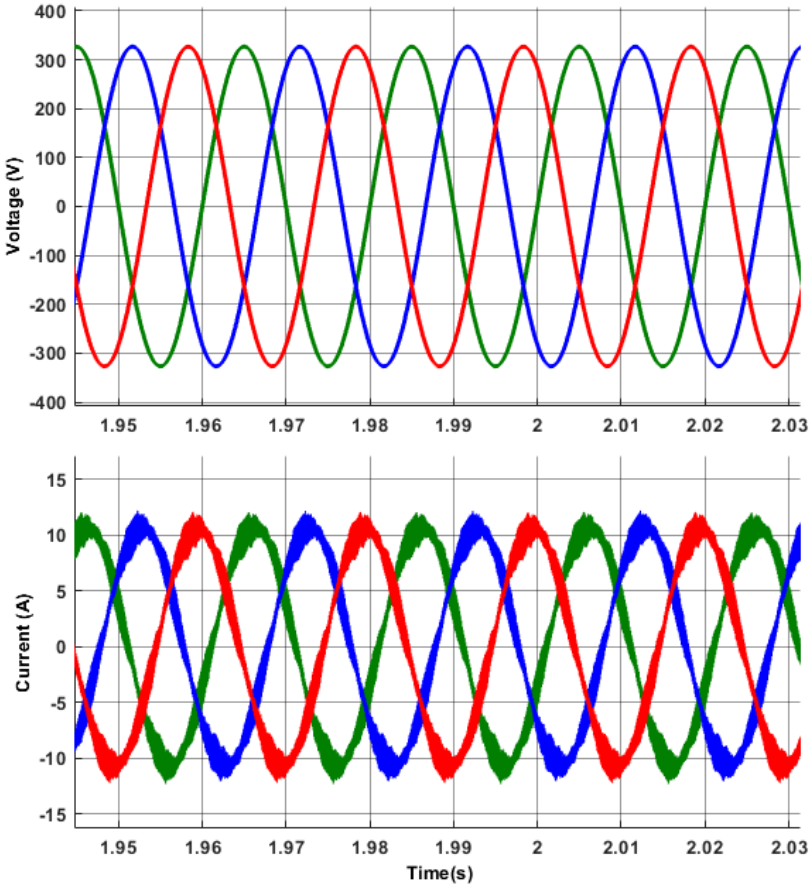

Figure 4.123. The voltage and current of inverter output for discharging mode

System THD is seen as close to 2% while the battery is being discharged as seen in Figure 4.124.

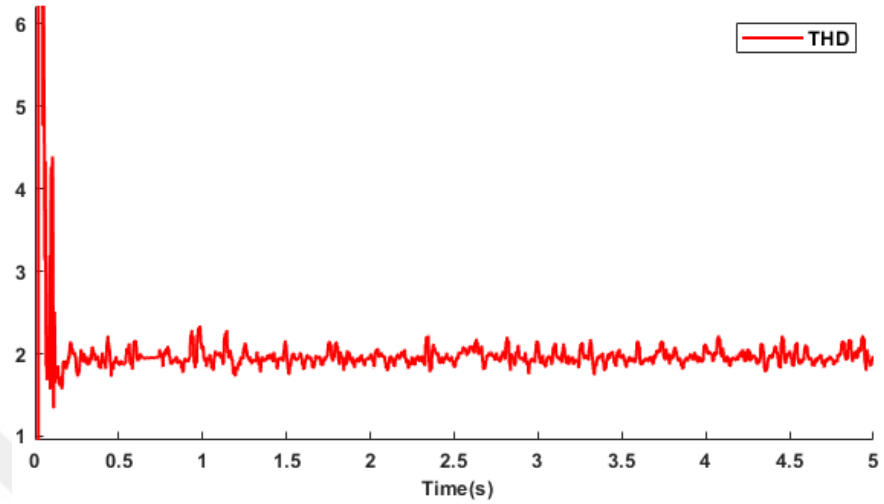

Figure 4.124. The THD of system for discharging mode

4.4. Real Solar Irradiation graph of a day at 25 ˚C

In this section, solar irradiation graph of a sunny day is created from real meteorological data of Tarsus / Mersin. The graph shown in the Figure 4.125 shows the variation of solar irradiation on a sunny day throughout the day. With this created variable solar irradiation, the sunny day scenario in Figure 3.21 is tested within the scope of energy management and the results of the MPPT methods are compared. The simulation time is 24 seconds. Since it takes a long time to charge the battery in the simulation environment, every second spent in the simulation is considered an hour. It is thought that our PV system starts to generate power at 05:00 am and simulation results are shown up to 19:00 pm.

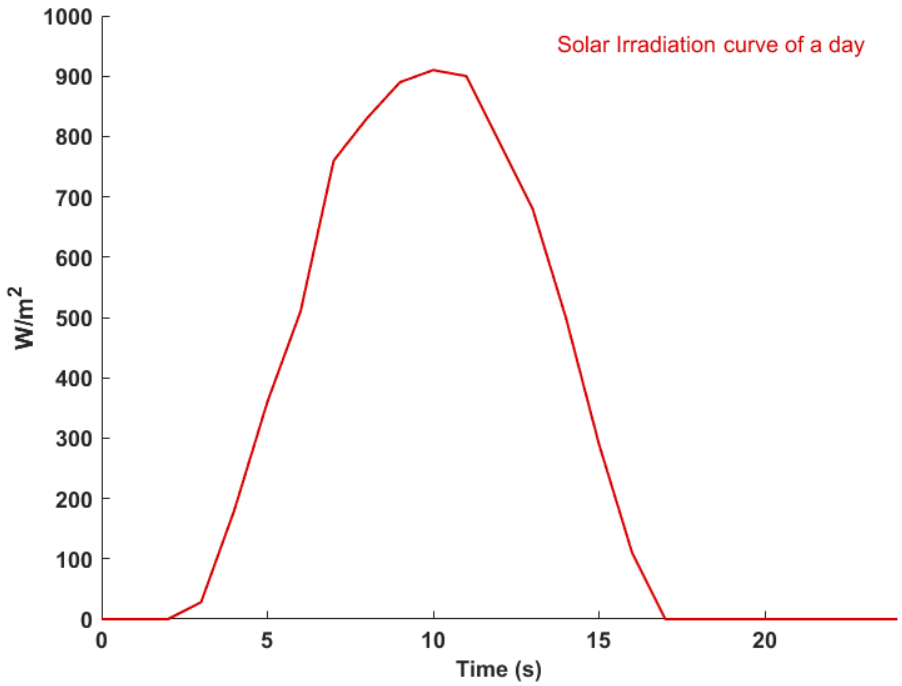

Figure 4.125. The solar irradiation of a day

According to the scenario in Figure 3.21 when the system starts to work with the irradiation given in the Figure 4.125; It works in PV to grid mode until the irradiation reaches 400 W/m^2. When the irradiance is greater than 400 W/m^2, the power generated from the PV is transmitted to both the battery and the grid, and the battery is charged. In this case, the battery is charged with low current since the irradiation is not very high. If the irradiance is higher than 750 W/m^2, the battery charging current increases. When the irradiance drops below 400 W/m^2, the battery stops charging and the generated power is transferred to the grid. When the PV power generation is less than 620 W, the PV stops producing power and the battery starts to discharge. The initial SOC of the battery is given as 51% to show the discharging processes clearly. The Figure 4.126 shows the SOC, current and voltage of the battery for INC, P&O and ANN-based MPPT methods. It is seen from the graphs of Figure 4.126 that the scenario is working well.

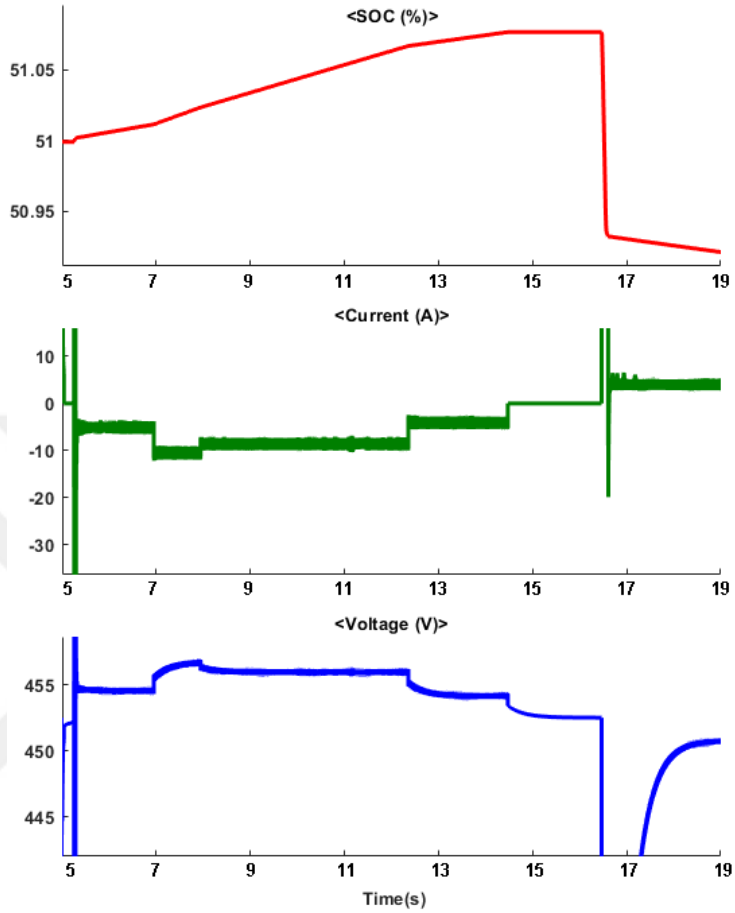

Figure 4.126. The SOC, current and voltage of battery for sunny day

As seen in Figure 4.126, when the irradiation exceeds 400W/m^2, the power generated from the PV is transferred to the batter and grid. This occurs between 5.25s and 14.5s. In this period, the battery current is charged with different current values according to the times when the irradiation is high and low. Between 14.5s and 16.5s, the power generated from the PV is only transferred to the grid. The energy stored in the battery is then transferred to the grid. While the battery is charged as in Figure 4.126, the power transferred to the grid varies. The voltage and current of inverter output is seen in Figure 4.127.

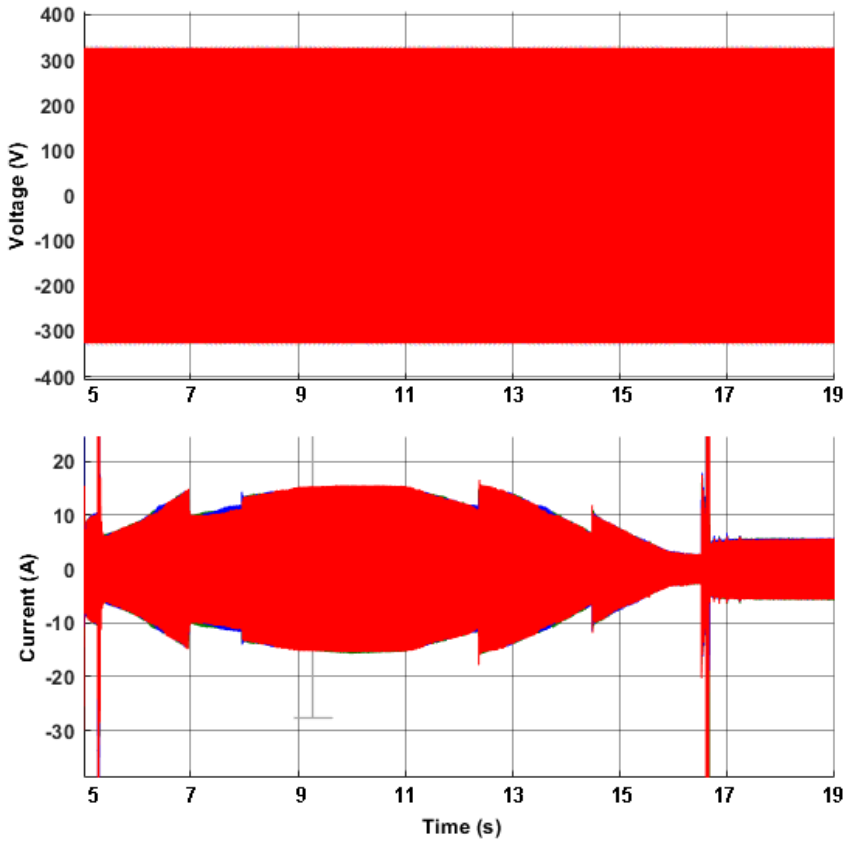

Figure 4.127. The voltage and current of inverter output for sunny day

The graph of the inverter output voltage current graph while the battery is charging for ANN-based MPPT method is given in the Figure 4.128.

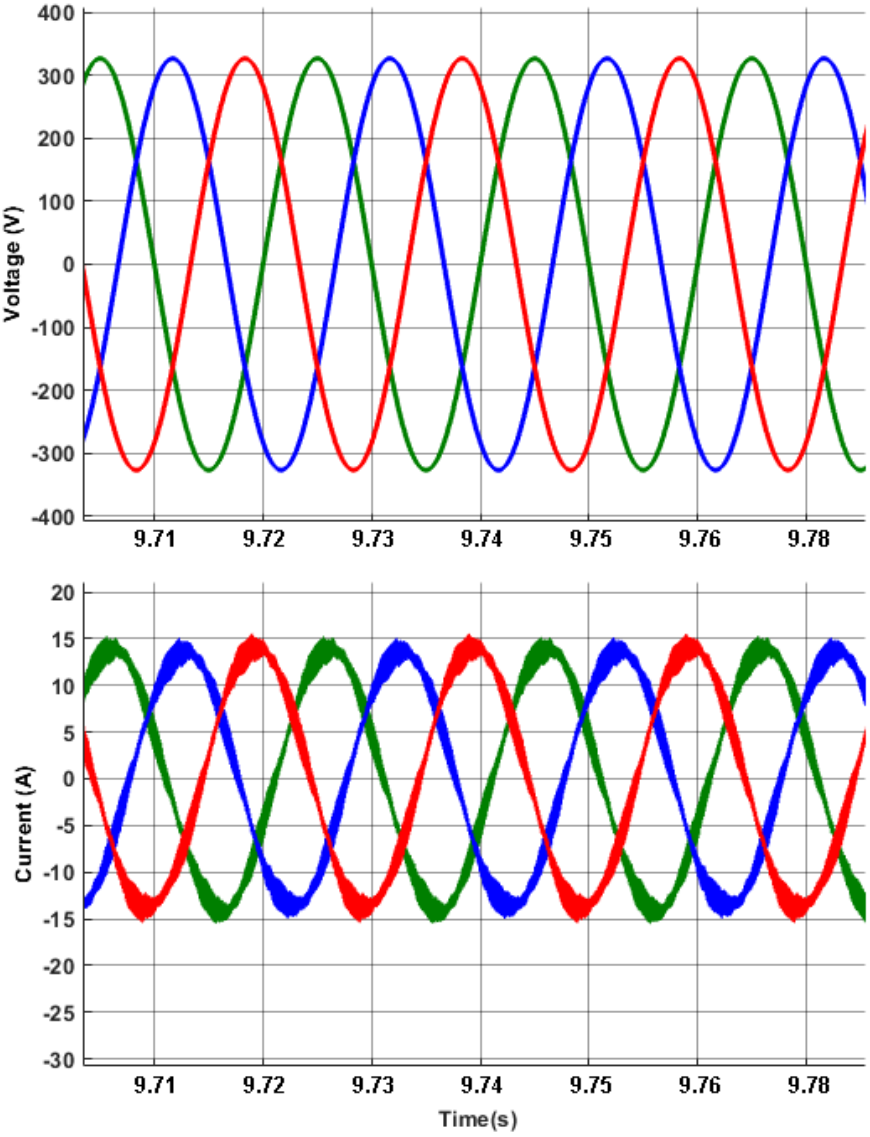

Figure 4.128. The voltage and current of inverter output for charging mode based on ANN method

The graph of the inverter output voltage current graph while the battery is charging for INC method is given in the Figure 4.129.

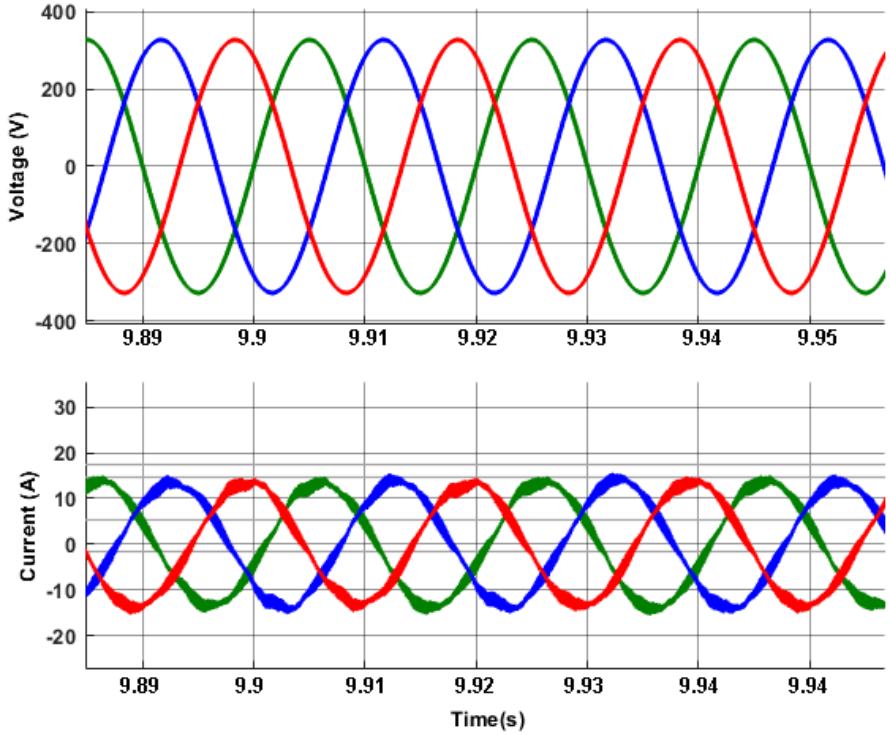

Figure 4.129. The voltage and current of inverter output for charging based on INC method

The graph of the inverter output voltage current graph while the battery is charging for P&O method is given in the Figure 4.130.

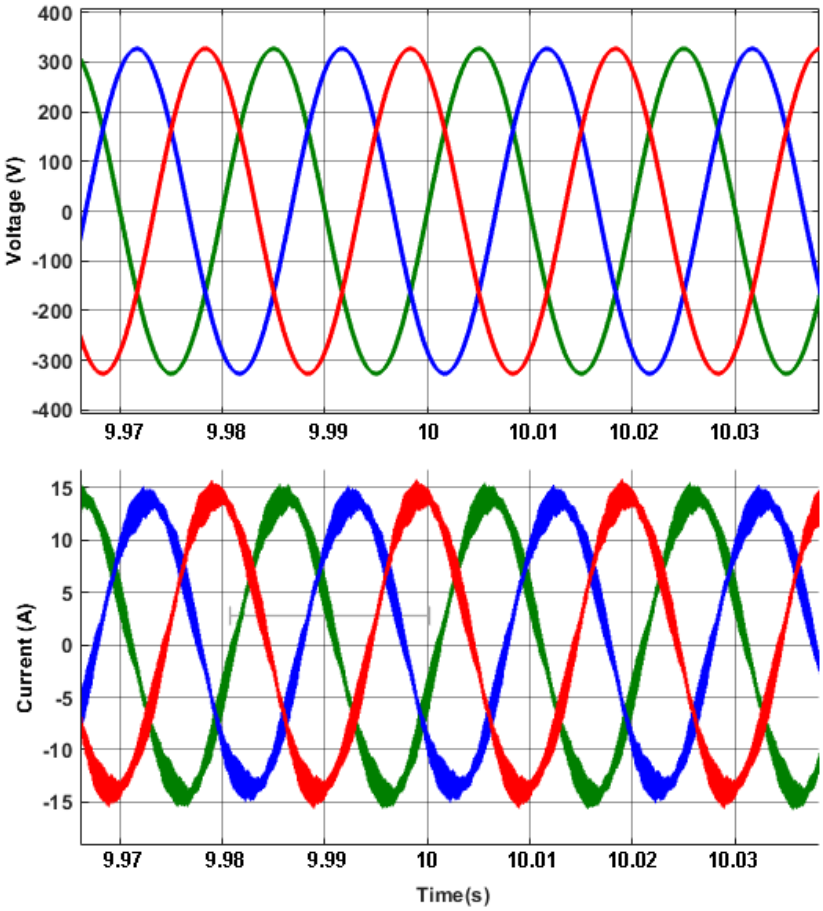

Figure 4.130. The voltage and current of inverter based on P&O method

The THD of the system operated with the ANN model is given in the Figure 4.131.

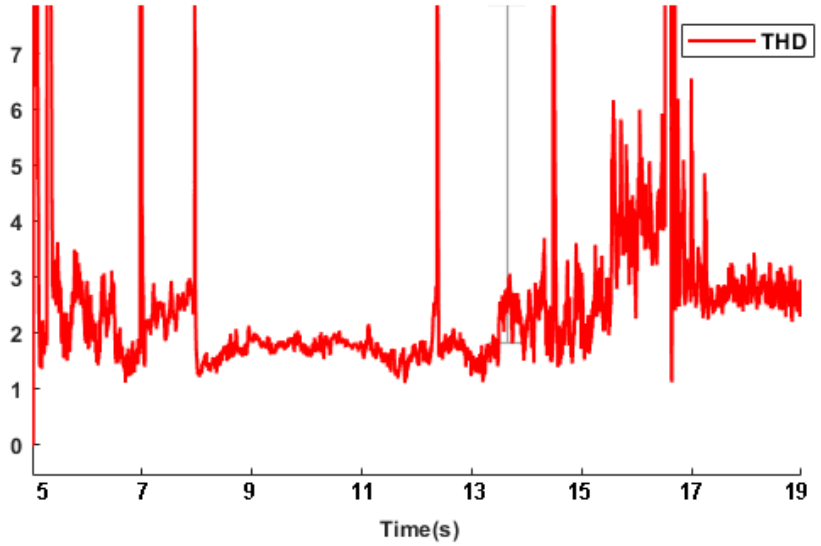

Figure 4.131. The THD of system based on ANN method

The THD of the system operated with the INC model is given in the Figure 4.132.

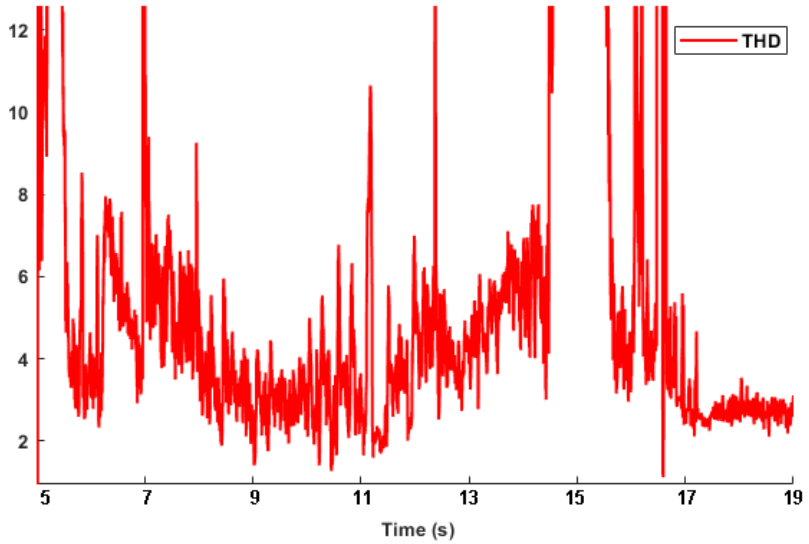

Figure 4.132. The THD of system based on INC method

The THD of the system operated with the P&O model is given in the Figure 4.133.

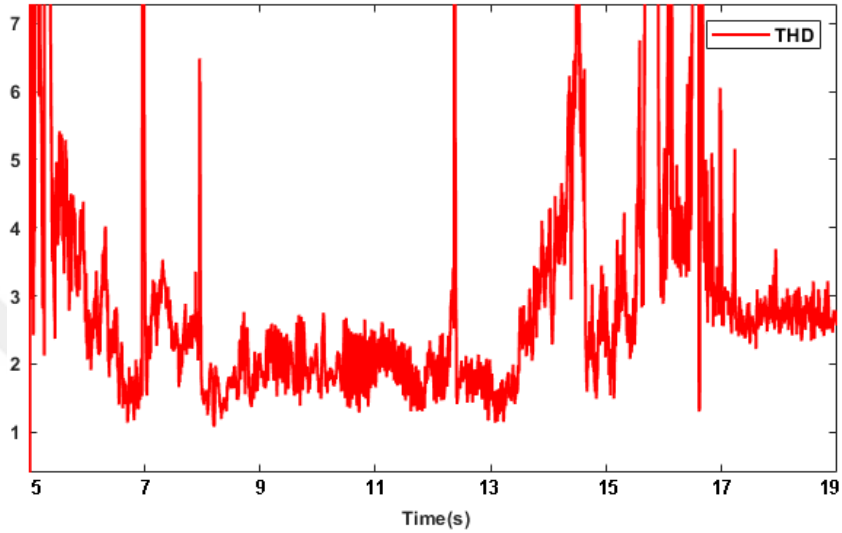

Figure 4.133. The THD of system based on P&O method

When the THD graphs are examined, it is seen that the THD of the ANN-based model responds more quickly to variable weather conditions and settles more quickly. While the system is operating in PV to grid transfer mode for up to 5.25s, a THD reduced to 2% in a short time is seen in the ANN-based method. While the battery is charging in the range of 5.25s and 7s, power is transferred to the grid and battery at the same time. In this time, the THD of the ANN-based model is mostly below 3%, while multi-oscillation THD values are seen in the Inc and P&O methods. In the 7s and 12s range, the THD of the ANN-based model is seen in the 1% and 2% range. In this case, the battery continues to charge. In this time, the THD of the Inc method is in the range of 2% and 4%, and the P&O method is in the range of 1% to 3%, but very oscillating. While the THD of other methods increases between 12s and 14.5s, the THD of the ANN-based method is below 3%. Between 17s and 19s,

the energy stored in the battery is transferred to the grid. In this case, the THD is between 2% and 3% for all MPPT methods.

4.5. Summary

In this section, the hybrid system created in MATLAB/Simulink is tested by adhering to the sunny day scenario. For 1000 W/m^2 and 500 W/m^2; Charge mode, discharge mode, PV-to grid mode is examined. In addition, the results of MPPT methods are compared with the real irradiation curve of a day, which is created with meteorological data of Tarsus /Mersin.

5. CONCLUSIONS AND FUTURE PERSPECTIVES

The optimal design of the PV-BES system is successfully performed with various operating modes and scenarios. The conclusions drawn from this study are listed below.

- The optimal design of a hybrid PV-BES system is performed with proposed ANN-based, Inc, P&O MPPT methods and the results are compared.
- In the study, the daily total solar irradiation estimation is performed by using the real meteorological data of the Tarsus / Mersin with LSTM, RNN, and FFBPNN models. The results are compared, and the best resulting model contributes to the system in terms of the effective consumption of the produced power. Thus, it can be decided how the power stored in the battery will be consumed by estimating the power to be produced from the PV system for the next day.
- Mitigation of harmonics in grid tied PV-BES system is carried out for.
  - PV to grid and battery mode at 1000 W/m^2 that called charging mode THD% < 1.5%,
  - PV to grid mode for 1000 W/m^2 THD% < 1%,
  - Battery to grid mode that called as discharging mode THD% < 3%, PV to grid and battery for 500 W/m^2 at charging mode THD% < 3%,
  - PV to grid mode for 500 W/m^2 THD% < 2% with proposed ANN-based method,
  - The Table 5.1 shows the THD results at constant irradiation values for all operating modes and MPPT methods.

Table 5.1. The THD values for all operating modes

Irradiation	**Operating Mode**	**Injected method**	**THD%**
1000 W/m^2	Charging	ANN	~1.3%
1000 W/m^2	Charging	P&O	1.5-2%
1000 W/m^2	Charging	INC	2- 4%
500 W/m^2	Charging	ANN	2- 3%
500 W/m^2	Charging	P&O	2- 4%
500 W/m^2	Charging	INC	6- 8%
1000 W/m^2	PV to grid mode	ANN	~ 0.85%
1000 W/m2	PV to grid mode	P&O	~ 1%
1000 W/m2	PV to grid mode	INC	1- 3%
500 W/m^2	PV to grid mode	ANN	1- 2%
500 W/m^2	PV to grid mode	P&O	2- 4%
500 W/m^2	PV to grid mode	INC	2- 4%
0	Discharging	-	~ 2%

- It is observed from the results of the system operated for 500 W/m^2 that the proposed ANN-based MPPT method at low irradiance slightly increases the system efficiency. While power efficiency is 84% and below in P&O and INC methods, the power efficiency is around 84.5% for the proposed ANN-based MPPT method.
- The system is operated for 3 different MPPT methods with the solar irradiation curve of a day created from the real data of Tarsus. The results of the proposed sunny day scenario are obtained and compared. Thus, more realistic results for variable weather conditions are obtained from the system tested with data from a real day.
- As a result of the data obtained from the system operated with the real solar irradiation curve; It is clearly seen in the graphs that the proposed

ANN-based MPPT method settles faster than the P&O and INC methods and the system works with lower THD for all operating modes.

- As a result, mitigation of harmonics in grid tied PV-BES system is carried out for PV to grid and battery mode at 1000 W/m^2 that called charging mode THD% < 1.5% , PV to grid mode for 1000 W/m^2 THD% < 1%, battery to grid mode that called as discharging mode THD% < 3%, PV to grid and battery for 500 W/m^2 at charging mode THD% < 3%, PV to grid mode for 500 W/m^2 THD% < 2% with proposed ANN-based method. Furthermore, the power efficiency of system is enhanced for lower irradiance weather conditions based on ANN method.

In future studies, it is planned to carry out studies on energy management and determination of the capacity of battery storage systems, as well as on the improvement methods of inverter power quality and inter harmonic issues.

REFERENCES

Abdelkhalek, C., Said, E. B., Younes, A., & Hassan, A. (2020). A Study and Implementation of Interleaved Boost Converter with a Novel MPPT Tactic for PV Systems. *2020 IEEE 2nd International Conference on Electronics, Control, Optimization and Computer Science, ICECOCS 2020*. https://doi.org/10.1109/ICECOCS50124.2020.9314470

Alexander, S. A. (2016). Development of solar photovoltaic inverter with reduced harmonic distortions suitable for Indian sub-continent. *Renewable and Sustainable Energy Reviews*, *56*, 694–704. https://doi.org/10.1016/j.rser.2015.11.092

Alexander, S. A., & Manigandan, T. (2014). Power quality improvement in solar photovoltaic system to reduce harmonic distortions using intelligent techniques. *Journal of Renewable and Sustainable Energy*, *6*(4). https://doi.org/10.1063/1.4893572

Alhafadhi, L., & Teh, J. (2020). Advances in reduction of total harmonic distortion in solar photovoltaic systems: A literature review. *International Journal of Energy Research*, *44*(4), 2455–2470. https://doi.org/10.1002/er.5075

Alharbi, B. M., Alhomim, M. A., & McCann, R. A. (2020). An efficient high voltage gain using two-stage cascaded interleaved boost converter for solar PV system with MPPT technique. *2020 IEEE Power and Energy Society Innovative Smart Grid Technologies Conference, ISGT 2020*, 2020–2023. https://doi.org/10.1109/ISGT45199.2020.9087720

Ali, A., Almutairi, K., Malik, M. Z., Irshad, K., Tirth, V., Algarni, S., Zahir, M. H., Islam, S., Shafiullah, M., & Shukla, N. K. (2020). Review of online and soft computing maximum power point tracking techniques under non-uniform solar irradiation conditions. *Energies*, *13*(12). https://doi.org/10.3390/en13123256

Ali, M. N., Mahmoud, K., Lehtonen, M., & Darwish, M. M. F. (2021). An Efficient

Fuzzy-Logic Based Variable-Step Incremental Conductance MPPT Method for Grid-connected PV Systems. *IEEE Access*, *4*, 1–1. https://doi.org/10.1109/access.2021.3058052

Alnejaili, T., Labdai, S., & Chrifi-Alaoui, L. (2021). Predictive management algorithm for controlling pv-battery off-grid energy system. *Sensors*, *21*(19). https://doi.org/10.3390/s21196427

Alrashidi, M., Alrashidi, M., Pipattanasomporn, M., & Rahman, S. (2019). Short-Term PV Output Forecasts with Support Vector Regression Optimized by Cuckoo Search and Differential Evolution Algorithms. *2018 IEEE International Smart Cities Conference, ISC2 2018*, 1–8. https://doi.org/10.1109/ISC2.2018.8656685

Amir, A., Amir, A., Che, H. S., Elkhateb, A., & Rahim, N. A. (2019). Comparative analysis of high voltage gain DC-DC converter topologies for photovoltaic systems. *Renewable Energy*, *136*, 1147–1163. https://doi.org/10.1016/j.renene.2018.09.089

Ansari, S., Chandel, A., & Tariq, M. (2021). A Comprehensive Review on Power Converters Control and Control Strategies of AC/DC Microgrid. *IEEE Access*, *9*, 17998–18015. https://doi.org/10.1109/ACCESS.2020.3020035

Athari, H., Niroomand, M., & Ataei, M. (2017). Review and Classification of Control Systems in Grid-tied Inverters. *Renewable and Sustainable Energy Reviews*, *72*(October 2016), 1167–1176. https://doi.org/10.1016/j.rser.2016.10.030

Basha, C. H., & Rani, C. (2020). Different conventional and soft computing MPPT techniques for solar PV systems with high step-up boost converters: A comprehensive analysis. *Energies*, *13*(2). https://doi.org/10.3390/en13020371

Bauer, J. (2010). Single Phase Voltage Source Inverter Photovoltaic Application. *Acta Polytechnica*, *50*(4), 7–11. https://doi.org/10.14311/1217

Behera, S., Meher, D., & Poddar, S. (2019). Comparative Study of MPPT Control

of Grid-Tied PV Generation by Intelligent Techniques. In *Advances in Intelligent Systems and Computing* (Vol. 711). Springer Singapore. https://doi.org/10.1007/978-981-10-8055-5_20

Besheer, A. H., & Adly, M. (2012). Ant colony system based PI maximum power point tracking for stand alone photovoltaic system. *2012 IEEE International Conference on Industrial Technology, ICIT 2012, Proceedings*, 693–698. https://doi.org/10.1109/ICIT.2012.6210019

Bhattacharyya, S., Kumar P, D. S., Samanta, S., & Mishra, S. (2021). Steady output and fast tracking MPPT (SOFT-MPPT) for P&O and InC algorithms. *IEEE Transactions on Sustainable Energy*, *12*(1), 293–302. https://doi.org/10.1109/TSTE.2020.2991768

Bollipo, R. B., Mikkili, S., & Bonthagorla, P. K. (2020). Critical Review on PV MPPT Techniques: Classical, Intelligent and Optimisation. *IET Renewable Power Generation*, *14*(9), 1433–1452. https://doi.org/10.1049/iet-rpg.2019.1163

Bollipo, R. B., Mikkili, S., & Bonthagorla, P. K. (2021). Hybrid, optimal, intelligent and classical PV MPPT techniques: A review. *CSEE Journal of Power and Energy Systems*, *7*(1), 9–33. https://doi.org/10.17775/CSEEJPES.2019.02720

Chauhan, S., & Singh, B. (2021). Control of solar PV-integrated battery energy storage system for rural area application. *IET Renewable Power Generation*, *15*(5), 1030–1045. https://doi.org/10.1049/rpg2.12086

Çukurova University Institute Of Natural And Applied Sciences Phd Thesis Özgür Çel İ K Controller Design And Experimental Verification Of Grid-Connected Microinverters For Photovoltaic Applications Department Of Electrical And Electronics Engineering Adan. (2019).

Di Piazza, M. C., Luna, M., La Tona, G., & Di Piazza, A. (2019). Improving grid integration of hybrid PV-storage systems through a suitable energy management strategy. *IEEE Transactions on Industry Applications*, *55*(1),

60–68. https://doi.org/10.1109/TIA.2018.2870348

EPDK. (2014). Elektrik Şebeke Yönetmeliği. In *Official Gazette* (Issue 29013).

Figueiredo, S. N., & Aquino, R. N. A. L. S. (2021). *Hybrid MPPT Technique PSO-P & O Applied to Photovoltaic Systems Under Uniform and Partial Shading Conditions*. *19*(10), 1610–1617.

Forouzesh, M., Siwakoti, Y. P., Gorji, S. A., Blaabjerg, F., & Lehman, B. (2017). Step-Up DC-DC converters: A comprehensive review of voltage-boosting techniques, topologies, and applications. *IEEE Transactions on Power Electronics*, *32*(12), 9143–9178. https://doi.org/10.1109/TPEL.2017.2652318

G, D., & Singh, S. N. (2017). Selection of non-isolated DC-DC converters for solar photovoltaic system. *Renewable and Sustainable Energy Reviews*, *76*(March), 1230–1247. https://doi.org/10.1016/j.rser.2017.03.130

Garud, K. S., Jayaraj, S., & Lee, M. Y. (2021). A review on modeling of solar photovoltaic systems using artificial neural networks, fuzzy logic, genetic algorithm and hybrid models. *International Journal of Energy Research*, *45*(1), 6–35. https://doi.org/10.1002/er.5608

Gonzalez-Castano, C., Restrepo, C., Kouro, S., & Rodriguez, J. (2021). MPPT Algorithm Based on Artificial Bee Colony for PV System. *IEEE Access*, *9*, 43121–43133. https://doi.org/10.1109/ACCESS.2021.3066281

Gorji, S. A., Sahebi, H. G., Ektesabi, M., & Rad, A. B. (2019). Topologies and control schemes of bidirectional DC–DC power converters: An overview. *IEEE Access*, *7*, 117997–118019. https://doi.org/10.1109/ACCESS.2019.2937239

Gowtham, M., Kaviyarasu, N., Dhayanithi, R., Praveen, C., & Hariprabhu, M. (2022). Maximum Power Tracking and Harmonic Reduction using Optimized P O MPPT Algorithm. *Proceedings of the 2nd International Conference on Artificial Intelligence and Smart Energy, ICAIS 2022*, 1674–1679. https://doi.org/10.1109/ICAIS53314.2022.9743092

Guerra, M. I. S., de Araújo, F. M. U., Dhimish, M., & Vieira, R. G. (2021). Assessing maximum power point tracking intelligent techniques on a pv system with a buck–boost converter. *Energies*, *14*(22). https://doi.org/10.3390/en14227453

Hannan, M. A., Wali, S. B., Ker, P. J., Rahman, M. S. A., Mansor, M., Ramachandaramurthy, V. K., Muttaqi, K. M., Mahlia, T. M. I., & Dong, Z. Y. (2021). Battery energy-storage system: A review of technologies, optimization objectives, constraints, approaches, and outstanding issues. *Journal of Energy Storage*, *42*(July), 103023. https://doi.org/10.1016/j.est.2021.103023

Hong, J., Yin, J., Liu, Y., Peng, J., & Jiang, H. (2019). Energy Management and Control Strategy of Photovoltaic/Battery Hybrid Distributed Power Generation Systems with an Integrated Three-Port Power Converter. *IEEE Access*, *7*, 82838–82847. https://doi.org/10.1109/ACCESS.2019.2923458

Ibnelouad, A., Kari, A. El, Ayad, H., & Mjahed, M. (2021). Multilayer Artificial Approach for Estimating Optimal Solar PV System Power Using the MPPT Technique. *Studies in Informatics and Control*, *30*(4), 109–120. https://doi.org/10.24846/V30I4Y202110

Ibrahim, A. W., Shafik, M. B., Ding, M., Sarhan, M. A., Fang, Z., Alareqi, A. G., Almoqri, T., & Al-Rassas, A. M. (2020). PV maximum power-point tracking using modified particle swarm optimization under partial shading conditions. *Chinese Journal of Electrical Engineering*, *6*(4), 106–121. https://doi.org/10.23919/CJEE.2020.000035

Iqbal, M. M. (2017). Design And Simulation Of A PV System With Battery Storage Using Bidirectional DC-DC Converter Using Matlab Simulink. *International Journal of Scientific & Technology Research 6 (07), 403-410 , July*.

Khan, M. N. H., Forouzesh, M., Siwakoti, Y. P., Li, L., Kerekes, T., & Blaabjerg, F. (2020). Transformerless Inverter Topologies for Single-Phase Photovoltaic

Systems: A Comparative Review. *IEEE Journal of Emerging and Selected Topics in Power Electronics*, *8*(1), 805–835. https://doi.org/10.1109/JESTPE.2019.2908672

Khan, S. U., Liu, L., Wang, L., & Yang, S. (2015). A modified particle swarm optimization algorithm for engineering optimizations. *Proceedings of Science*, *12-13-Sept*(January 2020). https://doi.org/10.22323/1.259.0004

Khezri, R., Mahmoudi, A., & Aki, H. (2022). Optimal planning of solar photovoltaic and battery storage systems for grid-connected residential sector: Review, challenges and new perspectives. *Renewable and Sustainable Energy Reviews*, *153*(September 2021), 111763. https://doi.org/10.1016/j.rser.2021.111763

Kummara, V. G. R., Zeb, K., Muthusamy, A., Krishna, T. N. V., Prabhudeva Kumar, S. V. S. V., Kim, D. H., Kim, M. S., Cho, H. G., & Kim, H. J. (2020). A comprehensive review of DC–DC converter topologies and modulation strategies with recent advances in solar photovoltaic systems. In *Electronics (Switzerland)* (Vol. 9, Issue 1). https://doi.org/10.3390/electronics9010031

Li, X., Wen, H., Hu, Y., Du, Y., & Yang, Y. (2021). A Comparative Study on Photovoltaic MPPT Algorithms under EN50530 Dynamic Test Procedure. *IEEE Transactions on Power Electronics*, *36*(4), 4153–4168. https://doi.org/10.1109/TPEL.2020.3024211

Liang, X., & Andalib-Bin-karim, C. (2017). Harmonic mitigation through advanced control methods for grid- connected renewable energy sources. *2017 IEEE Industry Applications Society Annual Meeting, IAS 2017*, *2017-Janua*, 1–12. https://doi.org/10.1109/IAS.2017.8101861

Liu, J., Chen, X., Cao, S., & Yang, H. (2019). Overview on hybrid solar photovoltaic-electrical energy storage technologies for power supply to buildings. *Energy Conversion and Management*, *187*(March), 103–121. https://doi.org/10.1016/j.enconman.2019.02.080

Liu, J., Chen, X., Yang, H., & Li, Y. (2020). Energy storage and management system

design optimization for a photovoltaic integrated low-energy building. *Energy*, *190*, 116424. https://doi.org/10.1016/j.energy.2019.116424

Malar, J. S. J., Bisharathu Beevi, A., & Jayaraju, M. (2020). Efficient Power Flow Management in Hybrid Renewable Energy Systems. *IETE Journal of Research*. https://doi.org/10.1080/03772063.2020.1853617

Mohammed, S. S., & Devaraj, D. (2015a). Simulation o f Incremental Conductance MPPT based J }. *2015 IEEE International Conference on Electrical, Computer and Communication Technologies (ICECCT)*, 1–6.

Mohammed, S. S., & Devaraj, D. (2015b). Simulation o f Incremental Conductance MPPT based J }. *2015 IEEE International Conference on Electrical, Computer and Communication Technologies (ICECCT)*, 1–6.

Mohandes, B., Wahbah, M., Moursi, M. S. El, & El-Fouly, T. H. M. (2021). Renewable energy management system: Optimum design and hourly dispatch. *IEEE Transactions on Sustainable Energy*, *12*(3), 1615–1628. https://doi.org/10.1109/TSTE.2021.3058252

Mumtaz, F., Zaihar Yahaya, N., Tanzim Meraj, S., Singh, B., Kannan, R., & Ibrahim, O. (2021). Review on non-isolated DC-DC converters and their control techniques for renewable energy applications. *Ain Shams Engineering Journal*, *12*(4), 3747–3763. https://doi.org/10.1016/j.asej.2021.03.022

Nahar, S., & Bashir Uddin, M. (2019). Analysis the performance of interleaved boost converter. *4th International Conference on Electrical Engineering and Information and Communication Technology, ICEEiCT 2018*, *8*, 547–551. https://doi.org/10.1109/CEEICT.2018.8628104

Narayanan, V., Kewat, S., & Singh, B. (2020). Solar PV-BES Based Microgrid System with Multifunctional VSC. *IEEE Transactions on Industry Applications*, *56*(3), 2957–2967. https://doi.org/10.1109/TIA.2020.2979151

Nespoli, A., Ogliari, E., Leva, S., Pavan, A. M., Mellit, A., Lughi, V., & Dolara, A. (2019). Day-ahead photovoltaic forecasting: A comparison of the most effective techniques. *Energies*, *12*(9), 1–15.

https://doi.org/10.3390/en12091621

Permatasari, I. (2015). No Title העיוורון על. *Journal of Geotechnical and Geoenvironmental Engineering ASCE*, *120*(11), 259.

Pogaku, N., Prodanović, M., & Green, T. C. (2007). Modeling, analysis and testing of autonomous operation of an inverter-based microgrid. *IEEE Transactions on Power Electronics*, *22*(2), 613–625. https://doi.org/10.1109/TPEL.2006.890003

Poongothai, C., & Vasudevan, K. (2019). Design of LCL filter for grid-interfaced PV system based on cost minimization. *IEEE Transactions on Industry Applications*, *55*(1), 584–592. https://doi.org/10.1109/TIA.2018.2865723

Priyadarshi, N., Padmanaban, S., Holm-Nielsen, J. B., Blaabjerg, F., & Bhaskar, M. S. (2020). An Experimental Estimation of Hybrid ANFIS-PSO-Based MPPT for PV Grid Integration under Fluctuating Sun Irradiance. *IEEE Systems Journal*, *14*(1), 1218–1229. https://doi.org/10.1109/JSYST.2019.2949083

Qays, M. O., Buswig, Y., Basri, H., Hossain, M. L., Abu-Siada, A., Rahman, M. M., & Muyeen, S. M. (2020). An Intelligent Controlling Method for Battery Lifetime Increment Using State of Charge Estimation in PV-Battery Hybrid System. *Applied Sciences*, *10*(24), 8799. https://doi.org/10.3390/app10248799

Rates, E. (2021). *Solar PV and Battery by Considering Flat and Time-of-Use*.

Reveles-Miranda, M., Flota-Banuelos, M., Chan-Puc, F., Ramirez-Rivera, V., & Pacheco-Catalan, D. (2020). A Hybrid control technique for harmonic elimination, power factor correction, and night operation of a grid-connected pv inverter. *IEEE Journal of Photovoltaics*, *10*(2), 664–675. https://doi.org/10.1109/JPHOTOV.2019.2961600

Reznik, A., Simoes, M. G., Al-Durra, A., & Muyeen, S. M. (2014). LCL Filter design and performance analysis for grid-interconnected systems. *IEEE Transactions on Industry Applications*, *50*(2), 1225–1232. https://doi.org/10.1109/TIA.2013.2274612

Roy, R. B., & Amin, N. (2021). A Comparative Performance Analysis of ANN Algorithms for MPPT Energy Harvesting in Solar PV System. *IEEE Access*, *PP*, 1. https://doi.org/10.1109/ACCESS.2021.3096864

Safari, A., & Mekhilef, S. (2011). Simulation and hardware implementation of incremental conductance MPPT with direct control method using cuk converter. *IEEE Transactions on Industrial Electronics*, *58*(4), 1154–1161. https://doi.org/10.1109/TIE.2010.2048834

Sefa, I., & Özdemir, Ş. (2009). Experimental study of interleaved MPPT converter for PV systems. *IECON Proceedings (Industrial Electronics Conference)*, 456–461. https://doi.org/10.1109/IECON.2009.5414965

Shafique, B. H., & Tjernberg, L. B. (2021). *Behind the Meter Strategies*. *September*, 112–119.

Sher, H. A., Murtaza, A. F., Noman, A., Addoweesh, K. E., Al-Haddad, K., & Chiaberge, M. (2015). A New Sensorless Hybrid MPPT Algorithm Based on Fractional Short-Circuit Current Measurement and P&O MPPT. *IEEE Transactions on Sustainable Energy*, *6*(4), 1426–1434. https://doi.org/10.1109/TSTE.2015.2438781

Sivakumar, S., Sathik, M. J., Manoj, P. S., & Sundararajan, G. (2016). An assessment on performance of DC-DC converters for renewable energy applications. *Renewable and Sustainable Energy Reviews*, *58*, 1475–1485. https://doi.org/10.1016/j.rser.2015.12.057

Sorte, P. K., Panda, K. P., & Panda, G. (2021). Current Reference Control Based MPPT and Investigation of Power Management Algorithm for Grid-Tied Solar PV-Battery System. *IEEE Systems Journal*, 1–11. https://doi.org/10.1109/JSYST.2021.3052959

Sun, J., Ma, X., & Kazi, M. (2018a). Comparison of decline curve analysis DCA with recursive neural networks RNN for production forecast of multiple wells. *SPE Western Regional Meeting Proceedings*, *2018-April*(April 2018). https://doi.org/10.2118/190104-ms

Sun, J., Ma, X., & Kazi, M. (2018b). Comparison of decline curve analysis DCA with recursive neural networks RNN for production forecast of multiple wells. *SPE Western Regional Meeting Proceedings*, *2018-April*(April). https://doi.org/10.2118/190104-ms

Taghvaee, M. H., Radzi, M. A. M., Moosavain, S. M., Hizam, H., & Hamiruce Marhaban, M. (2013). A current and future study on non-isolated DC-DC converters for photovoltaic applications. *Renewable and Sustainable Energy Reviews*, *17*, 216–227. https://doi.org/10.1016/j.rser.2012.09.023

Tahir, S., Wang, J., Baloch, M. H., & Kaloi, G. S. (2018). Digital control techniques based on voltage source inverters in renewable energy applications: A review. *Electronics (Switzerland)*, *7*(2). https://doi.org/10.3390/electronics7020018

Talbi, M., Mensia, N., & Ezzaouia, H. (2021). Modeling of a pv panel and application of maximum power point tracking command based on ann. *International Arab Journal of Information Technology*, *18*(4), 568–577. https://doi.org/10.34028/18/4/9

Teke, A. (2022). *Turkish Journal of Electrical Engineering and Computer Sciences Evaluation of artificial neural network methods to forecast short- term solar power generation : a case study in Eastern Mediterranean Region*. *30*(6). https://doi.org/10.55730/1300-0632.3921

Tofigh, M. A., Zainuddin, N. F., & Hasbi, A. F. (2021). Mitigation of Harmonic Distortion for Grid Connected PV Solar Using MPPT Controller. *Proceeding - 2021 IEEE 17th International Colloquium on Signal Processing and Its Applications, CSPA 2021*, *March*, 97–100. https://doi.org/10.1109/CSPA52141.2021.9377301

Wu, Z., Tazvinga, H., & Xia, X. (2015). Demand side management of photovoltaic-battery hybrid system. *Applied Energy*, *148*, 294–304. https://doi.org/10.1016/j.apenergy.2015.03.109

Yap, K. Y., Sarimuthu, C. R., & Lim, J. M. Y. (2020). Artificial Intelligence Based

MPPT Techniques for Solar Power System: A review. *Journal of Modern Power Systems and Clean Energy*, *8*(6), 1043–1059. https://doi.org/10.35833/MPCE.2020.000159

Yonis Buswig, Y. M., Qays, O., Affam, A., Albalawi, H., Othman, A. K., Julai, N., & Yi, S. S. (2020). Designing a control system based on SOC estimation of BMS for PV-Solar system. *International Journal of Integrated Engineering*, *12*(6), 148–157. https://doi.org/10.30880/ijie.2020.12.06.017

Zeb, K., Uddin, W., Khan, M. A., Ali, Z., Ali, M. U., Christofides, N., & Kim, H. J. (2018). A comprehensive review on inverter topologies and control strategies for grid connected photovoltaic system. *Renewable and Sustainable Energy Reviews*, *94*(June), 1120–1141. https://doi.org/10.1016/j.rser.2018.06.053

Zhang, X., Gamage, D., Wang, B., & Ukil, A. (2021). Hybrid maximum power point tracking method based on iterative learning control and perturb & observe method. *IEEE Transactions on Sustainable Energy*, *12*(1), 659–670. https://doi.org/10.1109/TSTE.2020.3015255

Zongo, O. A. (2021). Comparing the performances of MPPT techniques for DC-DC boost converter in a PV system. *Walailak Journal of Science and Technology*, *18*(2), 1–15. https://doi.org/10.48048/wjst.2021.6500

CURRICULUM VITAE

Helin BOZKURT. She graduated from 19 Mayıs Super High School in 2008. She received her BSc degree in Electrical and Electronics Engineering from Çukurova University in 2014. She has been working as a research assistant in the Electrical and Electronic Engineering Department of the Toros University Mersin since 2021. Her research interests include renewable energy systems, generation, transmission, and distribution of electrical energy, power electronic converters, and energy efficiency applications.